SPILLOVER MODELLING AND DYNAMICS IN MULTI-HOST PATHOGENS TRANSMISSION

YI TAN

A DISSERTATION SUBMITTED TO
THE FACULTY OF GRADUATE STUDIES
IN PARTIAL FULFILMENT OF THE REQUIREMENTS
FOR THE DEGREE OF
DOCTOR OF PHILOSOPHY

GRADUATE PROGRAM IN MATHEMATICS AND STATISTICS
YORK UNIVERSITY
TORONTO, ONTARIO

April 2025

Abstract

Many pathogens of concern to both human and animal populations exhibit a generalist nature of infecting multiple host species. The behavior and transmission dynamics within reservoir hosts not only influence outbreaks within their own population but also contribute to the spillover of pathogens to new target hosts. Although existing works have incorporated spillover transmission into zoonotic models, significant gaps remain in understanding the epidemic or endemic spread of disease in target hosts due to spillover, particularly in epizootic contexts. One typical example is the monkeypox. In this research, by delineating host roles and examining transmission dynamics of monkeypox, we can effectively assess the risk of spillover events and inform mitigation and control strategies.

We start with a foundational framework that models monkeypox transmission in a single host species. Two kinds of stochasticity, namely demographic and environmental stochasticity, are incorporated. We find population-size-dependent shift in the relative influence of demographic and environmental stochasticity on disease

dynamics. By developing a basic reservoir-target epidemic systems, we observe that the basic reproduction number of the system fails to capture interspecific transmissibility. Our novel threshold derived from the final size relation reflects the influence of spillover processes and intraspecific transmission within target hosts, providing an appropriate measure for quantifying the spillover phenomena. Subsequently, incorporating population demographics allows us to determine the population extinction threshold and the maximum persistence threshold. We further verify that stochasticity in the spillover rate induces Phenomenological bifurcation (P-bifurcation) within the model. These analyses reveal that the spillover rate is the most critical factor influencing the epidemic and endemic prevalence in target hosts.

Finally, we evaluate the effectiveness of reservoir control strategies such as quarantine and culling. Our findings indicate that the interactions between spillover events and the implementation of reservoir control strategies lead to complex dynamics due to the higher codimension bifurcations. A novel observation from our analysis and numerical simulations is the existence and collision of two limit cycles generated by distinct endemic equilibria within the system. Our study underscores the importance of controlling spillover events and managing reservoir prevalence as key interventions to mitigate spillover effects on target hosts.

Acknowledgements

Amidst the snowflakes swirling in frosty air and the vibrant life on York campus, I write this acknowledgment. Year after year, the snow continues its silent dance, and as my time in this cherished city comes to a close, I am filled with gratitude.

Studying in Toronto has been one of the most rewarding experiences of my life. This city's beauty is a constant companion: squirrels dart through trees, geese roam the verdant grass, and birds flit joyfully among blossoming branches. I am profoundly grateful for the serenity this place has offered—listening to the wind, watching the clouds, and reveling in the fiery hues of autumn maples. Some mornings, I rose early to run in the gym; other times, I found solace at the student center, watching life unfold below. The full moon illuminates my path home from the office, lunchbox in hand. These moments, balanced with the serious research, have made this chapter of my life uniquely meaningful.

My deepest gratitude goes to Professor Huaiping Zhu, whose guidance, care, and support have shaped every step of my journey. As my mentor in infectious disease

modeling and bifurcation analysis, his academic insights and profound expertise have been invaluable. Beyond academics, his patience and encouragement have helped me navigate challenges and grow as a researcher and individual. Reflecting on his lessons, I now fully appreciate their profound wisdom. As the Chinese saying goes, "Give a person a fish, and you feed them for a day; teach a person to fish, and you feed them for a lifetime." Under Professor Zhu's mentorship, I have gained not just knowledge but transformative ways of thinking—gifts I will carry forward.

I am also deeply grateful to my supervisory committee members, Professor Jane Heffernan and Professor Jude Kong. Their insightful suggestions and constructive feedback have been a constant source of inspiration, significantly shaping the direction and quality of this work.

I extend my heartfelt thanks to the members of the Lamps group—professors, senior colleagues, and peers—who have supported me throughout my research journey. In particular, I would like to express my appreciation to Pei Yuan, Elena Aruffo, Zhaowan Li, Guihong Fan, Juan Li, Steven Chen, Ziwang Deng, Xiaolan Zhou, Bing Hu, Shibing You, Haitao Song, Xinmiao Rong, Hao Zhou, Huidi Chu, Yao Wang, Boli Xie, Qi Li, Tingting Zheng, Mengyun Zhang, Jun Li, Mingju Ma, Shenggen Wu, Yunbo Tu, Hongyi Xie, Chunping Jia, Liwen Song, Wentao Fu, Miao Zhang, Sanaz Gholizadeh, and Sayeda Irin Akter for their generous assistance and encouragement.

I extend my gratitude to Professors Michael Haslam, Woldegebriel Assefa Woldegerima, Hyejin Ku, Dong Liang, and Seyed Moghadas. Their profound expertise during classes have significantly broadened my understanding in various domains.

I am deeply appreciative of the financial support from the China Scholarship Council (CSC) and the exceptional academic environment fostered by York University, particularly the Department of Mathematics and Statistics. Their resources and support have been instrumental in my success.

I would like to express my gratitude to my master's supervisor, Professor Sanyi Tang, who served as my guide into the world of doctoral research. It was under his encouragement that I began my exploration of stochastic modeling.

To the pioneers in biomathematics research, whose contributions have laid the foundation for my work, I offer my profound respect and admiration.

To my parents and family, your unwavering care and support have been my bedrock. A special thanks to my boyfriend, whose understanding and companionship over the past decade have been a constant source of strength and inspiration.

Finally, I wish to express my heartfelt gratitude to everyone who has supported and assisted me during this journey. Your encouragement and kindness have been instrumental in reaching this milestone, and I will cherish these memories forever. Wishing you all health, success, and happiness.

Table of Contents

List of Tables

List of Figures

1 Introduction

1.1 Multi-Host Pathogens

Multi-host pathogens, capable of infecting multiple host species, pose a significant challenge to both animal and human health [1, 2]. Cleaveland et al. [3] reported that approximately 77% of pathogens affecting livestock and 90% of pathogens affecting domestic carnivores are classified as multi-host pathogens. The emergence of infectious diseases in wildlife has been widely recognized as a major threat to biodiversity, agricultural productivity, and human health [4, 5]. Taylor et al. [6] estimated that over 60% of known human pathogens have zoonotic origins, emphasizing the critical role of animals in the emergence of infectious diseases. Among these, rodent-borne diseases constitute a notable category of multi-host pathogens capable of infecting humans, raising significant public health concerns (Table 1.1). The increasing prevalence of multi-host pathogens has been attributed to climate change [7], habitat destruction, and intensive farming practices [8]. A comprehen-

sive understanding of their transmission dynamics and cross-species interactions is crucial for effective disease risk management.

Distinguishing the hosts and their roles on pathogen circulation is a critical first step in modeling their effects. Haydon et al. [9] proposed that reservoirs can only be comprehensively understood in relation to specific target populations. Accordingly, they defined a reservoir as one or more epidemiologically connected populations or environments where the pathogen can be sustainably maintained and from which transmission to the defined target population occurs. The transmission of pathogens from reservoir hosts to new hosts is known as spillover [10, 11, 12, 13, 14], with target hosts serving as recipients in these events [11, 12, 15]. The spillover process is influenced by various factors (Figure 1.1), including the circulation within reservoir hosts, when and where to expect pathogen exertion, host's immune response, and behavioral changes aimed at reducing exposure [11, 14].

Recent outbreaks have revealed the widespread occurrence and significance of spillover events in disease transmission. For instance, since the onset of the SARS-CoV-2 pandemic, the virus has spilled over into more than 30 animal species, emphasizing the interconnectedness of human and animal health [16, 17]. Similarly, Nipah virus outbreaks in Bangladesh have occurred with alarming regularity, with 79 spillover events recorded between April 2001 and April 2014 [18]. Spillover dy-

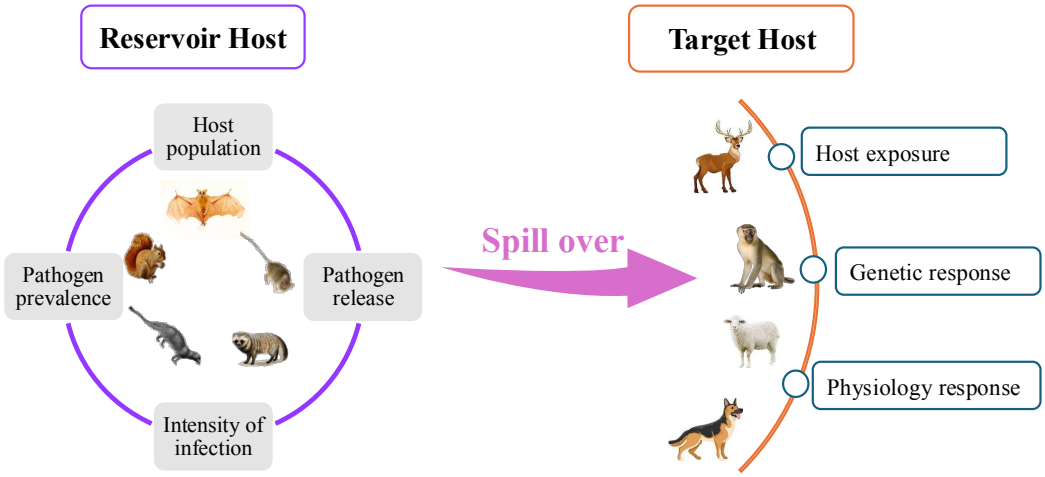

Figure 1.1: Factors affect spillover processes.

namics are also evident in highly pathogenic avian influenza (HPAI) H5N1, with 54 outbreaks documented in India involving transmission from wild birds to poultry between January 2006 and August 2010 [19]. More recently, by July 2024, spillover of H5N1 avian influenza from birds to cattle in the United States resulted in the infection of 157 herds across 13 states, along with four human cases, raising significant concerns about viral mutation and zoonotic transmission [20]. These incidents underscore the urgent need to develop and analyze reservoir-target disease models that incorporate spillover dynamics.

Wolfe et al. [13] proposed a framework outlining five evolutionary stages of zoonotic pathogen progression, beginning with exclusive infection in animal hosts

(stage I) and culminating in exclusive infection in humans (stage V). Building on this concept, we adopt an enhanced framework by Lloyd-Smith et al. [2], which considers four distinct stages of pathogen evolution (Figure 1.2). In the initial stage, reservoir hosts play a crucial role by exclusively harboring and transmitting the pathogen, ensuring its persistence and shedding within natural ecosystems. The subsequent stages are defined by the basic reproduction number of target hosts: stage II involves no intraspecific transmission among target hosts ($R_{0a} = 0$), stage III is characterized by stuttering chains with limited intraspecific transmission ($R_{0a} < 1$), and stage IV represents significant intraspecific transmission among target hosts ($R_{0a} > 1$).

In stage IV, the establishment of pathogens within target hosts is inevitable. Nevertheless, the outcomes of spillover events occurring during stages II and III remain uncertain, particularly whether they will lead to outbreaks or persistence within target host populations. Additionally, both theoretical and empirical studies highlight a concerning scenario where repeated powerful spillover events may exert significant pressures on target host populations, potentially driving them toward extinction [21]. Previous studies [21, 22] have only developed conceptual frameworks to outline potential spillover outcomes in target hosts, with a primary focus on transmission rates both within and between species (Figure 1.2).

In the management of spillover events, three primary strategies are widely em-

ployed [9]: (1) Target Control: focusing intervention efforts exclusively within the target population. A notable example is human vaccination program against monkeypox [23, 24]. (2) Spillover Tactics: implementing measures to substantially reduce interactions between species. For instance, minimizing human exposure to infected animals has been demonstrated to effectively control monkeypox transmission [25, 26]. (3) Reservoir Control: addressing infections within the reservoir population. An illustrative example is the culling of European badgers (*Meles meles*) to mitigate the transmission of Mycobacterium bovis to cattle, a well-documented vector for bovine tuberculosis (TB) [27]. The application of these approaches requires a deep understanding of host roles and spillover dynamics [14, 22, 28].

Two broad classes of stochasticity are commonly recognized in the context of pathogen transmission: environmental and demographic stochasticity [29, 30, 31]. Environmental stochasticity arises from fluctuations in temperature, rainfall, or host behavioral changes. This form of stochasticity induces random variations in key model parameters, which can affect disease dynamics at the population level. In contrast, demographic stochasticity is an intrinsic property of the system, driven by the probabilistic nature of individual-level events such as birth and death. This inherent variability is especially evident in small populations, where the resulting distributions of outcomes provide critical insights into the role of stochasticity in the

dynamics of disease spread.

Indeed, it is paramount to investigate the contribution of spillover events to pathogen prevalence and persistence in target hosts, identify threshold conditions, and inform applicable management measures. Monkeypox, a pathogen that has recently sparked public concern, offers an illustrative example for studying these crucial aspects. We examine the transmission dynamics of monkeypox within reservoir and target hosts in a hypothetical metropolitan area. Three distinct transmission pathways: (i) from reservoir to reservoir, (ii) from reservoir to target, and (iii) from target to target are incorporated. Our analysis of monkeypox clarifies that understanding of transmission dynamics can impact inference of control measures, and highlights the need to quantitatively evaluate spillover processes.

Table 1.1: Rodent-borne pathogens

Lassa Fever (LF)	
Main carriers	Reservoir: *Mastomys natalensis*
Human transmission route	Rodent-to-human, human-to-human and even human-to-rodent transmission patterns are possible
Human infections, region	Hemorrhagic fever common in areas of West Africa

Hantavirus Pulmonary Syndrome (HPS)	
Main carriers	The New York hantavirus, carried by the white-footed mouse, is associated with HPS cases in the northeastern US
Human transmission route	Rodent-to-human, rare cases of human-to-human transmission in Chile and Argentina
Human infections, region	America, Canada, Argentina, Bolivia, Brazil, Chile, Panama, Paraguay, and Uruguay
Hemorrhagic Fever with Renal Syndrome (HFRS)	
Main carriers	Known carriers include the striped field mouse (*Apodemus agrarius*), the reservoir for both the Saaremaa and Hantaan virus; the brown or Norway rat (*Rattus norvegicus*), the reservoir for Seoul virus; the bank vole (*Clethrionomys glareolus*), the reservoir for Puumala virus; and the yellow-necked field mouse (*Apodemus flavicollis*), which carries Dobrava virus
Human transmission route	Rodent-to-human

Human infections, region	HFRS is found throughout the world. Endemic in Europe and Asia
Leptospirosis	
Main carriers	Wild animals serve as reservoirs of leptospirosis, including rodents, bats, foxes, sea lions, and capybaras
Human transmission route	Human infection occurs through direct contact with secretions of an infected animal, especially urine, or through contact with contaminated water. Extremely rare human-to-human infection
Human infections, region	Leptospirosis is a widespread and potentially fatal zoonosis that is endemic in many tropical regions
Lujo Hemorrhagic Fever (LUHF)	
Main carriers	A range of mammalian species, particularly rodents and bats
Human transmission route	Rodent-to-human and human-to-human
Human infections, region	Identified in Southern Africa in 2008. Cases in humans are recorded each year globally

Lymphocytic Choriomeningitis (LCM)	
Main carriers	The primary host of LCMV is the common house mouse (*Mus musculus*). Other types of rodents, such as hamsters, are not the natural reservoirs but can become infected with LCMV from wild mice at the breeder, in the pet store, or home environment
Human transmission route	Human infection occurs through direct contact with infected rodents or contaminated environment. Person-to-person transmission has not been reported, with the exception of vertical transmission from infected mother to fetus, and rarely, through organ transplantation
Human infections, region	Hemorrhagic fever common in areas of West Africa
Omsk Hemorrhagic Fever (OHF)	

Main carriers	Rodents serve as the primary host for OHFV, which is transmitted to rodents from the bite of an infected tick. Common tick vectors include *Dermacentor reticulatus*, *Dermacentor marginatus*, and *Ixodes persulcatus*. Common rodents infected with OHFV include the muskrat (*Ondatra zibethica*), water vole (*Arvicola terrestris*), and narrow-skulled voles (*Microtus gregalis*)
Human transmission route	Humans can become infected through tick bites or through contact with the blood, feces, or urine of an infected, sick, or dead animal – most commonly, rodents. Transmission may also occur with contaminated environment. No human-to-human transmission of OHFV has been documented but infections due to lab contamination have been described
Human infections, region	OHF occurs in the western Siberia regions of Omsk, Novosibirsk, Kurgan, and Tyumen

Rat-Bite Fever (RBF)	
Main carriers	The primary hosts are rats, both the black rat (*Rattus rattus*) and the Norwegian rat (*Rattus norvegicus*), kept as pets and used in animal research. Other rodents can also carry and spread the bacteria
Human transmission route	Rodent-to-human, environment-to-human
Human infections, region	RBF is an infectious disease caused by two distinct bacterial pathogens: Streptobacillus moniliformis, which is the reported causative agent of RBF in North America (streptobacillary RBF), and Spirillum minus, which is more commonly found in Asia (spirillary RBF, also known as sodoku).
Chapare Hemorrhagic Fever (CHHF)	
Main carriers	Rodents
Human transmission route	Rodent-to-human, environment-to-human

Human infections, region	The only documented outbreaks of CHHF to date have occurred in the Cochabamba and Caranavi regions of Bolivia
Tularemia	
Main carriers	Arthropods (ticks and deer flies) are the main transmission vector, and small animals (rabbits, hares, and muskrats) serve as reservoir hosts
Human transmission route	The pathogen can be transmitted to humans from animals, vectors, food and water, or the environment
Human infections, region	Endemic in North America and parts of Europe and Asia

1.2 Monkeypox

The monkeypox virus is a member of the Orthopoxvirus genus, first isolated from cynomolgus macaque (*Macaca fascicularis*) in 1958 [32], hence its nomenclature. There are four recognized variants of the monkeypox virus, categorized into clades Ia, Ib, IIa, and IIb [33]. The clade Ia virus is of particular interest in our study as they

represent one of the ancestral strains impacting both animals and humans [33, 34]. Historically, transmission of clade Ia has been primarily zoonotic, occurring from animals to humans within Central Africa. However, recent research [35] indicates that clade Ia may now be circulating persistently among humans, potentially facilitated by sexual transmission, particularly in the Democratic Republic of the Congo (DRC). Notably, clade Ia is associated with higher virulence, with human case fatality rates in certain African outbreaks estimated at approximately 10% [36].

Clade Ib, identified in late 2023, has since led to a notable increase in cases in Central Africa [37]. This clade has also been detected in the United Kingdom, Sweden, Thailand, India, Germany, and six African nations with no prior reports of monkeypox cases [33]. The DRC has experienced a significant impact, reporting nearly 36 000 suspected infections and over 1 000 deaths due to monkeypox in 2024 [33]. Clade Ib is known to transmit from person to person, including via sexual contact.

Clade IIa viruses have been associated with sporadic human infections, primarily within West Africa. Human infections due to clade IIa has occurred in other parts of the world through importation of African rodents into the United States in 2003 and by travelers from Africa [38]. During the mid-2010s, a similar clade II strain, labeled IIb, was identified as capable of transmission through sexual contact. Clade IIb is

responsible for the still-simmering 2022 global outbreak [33]. Since mid-May 2022, monkeypox virus has spread to over 130 countries across Europe, the Americas, the Middle East, additional African regions, South Asia, and Australia [39]. This spread marks the first recorded instances of sustained transmission in areas with no direct epidemiological links to West or Central Africa. Human mortality rate associated with clade IIb remains low, though they may be underestimated [36]. Whereas clades Ia and IIa are primarily zoonoses, clade IIb has exhibited extensive human-to-human spread [38].

Factors such as urbanization and the increasing frequency of human-animal interactions serve as key drivers for the rising incidence of monkeypox cases [40, 41, 42, 43]. Numerous human cases on the continent have been associated with contact with wild animals or the use of animal products for medicinal or cultural purposes. Spillover events between animal hosts, have posed a recurrent challenge in past outbreaks. Notably, an interspecies transmission occurred at Rotterdam Zoo in 1964, when American giant anteaters and non-human primates housed in close proximity facilitated the transmission of monkeypox virus, marking the first indications of its broad host range [44]. In 2003, an outbreak originating from rodents imported from Ghana to the United States marked the first documented spread of monkeypox virus in the Western Hemisphere [45]. Subsequent transmissions within the United States led to

infections in various animals and 47 documented cases in humans with close contact to infected animals [46].

Despite its initial association with primate hosts, the virus has exhibited a broader host range [47, 48, 49, 50, 51]. Existing studies suggest that there may be no one reservoir; rather, multiple animal species may support monkeypox virus [52]. In Africa, evidence of monkeypox infection has been found in various rodents: rope squirrels (*Funisciurus* spp.), sun squirrels (*Heliosciurus* spp.), giant pouched rats (*Cricetomys* spp.), African dormice (*Graphiurus* spp.), and ground squirrels (*Xerus* spp.) [50, 53]. Notably, scientific studies [36, 54, 55, 56, 57, 58, 59] have spotlighted the *Funisciurus* spp. as potential natural reservoir hosts for monkeypox.

In areas where *Funisciurus* spp. are less common or entirely absent, other species — including incidentally infected wild hosts and captive animals — play a role in sustaining viral prevalence [60]. North American rodents, especially ground squirrels, have demonstrated susceptibility to the virus, indicating a possible pathway for cross-geographic spread [61, 62]. With the high reproductive rate of rodents in North American countries [63, 64], there is a significant resource for virus transmission and circulation. The Centers for Disease Control and Prevention (CDC) has issued a report cautioning about the potential establishment of the monkeypox virus within one or more animal populations in the United States [65].

Recent experimental investigations have shown that animals can be infected with clades Ia, IIa, or IIb of the monkeypox virus, though notable differences in morbidity and viral replication rates have been observed among infected animals [36, 38]. Studies in animals suggest that clade I is more lethal than clade II [36, 37]. Warner and coworkers [36] demonstrated that mice do not succumb to infection with the clade IIb, although they are highly susceptive to clade Ia and IIa and developed fatal disease upon challenge. Further research involving clades Ib and IIb could reshape our understanding of monkeypox infection across animal species, highlighting the need for additional studies.

Animals can acquire monkeypox through multiple routes of transmission, including direct contact with infected animals or their bodily fluids [50, 54]. Primates susceptible to the virus may become infected if virus-carrying small mammals, such as rodents, pass beneath them [66]. Furthermore, studies have shown that the monkeypox virus can persist and remain viable on surfaces or fomites for extended periods, underscoring the potential for indirect transmission [67, 68].

Rosa et al. [36] offered a comprehensive review of the symptoms associated with monkeypox virus infections in animals. Clinical manifestations may include lethargy, reduced appetite, fever, coughing, ocular crusting or clouding, limb swelling due to lymphadenopathy, and the development of a bumpy or blister-like rash [69]. Notably,

species-specific differences are observed. For instance, prairie dogs (*Cynomys ludovicianus*) can shed the virus before the onset of symptoms [36, 70]. Similarly, Gambian pouched rats (*Cricetomys gambianus*) can harbor and shed the virus asymptomatically, as infected individuals often do not exhibit signs of severe disease or become moribund [50]. In *Funisciurus* spp., initial skin lesions typically appear three days post-exposure, with classic poxviral lesions emerging by day six [50].

1.3 Disease Modelling and Literature Review

Population Growth Models

Central to many epidemic models is the assumption of a constant total population, neglecting population demogarphics [71]. This assumption is applicable when examining disease progression over a short time frame. In reality, population growth or decline can significantly influence disease dynamics, potentially altering transmission processes and shaping the course of an epidemic [72, 73]. There are three primary methods for incorporating population growth. A fundamental approach is to assume that both birth and death rates are directly proportional to the population size. Anderson and May [74], Busenberg and van den Driessche [75], and Derrick and van den Driessche [76] proposed that in the absence of the disease, the total population $N(t)$ satisfies

$$\frac{dN(t)}{dt} = (b - d)N,$$

where b is the birth rate and d is the natural death rate. A modification is to assume constant immigration and deaths proportional to the population size, leading the population to approach an equilibrium state. Jacquez et al. [77], Mena-Lorcat and Hethcote [78], and Zhou and Hethcote [79] represented the equation

$$\frac{dN\,(t)}{dt} = A - dN,$$

where A is the recruitment rate. In this model, if the initial populaiton $N_0 < \frac{A}{d}$, the population grows up to the maximum value $\frac{A}{d}$ [78]. Adversely, some epidemiological models incorporate a natural demographic process with restricted growth due to density dependence. Anderson et al. [80], Brauer [81], and Bremermann and Thieme [82] put forward the model

$$\frac{dN\,(t)}{dt} = \Lambda N\left(1 - \frac{N}{K}\right),$$

where Λ is the intrinsic birth rate and K is the maximal carrying capacity. Here, the population initially grows exponentially, eventually stabilizing as it approaches the carrying capacity [83]. Other approaches assume density-dependent death rates to capture population constraints [84, 85].

Deterministic Models

The compartmental model, pioneered by Bernoulli in 1760 [86], Ross in 1911 [87], and Kermack and McKendrick in 1927 [88], has become a cornerstone in studying the transmission dynamics of infectious diseases. Typically, the population is categorized into exclusive classes, including susceptible, exposed, infected, and recovered [74]. The choice of which compartments to include in a model depends on the characteristics of the particular disease being modeled and the purpose of the model [71].

For many infectious diseases prevalent in heterogeneous host populations, it is often more suitable to propose multigroup epidemic models. Ross [87, 89] developed pioneering differential equation models for malaria as a host-vector disease in 1911. Ross's models notably distinguish between the disease progressions within human hosts and mosquito vectors, acknowledging the distinct roles and dynamics each plays within the transmission cycle.

In 1906, Hamer [90] formulated and analyzed a discrete-time model to investigate the recurrence of measles epidemics. His model may have been the first to assume that the incidence depends on the product of the densities of the susceptibles and infectives [71]. Nowadays, disease transmission is typically modeled using functional forms reflecting assumptions of whether the transmission modes are density

dependent or frequency dependent [91, 92]. In density dependent disease transmission, contact rates increase as density increases, therefore disease transmission also increases. Frequency dependent disease transmission occurs when there is no relationship between contact rates and density of a population.

The basic reproduction number (R_0), also known as the basic reproduction ratio or rate or the basic reproductive rate, is an epidemiologic metric used to describe the contagiousness or transmissibility of infectious agents [71, 93, 94, 95]. It is defined as the average of secondary cases generated by a primary infectious individual in a totally susceptible population within its infectious period. An outbreak is expected to continue if $R_0 > 1$ and to end if $R_0 < 1$ [96]. Diekmann et al. [93] introduced a pioneering methodology known as the Next Generation Matrix method, which was later refined and expanded by Van Den Driessche and Watmough [97]. Recently, there has been some discussion regarding the limitations of R_0 [98].

Stochastic Models

McKendrick [99] introduced an early stochastic epidemic model in 1926, establishing a foundational framework for understanding epidemic dynamics from a stochastic perspective. Since then, numerous researchers have further advanced the field of stochastic epidemic modeling [100, 101, 102, 103]. Stochasticity in epidemiological systems is generally classified into two primary types. The first type consists of

external perturbations, which arise from random fluctuations in model parameters due to environmental variability and other external factors [30]. The second type involves intrinsic stochastic processes, where individuals change their status through random chance [104].

Environmental stochasticity leads to random variations in multiple model parameters, including species decay rate, infectious period, recovery rate and transmission rate [30, 105, 106, 107, 108, 109, 110]. A common approach incorporates environmental variability either as additive Gaussian white noise or as multiplicative noise that scales with population density [30, 111]. The use of a linear function of Gaussian white noise is a standard approach in stochastic modeling, as it facilitates the derivation of analytical results [112, 113]. Alternatively, environmental noise can be modeled using a mean-reverting process, often referred to as colored noise [109, 114, 115]. The presence of environmental stochasticity introduces systematic deviations from deterministic system behavior [31, 116]. These deviations can manifest in various ways, including transient phenomena and stochastic bifurcations, which contribute to the emergence of complex dynamics [30, 107, 117, 118, 119, 120, 121, 122, 123, 124].

Demographic stochasticity refers to random fluctuations in population dynamics caused by the discrete and probabilistic nature of individual-level events, such as birth, death, infection, and recovery processes [100, 125]. This phenomenon be-

comes particularly significant in small populations, where the impact of individual events on the overall population is magnified. To systematically incorporate demographic stochasticity into epidemic models, Allen [109, 126, 127, 128] proposed a methodological framework. This approach transitions from a deterministic model to a continuous-time Markov chain (CTMC), capturing the probabilistic nature of processes. The CTMC is then approximated by an Itô stochastic differential equation (SDE), enabling both analytical and numerical exploration of stochastic dynamics. Studies have demonstrated that demographic stochasticity can significantly alter outbreak dynamics and increase the likelihood of disease extinction [104, 109, 127].

Modelling Multi-Host Pathogen Dynamics and Transmission

The ongoing advancement of multivariate modeling frameworks plays a pivotal role in understanding transmission dynamics [2, 128, 129, 130, 131, 132, 133, 134]. By modelling the transmission of vector-borne parasites, prior studies have emphasized the crucial significance of host species diversity in amplifying transmission potential to humans [135, 136, 137, 138, 139]. Craft et al. [140] developed a stochastic model to describe the spatial and temporal dynamics of a pathogen in a spatially structured, multi-host community. The model accounted for host social behaviors and variations in disease transmission rates both within and between host groups. Their findings on multi-host disease dynamics provided a key insight: species characterized by

low neighbor-to-neighbor intraspecific transmission bear the most substantial costs associated with interspecific transmission.

By encompassing data across multiple scales, including ecological interactions, population dynamics, pathogen biology, and host immune responses, predictive frameworks offer a powerful means to efficiently predict the relative importance and risk of spillover events [131, 132, 141, 142]. Childs et al. [129] developed and validated a mechanistic model of pathogen spillover to forecast yellow fever risk among human populations in Brazil. Their study highlighted how the complex ecological interactions among environmental factors, vectors, reservoir hosts, and human populations can serve as reliable predictors of spillover events.

Existing research on monkeypox has primarily focused on studying outbreaks in human populations, employing a deterministic approach [143, 144, 145, 146, 147, 148, 149]. These studies largely emphasize the existence of equilibrium states in epidemic modesl and analyze their stability properties [144, 145, 146, 147, 149], while incorporating additional aspects such as vaccination [144, 148], isolation measures [149], optimal control strategies [143], and parameter sensitivity analyses [148]. Building on these findings, it has been suggested that if monkeypox persists within animal populations and is able to be transmitted to humans, the disease is likely to establish itself as endemic among humans, irrespective of the spillover rate [147, 148, 150].

However, it has been emphasized that an increasing frequency of spillover events may contribute to unexpectedly large outbreaks [22, 151].

Several works have examined the basic reproduction number to better understand and quantify the impacts of spillover events [12, 150, 152, 153, 154, 155, 156]. For instance, Binkley et al. [157] derived a mathematical expression for the basic reproduction number of rabies in Ethiopia based on intra- and interspecies contact rates. They highlighted multiple urban carnivores as key species for rabies maintenance, with hyenas posing the greatest risk due to high intraspecific transmission rates. Bolzoni et al. [158] contributed to the comprehension of pathogen dynamics in multi-host communities, particularly focusing on the SEI model, which considers susceptible, exposed, and infectious stages. Their analyses demonstrated that the basic reproduction number for limit cycles to occur depends on the ratio between host sizes, that the oscillation period in a multi-host community is set by the smaller species dynamics, and that intermediate interspecific disease transmission can stabilize the epidemic occurrence in wildlife communities. The research conducted by Bielby et al. [159] investigated the complexities of amphibian parasite dynamics, focusing on Batrachochytrium dendrobatidis (Bd) and Ranavirus, which infect multiple host species. By studying these parasites within a community of five amphibian species, they unraveled the relative importance of hosts in parasite persistence and

discerned spatial and temporal variations in these patterns.

Indeed, while the thresholds derived in these works provide valuable insights into spillover dynamics of multi-host pathogen, they typically assume bidirectional transmission between reservoir and target hosts. For pathogens unable to spill back into reservoir hosts, such as certain zoonotic diseases, the effects of spillover may not be adequately captured by these thresholds. Furthermore, as discussed by Jesse et al. [160], for homogeneous populations, the basic reproduction number serves as a robust indicator. For metapopulations, defining such an indicator is not straightforward. Consequently, the potential for spillover events to initiate and sustain outbreaks in target host populations warrants deeper investigation.

Recent research has extensively examined novel outbreak thresholds [160, 161, 162, 163, 164, 165, 166, 167, 168, 169]. Roberts and Heesterbeek [170] proposed a refined framework for redefining the basic reproduction number in the context of tuberculosis (TB) transmission among possums, accounting for heterogeneity in host types. Their study demonstrated that the persistence threshold of TB within a given host type is influenced not only by within-group transmission but also by transmission rates among all interacting host types. Building on this foundation, Greenman and Hoyle [171] introduced the pathogen invasion matrix, underscoring its applicability across diverse epidemiological models. Their analysis also provided

critical insights into optimizing culling strategies for effective pathogen control.

There are three primary strategies for managing disease spread in target host populations. In addition to blocking transmission between reservoir and target populations [19, 172], control measures can focus directly on reservoir or target hosts [9, 173]. For example, mass culling of animal hosts remains a key tool for reducing human cases of zoonotic diseases [174, 175, 176, 177]. The effectiveness of culling badgers to prevent the spillover of Mycobacterium bovis, the causative agent of TB, to cattle has been reviewed and discussed in detail [178]. Additionally, vaccination of target hosts has been proposed both as a means of protecting valuable livestock and as an effective method for controlling overall epidemics [179].

Culling Strategies

Culling of wildlife and domestic animals has been implemented as disease control strategy to eradicate infectious diseases [174, 180, 181, 182, 183, 184, 185, 186], especially when vaccination is unavailable or impractical. There are two primary approaches to culling: selective culling [175, 176, 187], which involves removing only infected animals, and mass culling [178, 182], which involves removing entire populations regardless of infection status. The choice of a culling strategy depends on various factors, including the type of reservoir host (wildlife versus domestic animals), the objectives of the control program (eradication versus conservation), and

the practical feasibility of implementation [27, 178]. Gulbudak and Martcheva [182] conducted a comparative analysis of these strategies by modelling per capita culling rates as general functions of the infected population size.

Culling of infected hosts generally has a stronger impact on disease control than mass culling and tends to select for higher virulence within both wildlife and livestock systems [176]. However, in practice, distinguishing between infected and susceptible individuals is often challenging or inefficient. Consequently, mass culling, which indiscriminately targets both susceptible and infected animals, is commonly implemented [173, 174, 183, 185, 188]. Furthermore, if the wildlife reservoir lacks conservation significance, then culling without regard to infection status—even to the point of local extinction—may be an acceptable strategy [178].

The effectiveness of culling in disease control varies depending on model assumptions. While some studies report significant reductions in disease prevalence following culling interventions [173, 178, 183, 184, 189, 190], others suggest that culling may paradoxically increase disease prevalence [189, 191]. Badger culling, in particular, has been highly controversial, as both experimental and modeling studies have produced conflicting results [27, 178]. A possible explanation for this discrepancy is the counterproductive effects of insufficiently severe population reductions. Prentice et al. [189] demonstrated through modelling that when culling fails to significantly

decrease host density, it can enhance disease transmission, ultimately sustaining or even increasing infection levels. Furthermore, culling-induced disturbances can facilitate pathogen spread by increasing host dispersal, as observed in species such as vampire bats (*Desmodus rotundus*) and badgers (*Meles meles*) [192].

Recent studies have improved the understanding of how to design and implement effective culling interventions [193, 194]. Wasserberg et al. [195] developed a deterministic matrix model that incorporated both sex and age structure to evaluate the effectiveness of mass culling. Their model analyzed the outcomes under frequency- and density-dependent incidence, predicting that control efforts are more feasible under density-dependent incidence than frequency-dependent incidence. Gross and Miller [196], employing an individual-based model, concluded that targeted test-and-cull approaches are more effective for disease control than indiscriminate culling strategies. Furthermore, the appropriate combination of recruitment and culling can reduce disease prevalence and sustain this reduction over time, potentially leading to disease eradication [197]. Choisy et al. [198] highlighted that sufficiently high density-dependent recruitment at low host densities can counterbalance population reductions caused by culling interventions.

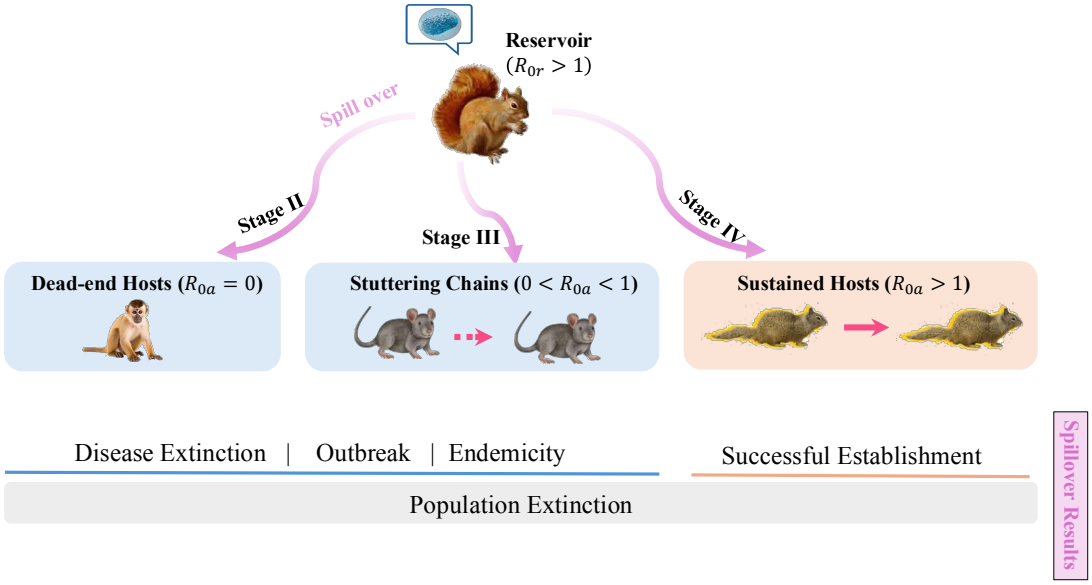

Figure 1.2: Schematic representation of pathogen evolution and spillover outcomes in target hosts. In stage II, target hosts serve as dead-end hosts, where no intraspecific transmission occurs. When intraspecific transmission within target hosts is limited, pathogen evolves to the stage III. Conversely, when significant intraspecific transmission occurs, target hosts are termed sustained hosts, and the pathogen progresses to stage IV. Spillover events in stages II or III may either succeed or fail in triggering epidemic or endemic spread within target hosts. For pathogen in stage IV, successful establishment within target hosts is evident. Additionally, under conditions of strong spillover, target hosts may face extinction. R_{0r} and R_{0a} represent the basic reproduction number in reservoir and target hosts, respectively.

1.4 Objectives of the Dissertation

The primary objective of this dissertation is to examine the consequences of spillover events, with a particular focus on scenarios involving disease eradication, outbreaks, and the sustained presence of multi-host pathogens within target populations. To this end, we develop both epidemic and endemic transmission models for monkeypox. Our analysis explores key factors influencing disease transmission in target hosts, including the basic reproduction number of reservoir hosts, interspecies contacts, and critical stochastic variations. By comparing reservoir control, spillover control, and target control strategies, we aim to provide insights that inform practical intervention measures and applications.

In Chapter 2, we develop a foundational framework for modelling monkeypox transmission within a single host population. Our analysis begins with an investigation of the fundamental properties of the deterministic model, including the existence of a unique endemic equilibrium and its global stability. We then extend the model by incorporating both demographic and environmental stochasticity to assess their respective impacts on the system's dynamic behavior. The global stability of the system under environmental stochasticity is analytically investigated, while numerical methods are employed for further investigation. We first simulate the effects of demographic and environmental noise separately and subsequently compare them

within the hybrid model.

In chapter 3, we develop a minimalist two-species epidemiological framework to model spillover dynamics from reservoir hosts to target hosts during stages II and III. By employing the total number of infections in target hosts as a key epidemiological metric, we derive an outbreak threshold that quantifies spillover results. To evaluate the robustness of this threshold, we perform numerical simulations, including contour plots and sensitivity analysis. The results confirm the feasibility and applicability of the proposed threshold.

In Chapter 4, we extend our model to an endemic context for spillover transmission in stage II, incorporating control strategies aimed at target hosts. Our objective is to assess the spillover impacts on the success or failure of pathogen establishment within target hosts. We identify critical thresholds for disease persistence, maximum endemic prevalence, and potential population extinction in target hosts. Furthermore, the effectiveness of various control measures is systematically evaluated based on the analytical findings.

In Chapter 5, we extend the model developed in Chapter 4 to investigate spillover effects on target hosts during stage III. The extended deterministic framework incorporates an exposed compartment and accounts for intraspecific transmission among target hosts. The threshold conditions derived are compared with the results from the

previous chapter to assess their implications. Furthermore, we introduce stochasticity into the spillover rate to evaluate its impact on system dynamics. Using simulation-based methods, we analyze variations in the stationary distribution of infected target hosts under increasing volatility.

In Chapter 6, we develop a generalized reservoir-to-target transmission model for monkeypox, applicable to stages II through IV. The model is further extended to incorporate quarantine and culling of reservoir hosts, triggered by infections in target hosts. We analyze and compare the equilibrium states and dynamics of the models with and without reservoir control strategies. In particular, we examine the occurrence of higher codimension bifurcations resulting from the interplay between spillover events and the implementation of reservoir control measures.

In chapter 7, we present our conclusions and future works.

2 Demographic and Environmental Stochasticity in Monkeypox Transmission Dynamics

2.1 Introduction

The transmission dynamics of monkeypox virus clade Ia among animal hosts warrant significant attention, as they play a crucial role in facilitating potential spillover events into susceptible populations. Animals such as prairie dogs (*Cynomys ludovicianus*), rope squirrels (*Funisciurus* spp.), and nonhuman primates (*Macaca mulatta*) can shed the virus before showing symptoms. In this chapter, we embark on our investigation by adopting a single host SEIR (S, Susceptible, E, Exposed, I, Infectious and R, Removed) transmission model. By focusing on a single host, we aim to elucidate the effects of demographic and environmental stochasticity on monkeypox transmission dynamics.

The isolation of the monkeypox virus from wild animals has been a rare occur-

rence, documented only twice in history [199]. The first instance occurred in 1985, when the virus was isolated from a moribund Thomas's rope squirrel (*Funisciurus anerythrus*), and the second in 2012, from a deceased sooty mangabey (*Cercocebus anerythrus*) [32, 200]. Squirrels of the *Funisciurus* genus have been identified as the most likely reservoir hosts in endemic regions [32, 36, 55, 56, 59]. Among the species within this genus, five (*F. anerythrus, F. carruthersi, F. congicus, F. lemniscatus,* and *F. pyrropus*) have tested positive for monkeypox virus infection, with *F. anerythrus* emerging as a particularly strong candidate for a primary reservoir [53]. Historical evidence suggests that monkeypox virus has been circulating within *Funisciurus* populations as early as 1899 [53]. The high population densities of *Funisciurus* spp. are considered a key factor in sustaining viral prevalence within the ecosystem [53, 201]. Furthermore, the social behavior of these squirrels, characterized by frequent interactions both within their species and with other animals, likely facilitates virus transmission across various hosts throughout Africa [53].

Infected animals are able to transmit the virus to animals or humans via direct contact [50, 52]. Notably, large mammals exhibit pathological manifestations similar to those observed in human cases. Additionally, the perpetuation of acute viral infections in small mammals is often theorized to necessitate either virus persistence or latency in the host [36, 202]. In *Cercopithecus* spp., initial symptoms, such as fever,

typically appear between 5 and 9 days post-infection [36, 48], before which the virus remains undetectable. Experimental studies indicate that viral shedding occurs between 21 and 27 days post-infection [70, 203, 204]. Notably, *Funisciurus anerythrus* presents with clinical signs including increased respiratory rate, nasal discharge, oral lesions, respiratory distress, weight loss, and marked lethargy, accompanied by prolonged periods of viral shedding [32, 36].

Existing research on the transmission of the monkeypox virus within animal populations has explored various modelling assumptions and methodologies. Madubueze et al. [205] developed a basic SI model to depict the dynamics of animal infections and investigated the impact of environmental transmission on human infection. Majee et al. [148] extended this approach by constructing a SIS model, demonstrating the occurrence of a transcritical bifurcation in the disease dynamics. Additionally, several studies have employed a SIR type model with standard incidence to examine monkeypox transmission within animal populations [145, 146, 147]. Other researchers have built a SEI model to examine the conditions under which the epidemic becomes endemic in both human and animal populations [144, 149, 206, 207]. Notably, all these studies have assumed a constant growth rate of the animal population.

Selective culling, a practice that targets only infected animals, aims to lower the density of infected individuals in a population, thereby reducing the opportunities

for disease transmission [208]. However, in practice, distinguishing between infected and susceptible individuals can be challenging or inefficient [190], leading to the adoption of mass culling, where the culling rate applies equally to both susceptible and infected individuals [173, 174, 183, 185, 188, 209, 210]. In one study investigating monkeypox transmission using a constant culling rate, researchers found that the effectiveness of culling strongly depends on the demographic and epidemiological characteristics of the animal reservoirs involved [174]. Specifically, if reproduction is density-dependent and infection follows frequency-dependent incidence, culling may have the unintended effect of increasing monkeypox transmission among children, highlighting the complex dynamics of disease control in such settings.

Extensive research has examined culling as strategies to control infectious diseases within animal populations. Potapov et al. [197] proposed that a sufficiently high density-dependent recruitment can offset the population reduction caused by culling. They found that the appropriate combination of recruitment and culling levels may significantly decrease disease prevalence and maintain this reduction long enough to potentially achieve eradication. However, other research suggests that population reduction through culling may hinder the evolution of host resistance [183] and result in enhanced disease transmission [189]. Tanner et al. [184] emphasized the narrow threshold between culling levels that could lead to disease eradication and those

that risk population extinction. Additionally, incorporating a saturation function into culling models adds complexity to the system dynamics, potentially resulting in saddle-node, generalized Hopf, and Bogdanov-Takens bifurcations [187].

Demographic stochasticity describes the natural truth that individuals shift status by chance [211, 212, 213]. This stochasticity not only introduces variation in the population size of each state, but also induces systematic deviations from deterministic dynamics [213]. Allen et al. [109, 214, 215] demonstrated that the reproduction number derived from ordinary differential equations (ODE) serves as a threshold for disease extinction in stochastic models that incorporate demographic stochasticity. Consequently, the probability of a disease outbreak can be determined by these stochastic frameworks [175].

Environmental stochasticity encompasses the variations in environmental conditions that lead to models with differing parameter values, such as transmission rate. Randomness in transmission rate arises from multiple influencing factors. For instance, environmental conditions like temperature, humidity, and resource availability can lead to fluctuations in disease transmissibility. Additionally, individual characteristics—such as species-specific traits, immunity levels, and behavioral tendencies—affect both the frequency and intensity of behaviors that facilitate disease spread. Social interactions within animal groups, including dominance hierarchies

and group dynamics, further modulate the timing and occurrence of disease transmission. These factors alter contact likelihood among individuals, infection probabilities, and disease progression pathways.

The threshold of stochastic models in the presence of environmental stochasticity has been a subject of ongoing debate in epidemiological research. Studies by Gray et al. [216], suggested that the basic reproduction number in stochastic differential equation (SDE) models with environmental stochasticity is lower than that in ODE models. This reduction implies that additional noise conditions are required for disease persistence [111, 217, 218]. However, recent findings have challenged this perspective, arguing that the asymptotic behavior of SDE models is governed by the same reproduction number as their deterministic counterparts [219]. Zhu and Hu [220] demonstrated that the reproduction number remains unchanged between SDE and ODE models, while Lahrouz et al. [221] proved that the solution of an SDE model with environmental stochasticity almost surely leads to disease extinction when the reproduction number of the corresponding ODE model is less than one.

Environmental stochasticity has the potential to destabilize disease dynamics by disrupting the persistent coexistence of susceptible and infected populations. Stochastic perturbations may drive infections to extinction [192, 222] or even lead to the collapse of the entire population system [107]. Nevertheless, stochastic models

can exhibit long-term persistence under specific conditions. For instance, Nguyen et al. [111] demonstrated that when the reproduction threshold exceeds one, stochastic solutions may converge to an invariant measure, ensuring the continued presence of the disease. Xu [169] further investigated the global dynamics of a stochastic SIS model originally studied by Gray et al., proposing that environmental stochasticity could exacerbate disease severity. Additionally, stochastic effects may induce transient dynamics, adding complexity to the system's behavior [107]. Despite efforts to develop hybrid models incorporating both demographic and environmental stochasticity [223, 224], a detailed comparison of their roles in shaping disease dynamics remains unexplored.

In our work, we construct an ODE model that incorporates mass quarantine and culling strategies to model the transmission dynamics of monkeypox clade Ia within an animal host population. We begin by analyzing the fundamental properties of the ODE model. Building on this, we formulate a continuous-time Markov chain (CTMC) model and a corresponding SDE model to assess the impact of demographic variability. Subsequently, we develop an alternative SDE model that incorporates time-dependent environmental variability in the transmission rate. By integrating both demographic and environmental stochastic effects, our ultimate objective is to investigate the combined influence of these two types of stochasticity. For our

analysis, we select parameters representative of a hypothetical metropolitan area in an endemic region and conduct numerical simulations. We generate sample paths and probability distributions to illustrate the likelihood of an outbreak under the combined influences of demographic and environmental stochasticity.

2.2 Deterministic Model and Methods

2.2.1 Model

We develop a generalized mathematical model to describe the transmission dynamics of monkeypox virus clade Ia within a suspect animal population. A generalized approach is appropriate, as animal models of clade Ia infection have revealed similar pathology as observed in humans [36, 50]. Considering the presence of a latent phase in certain species, such as prairie dogs (*Cynomys ludovicianus*) and macaque (*Macaca fascicularis*) [36, 50, 70], we divide the total animal population (N) into four distinct classes: susceptible (S), exposed (E), infected (I), and recovered (R), such that $N = S + E + I + R$.

We assume the animal population follows logistic growth with a carrying capacity K and an intrinsic growth rate Λ. Additionally, the population is subjected to mass quarantine and culling at a constant rate c, which further reduces its size [174, 198]. Accordingly, in the absence of disease, the total population N satisfies the following

equation

$$N' = \Lambda N\left(1 - \frac{N}{K}\right) - cN.$$

It is obvious that the population approaches a positive equilibrium $\frac{(\Lambda - c)K}{\Lambda}$ if $c < \Lambda$; otherwise the population will die out as $t \to \infty$ [180]. Hence, we assume $\Lambda > c$ in the following analysis, ensuring that the population approaches a steady state.

We assume newborns are susceptible. Let β denote as the transmission rate among hosts, and we use the frequency-dependent incidence to describe the process by which susceptible animals become infected through interactions with infected individuals. The differential equation for the susceptible hosts yields

$$S' = \Lambda N\left(1 - \frac{N}{K}\right) - \frac{\beta IS}{N} - cS.$$

After a latent period, exposed hosts will develop first symptoms, including fever, diarrhea, headache, sore throat, rash, etc., and become infectious [36, 48, 202]. The rate of change of exposed hosts satisfies the following equation

$$E' = \frac{\beta IS}{N} - \tau E - cE.$$

The number of infected hosts diminishes by recovery at a rate γ [70, 203, 204], disease-induced death at a rate μ [203], and control measures such as quarantine and culling at a rate c [25, 225, 226]. The rate of change of infected hosts satisfies

$$I' = \tau E - \gamma I - \mu I - cI.$$

Incorporating the processes of recovery, quarantine, and culling, the rate of change of recovered hosts satisfies

$$R' = \gamma I - cR.$$

Therefore, the system of equations describing the dynamics of monkeypox infection in an animal host population is given by

$$\begin{cases} S' &= \Lambda N\left(1 - \frac{N}{K}\right) - \frac{\beta IS}{N} - cS, \\ E' &= \frac{\beta IS}{N} - \tau E - cE, \\ I' &= \tau E - \gamma I - \mu I - cI, \\ R' &= \gamma I - cR. \end{cases} \tag{2.1}$$

The descriptions of model variables and parameters are summarised in Table 2.1. Let N_0 denote the initial population size. The initial states of equation (2.1) are $(S_0, E_0, I_0, 0)$, such that $S_0 + E_0 + I_0 = N_0$.

The model (2.1) with $c = 0$ has been explored in [227, 228, 229]. Through comparative analysis, authors discussed that the SEIR model with frequency-dependent incidence does not exhibit periodic solutions, while density-dependent incidence serves as the trigger for Hopf bifurcation in such models [229]. Furthermore, Zhang et al. [84] studied the SIR model with standard incidence and demonstrated that the system stables at the endemic equilibrium when it exists. In the subsequent sections, we analyze the fundamental properties of the model incorporating mass quarantine

and culling strategies.

2.2.2 Disease-Free Equilibrium and the Basic Reproduction Number

System (2.1) always exhibits a disease-free equilibrium $\left(\frac{(\Lambda-c)K}{\Lambda}, 0, 0, 0\right)$, whose stability is determined by the basic reproduction number (denoted as R_0). By employing the Next Generation Matrix approach [97], R_0 yields

$$R_0 = \frac{\beta\tau}{(\tau+c)(\gamma+c+\mu)}.$$

It is observed that an increase in the quarantine and culling rate effectively reduces the basic reproduction number, thereby contributing to disease eradiction.

Theorem 2.2.1. *The disease-free equilibrium* $\left(\frac{(\Lambda-c)K}{\Lambda}, 0, 0, 0\right)$ *of system* (2.1) *is globally stable if* $R_0 \leq 1$.

Proof. Consider the Lyapunov function $V_1 = E + \frac{\tau+c}{\tau} I$, then

$$\frac{dV_1}{dt} = \left[(R_0 - 1)\, S - (E + I + R)\right] \frac{\tau + c}{\tau} (\gamma + c + \mu) \frac{I}{N} \leq 0.$$

The equality holds when $I = 0$. Define the set $S_1 = \left\{(S, E, I, R) : \frac{dV_1}{dt} = 0\right\}$, and M be the largest invariant set within S_1. On the plane S_1, we obtain $E \to 0$, $R \to 0$, $S \to \frac{(\Lambda-c)K}{\Lambda}$ as $t \to +\infty$. It follows from Lyapunov-Lasalle theorem that the disease-free equilibrium is globally stable [230].

□

Table 2.1: Model variables and parameters.

Variables and their initial values		
Notation	**Definition**	**Initial value**
$S(t)$	Number of susceptible hosts on day t	[799.9, 7 998 000]
$E(t)$	Number of exposed hosts on day t	$[0.1, 1\ 000]$
$I(t)$	Number of infected hosts on day t	$[0, 1\ 000]$
$R(t)$	Number of recovered hosts on day t	0
$N(t)$	Number of total host population on day t	[800, 8 000 000]
Parameters for monkeypox transmission		
Notation	**Definition**	**Range**
Λ	Intrinsic birth rate	0.01685
K	Maximal carrying capacity	[800, 8 000 000]
β	Transmission rate	$[0.0505, 0.0514]$
$1/\tau$	Latent period	1/7
c	Quarantine and culling rate	0.0002
μ	Disease-induced death rate	0.0050
γ	Recovery rate	0.0452
σ	Volatility of transmission rate	$[0, 5]$

This theorem emphasize the significance of implementing effective management strategies to reduce the basic reproduction number of animal hosts. By doing so, the risk of disease can be eliminated.

2.2.3 Endemic Equilibrium and Stability

To determine the conditions for the existence of a unique endemic equilibrium in the monkeypox model (2.1), we set the right-hand sides of system (2.1) to zero, resulting in the following expressions

$$S^* = \frac{(\tau + c)(c + \gamma + \mu)}{\beta\tau}, \quad E^* = \frac{(c + \gamma + \mu)\, I}{\tau}, \quad R^* = \frac{\gamma I}{c},$$

$$I^* = \frac{c\,(\tau + c)\,(c + \gamma + \mu)\,(R_0 - 1)}{(\tau c + \gamma\tau + c\,(c + \gamma + \mu))\,\beta} N,$$

$$N^* = \frac{K\left[(((c + \gamma)\,(\tau + c) + c\mu)\Lambda - (c + \gamma + \mu)\,(\tau + c)\,c)\beta + (\tau + c)\,(c + \gamma + \mu)\,c\mu\right]}{\Lambda\beta\,(c^2 + \gamma\tau + c\,(\tau + \gamma + \mu))}.$$

Positivity constraints on the endemic coordinates are required. Thus, we conclude that system (2.1) possesses a unique endemic equilibrium $(S^*, E^*,\ I^*, R^*)$ if the following conditions are met: either

a. $R_0 > 1$ and $\Lambda \geq \frac{(c+\gamma+\mu)(\tau+c)c}{(c+\gamma)(\tau+c)+c\mu}$, or

b. $R_0 > 1$, $\Lambda < \frac{(c+\gamma+\mu)(\tau+c)c}{(c+\gamma)(\tau+c)+c\mu}$, and $\beta < \frac{(\tau+c)(c+\gamma+\mu)c\mu}{\tau\mu\Lambda-(c+\gamma+\mu)(\tau+c)(\Lambda-c)}$.

It is observed that when the birth rate is low and the transmission rate is high, achieving an endemic equilibrium becomes increasingly challenging. In such scenar-

ios, the entire population is at risk of extinction due to insufficient replenishment from new births.

Theorem 2.2.2. *In system* (2.1)*, if the conditions* $\mu < \frac{\Lambda - c}{2}$ *and* $\mu \leq c$ *are satisfied, then the endemic equilibrium exists and is globally stable.*

Proof. Given that system (2.1) admits a unique endemic equilibrium, we analyze its global stability by employing Lyapunov functions in appropriate subspaces. First, if $\{N > N^*, I > I^*\}$, we consider the Lyapunov function

$$V_2 = N - N^* - N^* \ln \frac{N}{N^*}.$$

We compute the time derivative along the solutions of the system as follows

$$\dot{V_2} = \frac{N - N^*}{N} \left(\Lambda N \left(1 - \frac{N}{K} \right) - cN - \mu I \right).$$

Using the relation $\Lambda N^* \left(1 - \frac{N^*}{K}\right) - cN^* - \mu I^* = 0$, we have

$$\begin{aligned} \dot{V_2} &= (N - N^*) \left(\frac{\Lambda}{K} N^* + \frac{\mu I^*}{N^*} - \frac{\Lambda}{K} N - \frac{\mu I}{N} \right) \\ &= \left(-\frac{\Lambda}{K} + \frac{\mu I^*}{N N^*} \right) (N - N^*)^2 - \frac{\mu}{N} (I - I^*) (N - N^*). \end{aligned}$$

Additionally, if $N < \frac{\Lambda - c - \mu}{\Lambda} K$, then the equation of $N(t)$ satisfies

$$\frac{dN(t)}{dt} = \Lambda N \left(1 - \frac{N}{K} \right) - cN - \mu I \geq N \left[\Lambda \left(1 - \frac{N}{K} \right) - c - \mu \right] > 0.$$

This implies that the solution cross the plane $N = \frac{\Lambda-c-\mu}{\Lambda}K$ in finite time and remains above this plane afterwards. Additionally, according to the comparison theorem, the solution satisfies $N^* > \frac{\Lambda-c-\mu}{\Lambda}K$. Therefore, if $\mu < \frac{\Lambda-c}{2}$, we derive

$$-\frac{\Lambda}{K} + \frac{\mu I^*}{NN^*} < -\frac{\Lambda}{K} + \frac{(\Lambda - c)\Lambda}{2(\Lambda - c - \mu)K} < 0.$$

Thus, we obtain $\dot{V}_2 < 0$. Furthermore, condition (a) is satisfied when $\mu < \frac{\Lambda-c}{2}$. Under this condition, the endemic equilibrium is stable in the subspace $\{N > N^*, I > I^*\}$.

Second, if $\{N > N^*, I < I^*, S < S^*\}$, we consider the Lyapunov function

$$V_3 = N - N^* - N^* \ln \frac{N}{N^*} + \frac{\mu}{2N\tau}(I - I^*)^2 + \frac{\mu}{2N\gamma}(R - R^*)^2.$$

We compute the time derivative of the Lyapunov function V_3 along the solutions and by substituting the relation $\Lambda N^*\left(1 - \frac{N^*}{K}\right) - cN^* - \mu I^* = 0$, $\tau E^* - \gamma I^* - cI^* - \mu I^* = 0$, and $\gamma I^* - cR^* = 0$, we obatin

$$\begin{aligned}
\dot{V}_3 &= \left(-\frac{\Lambda}{K} + \frac{\mu I^*}{NN^*}\right)(N - N^*)^2 - \frac{\mu}{N}(I - I^*)^2 - \frac{\mu}{N}(I - I^*)(S - S^*) \\
&\quad -\frac{\mu}{N}(I - I^*)((E - E^*) + (R - R^*)) \\
&\quad +\frac{\mu}{\tau N}(I - I^*)[(\tau E - \tau E^*) + (\gamma + c + \mu)(I^* - I)] \\
&\quad -\frac{\mu}{2\tau N^2}(I - I^*)^2\left[\Lambda N\left(1 - \frac{N}{K}\right) - cN - \mu I\right] \\
&\quad +\frac{\mu}{\gamma N}(R - R^*)[\gamma(I - I^*) + c(R^* - R)] \\
&\quad -\frac{\mu}{2\gamma N^2}(R - R^*)^2\left[\Lambda N\left(1 - \frac{N}{K}\right) - cN - \mu I\right]
\end{aligned}$$

$$
\begin{aligned}
= & \left(-\frac{\Lambda}{K}+\frac{\mu I^*}{NN^*}\right)\left(N-N^*\right)^2-\frac{\mu\Lambda}{2\tau N}\left(1-\frac{N}{K}\right)\left(I-I^*\right)^2 \\
& -\frac{\mu\Lambda}{2\gamma N}\left(1-\frac{N}{K}\right)\left(R^*-R\right)^2-\frac{\mu}{N}\left(I-I^*\right)\left(S-S^*\right) \\
& -\frac{\mu}{N}\left[1+\frac{\gamma+c+\mu}{\tau}-\frac{c}{2\tau}-\frac{\mu I}{2\tau N}\right]\left(I-I^*\right)^2 \\
& -\frac{\mu}{2\gamma N}\left(c-\frac{\mu I}{N}\right)\left(R-R^*\right)^2.
\end{aligned}
$$

If $\mu \leq c$, then the following inequalities hold

$$
1+\frac{\gamma+c+\mu}{\tau}-\frac{c}{2\tau}-\frac{\mu I}{2\tau N}>0, \quad c-\frac{\mu I}{N}>0.
$$

Therefore, the derivative $\dot{V}_3 < 0$, and the endemic equilibrium is stable in the subspace $\{N > N^*, I < I^*, S < S^*\}$ given that $\mu < \frac{\Lambda - c}{2}$ and $\mu \leq c$.

Third, if $\{N > N^*, I < I^*, S > S^*\}$, we consider the Lyapunov function

$$
V_4=\int_{S^*}^{S} 1-\frac{f\left(S^*, I^*\right)}{f\left(u, I^*\right)} du+E-E^*-E^* \ln \frac{E}{E^*}+\frac{\tau+c}{\tau}\left(I-I^*-I^* \ln \frac{I}{I^*}\right),
$$

where $f(S, I) = \frac{\beta I S}{N}$. It is obvious that the function $f(S, I)$ is strictly increasing with respect to S for any fixed $I > 0$. The time derivative of V_4 along the solutions is given by

$$
\begin{gathered}
\frac{dV_4}{dt}=\left[1-\frac{f\left(S^*, I^*\right)}{f\left(S, I^*\right)}\right]\left[\Lambda N\left(1-\frac{N}{K}\right)-f\left(S, I\right)-cS\right]+\left(1-\frac{E^*}{E}\right)\left[f\left(S, I\right)-(\tau+c) E\right] \\
+\frac{\tau+c}{\tau}\left(1-\frac{I^*}{I}\right)\left[\tau E-(\gamma+c+\mu) I\right].
\end{gathered}
$$

Since (S^*, E^*, I^*, R^*) represents the endemic equilibrium of the system, we have

$$
\frac{dV_4}{dt} = \left(1-\frac{f\left(S^*, I^*\right)}{f\left(S, I^*\right)}\right)\left(\Lambda \mathrm{N}\left(1-\frac{N}{K}\right)-\Lambda N^*\left(1-\frac{N^*}{K}\right)-cS+cS^*\right)
$$

$$
\begin{aligned}
&+\left(1-\frac{f\left(S^{*},I^{*}\right)}{f\left(S,I^{*}\right)}\right)\left(f\left(S^{*},I^{*}\right)-f\left(S,I\right)\right)\\
&+f\left(S^{*},I^{*}\right)\left(\frac{f\left(S,I\right)}{f\left(S^{*},I^{*}\right)}-\frac{I^{*}E}{E^{*}I}-\frac{E^{*}f\left(S,I\right)}{Ef\left(S^{*},I^{*}\right)}-\frac{\left(\gamma+c+\mu\right)I}{\tau E^{*}}+2\right)\\
=\;&\Lambda\left(1-\frac{f\left(S^{*},I^{*}\right)}{f\left(S,I^{*}\right)}\right)\left(N-N^{*}\right)\left(1-\frac{N+N^{*}}{K}\right)\\
&-c\left(1-\frac{f\left(S^{*},I^{*}\right)}{f\left(S,I^{*}\right)}\right)\left(S-S^{*}\right)+f\left(S^{*},I^{*}\right)\left(3-\frac{f\left(S^{*},I^{*}\right)}{f\left(S,I^{*}\right)}+\frac{f\left(S,I\right)}{f\left(S,I^{*}\right)}\right)\\
&+f\left(S^{*},I^{*}\right)\left(-\frac{I^{*}E}{E^{*}I}-\frac{E^{*}f\left(S,I\right)}{Ef\left(S^{*},I^{*}\right)}-\frac{\left(\gamma+c+\mu\right)I}{\tau E^{*}}\right).
\end{aligned}
$$

According to [84], if $\mu<\frac{\Lambda}{2}$, then $1-\frac{N+N^{*}}{K}<0$. Furthermore, defining the function $g\left(x\right)=1-x+\ln x$, we obtain

$$
4-\frac{f\left(S^{*},I^{*}\right)}{f\left(S,I^{*}\right)}-\frac{I^{*}E}{E^{*}I}-\frac{E^{*}f\left(S,I\right)}{Ef\left(S^{*},I^{*}\right)}-\frac{If\left(S,I^{*}\right)}{I^{*}f\left(S,I\right)} \tag{2.2}
$$

$$
=g\left(\frac{f\left(S^{*},I^{*}\right)}{f\left(S,I^{*}\right)}\right)+g\left(\frac{I^{*}E}{E^{*}I}\right)+g\left(\frac{E^{*}f\left(S,I\right)}{Ef\left(S^{*},I^{*}\right)}\right)+g\left(\frac{If\left(S,I^{*}\right)}{I^{*}f\left(S,I\right)}\right)\leq 0. \tag{2.3}
$$

One can verify that

$$
\frac{If\left(S,I^{*}\right)}{I^{*}f\left(S,I\right)}+\frac{f\left(S,I\right)}{f\left(S,I^{*}\right)}-\frac{I}{I^{*}}-1=\left(\frac{I}{I^{*}}-\frac{f\left(S,I\right)}{f\left(S,I^{*}\right)}\right)\left(\frac{f\left(S,I^{*}\right)}{f\left(S,I\right)}-1\right)=0, \tag{2.4}
$$

$$
\frac{I}{I^{*}}-\frac{\left(\gamma+c+\mu\right)I}{\tau E^{*}}=0. \tag{2.5}
$$

By summing equations (2.2)-(2.5), we obtain $\frac{dV_{4}}{dt}<0$. Thus, the endemic equilibrium is stable in the subspace $\{N>N^{*},I<I^{*},S>S^{*}\}$ given that $\mu<\frac{\Lambda-c}{2}$ and $\mu\leq c$.

On the other hand, for the case where $\{N<N^{*}\}$, it can be verified that the endemic equilibrium remains stable if $\mu<\frac{\Lambda-c}{2}$ and $\mu\leq c$. The detailed proof is omitted for brevity. □

We observe that while Theorem (2.2.2) imposes constraints on the disease-induced death rate to ensure global stability, it is not a necessary condition.

2.3 Stochastic Models and Methods

2.3.1 Demographic Stochasticity

We extend the ODE model by incorporating demographic variability to gain insights into its impact on the likelihood of disease outbreaks. To achieve this, we first derive a CTMC model. We use the same notation for the discrete random variables in the CTMC model as in the ODE model; specifically, $X = (S, E, I, R)$ represents the state vector of the population, and $\Delta X = (\Delta S, \Delta E, \Delta I, \Delta R)$ represents the change in population over a short time interval Δt. There are eight possible types of changes, with only one occurring between any of the four compartments during a small Δt. The probability of each transition is given by the product of its transition rate and the time Δt. Table 2.2 summarizes all possible transitions among the four compartments along with their respective probabilities.

As $\Delta t \to 0$ in the transition probabilities in Table 2.2, an approximation to an *Îto* SDE model with continuous variables can be derived as

$$dX(t) = F(X(t), t)\, dt + G(X(t), t)\, d\widetilde{W}(t),$$

where $\widetilde{W}(t)$ represents a vector of independent Wiener processes. The drift vector $F(X(t),\ t)$ with dimensions 4×1, corresponds to the rates defined in the ODE model. The diffusion matrix G is a 4×8 matrix, where 4 represents the number of random variables and 8 corresponds to the number of events [211, 231, 232]. The diffusion matrix satisfies $G(t)G(t)^T = Cov(t)$, where $Cov(t)$ denotes the covariance matrix of the corresponding CTMC.

$$G = \begin{bmatrix} \sqrt{\Lambda \mathrm{N}\left(1-\frac{N}{K}\right)} & -\sqrt{\frac{\beta IS}{N}} & -\sqrt{cS} & 0 & 0 & 0 & 0 & 0 \\ 0 & \sqrt{\frac{\beta IS}{N}} & 0 & -\sqrt{\tau E} & -\sqrt{cE} & 0 & 0 & 0 \\ 0 & 0 & 0 & \sqrt{\tau E} & 0 & -\sqrt{\gamma I} & -\sqrt{(c+\mu)\, I} & 0 \\ 0 & 0 & 0 & 0 & 0 & \sqrt{\gamma I} & 0 & -\sqrt{cR} \end{bmatrix}.$$

The explicit $\hat{I}to$ SDE model with demographic stochasticity yields

$$\begin{cases} dS &= \Lambda \mathrm{N}\left(1-\frac{N}{K}\right) dt - \frac{\beta IS}{N} dt - cSdt + \sqrt{\Lambda \mathrm{N}\left(1-\frac{N}{K}\right)} dW_1(t) \\ & \quad -\sqrt{\frac{\beta IS}{N}} dW_2(t) - \sqrt{cS} dW_3(t), \\ dE &= \frac{\beta IS}{N} dt - \tau Edt - cEdt + \sqrt{\frac{\beta IS}{N}} dW_2(t) - \sqrt{\tau E} dW_4(t) - \sqrt{cE} W_5(t), \\ dI &= \tau Edt - \gamma Idt - cIdt - \mu Idt + \sqrt{\tau E} dW_4(t) \\ & \quad -\sqrt{\gamma I} dW_6(t) - \sqrt{(c+\mu)\, I} dW_7(t), \\ dR &= \gamma Idt - cRdt + \sqrt{\gamma I} dW_6(t) - \sqrt{cR} dW_8(t). \end{cases} \tag{2.6}$$

Previous research has demonstrated consistency between the outcomes of the CTMC model and the corresponding approximated $\hat{I}$to SDE model (2.6) in scenarios with large

population sizes [109, 223, 224]. Given the computational efficiency of the SDE model with demographic variability [223], we employ this framework to analyze the effects of demographic stochasticity.

To further extend the model, we incorporate environmental variability in the transmission rate, capturing fluctuations in disease transmission due to external factors. Ultimately, a hybrid model is constructed by integrating both demographic and environmental stochasticity.

Table 2.2: Possible changes of X during the time Δt for the CTMC model.

Possible change	**Probability**
$[+1, 0, 0, 0]$	$\Lambda N \left(1 - \frac{N}{K}\right) \Delta t$
$[-1, +1, 0, 0]$	$\frac{\beta IS}{N} \Delta t$
$[-1, 0, 0, 0]$	$cS\Delta t$
$[0, -1, +1, 0]$	$\tau E \Delta t$
$[0, -1, 0, 0]$	$cE\Delta t$
$[0, 0, -1, +1]$	$\gamma I \Delta t$
$[0, 0, -1, 0]$	$(c + \mu) I \Delta t$
$[0, 0, 0, -1]$	$cR\Delta t$

2.3.2 Environmental Stochasticity

Contacts within animal hosts are influenced by environmental factors, particularly seasonal variations in temperature, humidity, and rainfall, which affect food availability and habitat conditions [233]. Additionally, viral mutations occur randomly, introducing stochasticity to the probability of infection. These sources of randomness are encapsulated in a stochastic transmission rate β, which becomes a time-dependent random variable $\hat{\beta}(t)$. A commonly used approach for modelling environmental variability is to express it as a linear function of Gaussian white noise [216, 234]. Specifically, we represent the random variable as

$$\hat{\beta}(t)dt = \beta dt + \sigma dW,$$

where σ is the noise volatility, and $W(t)$ is a one-dimensional Wiener process. This formulation gives the mean $E\left[\hat{\beta}(t)\,dt\right] = \beta dt$ and the variance $var\left[\hat{\beta}(t)\,dt\right] = \sigma^2 dt$. Consequently, incorporating environmental variability in the transmission rate leads to an alternative *Itô* SDE model of the form

$$\begin{cases} dS &= \Lambda \mathrm{N}\left(1-\frac{N}{K}\right)dt - \frac{\beta IS}{N}dt - cSdt - \frac{\sigma IS}{N}dW(t), \\ dE &= \frac{\beta IS}{N}dt - \tau Edt - cEdt + \frac{\sigma IS}{N}dW(t), \\ dI &= \tau Edt - \gamma Idt - cIdt - \mu Idt, \\ dR &= \gamma Idt - cRdt. \end{cases} \tag{2.7}$$

In the following analysis, we investigate the dynamic behavior of the SDE model (2.7).

We begin by establishing the global existence and positivity of solutions to ensure that the model remains biologically meaningful under stochastic fluctuations.

Proposition 2.3.1. *For any given initial values* $(S_0, E_0, I_0, 0)$ *satisfying* $S_0 + E_0 + I_0 = N_0 < K$*, there exists a local solution to system* (2.7) *such that* $N(t) < K$ *almost surely.*

Proof. For system (2.7), the functions on the right-hand side satisfy the locally Lipschitz condition, ensuring the existence of a unique local solution. Let $S_0 + E_0 + I_0 < K$. Using the $Itô$ formula, we derive the equation for $N(t)$, which yields

$$dN(t) = \Lambda N\left(1 - \frac{N}{K}\right)dt - cNdt - \mu Idt. \tag{2.8}$$

For all $0 \leq s \leq t$, we obtain the following inequality almost surely (a.s.)

$$dN(s) < \Lambda N\left(1 - \frac{N}{K}\right)ds - cNds, \qquad a.s.$$

This inequality ensures that $N(t)$ remains bounded almost surely [221]. Consequently, we conclude that

$$S(s), E(s), I(s), R(s) \in (0, K) \quad for\ all\ s \in [0, t], \qquad a.s.$$

Thus, the solutions remain within biologically feasible bounds almost surely, completing the proof. □

Theorem 2.3.2. *For any given initial value* $(S_0, E_0, I_0, 0)$ *satisfying* $S_0+E_0+I_0 = N_0 < K$*, the system* (2.7) *has a unique positive solution* $(S(t), E(t), I(t), R(t)) \in \mathbb{R}^4_+$ *almost surly.*

Proof. Suppose that there exists a unique solution $(S(t), E(t), I(t), R(t))$ on $t \in [0, \tau_e)$, where τ_e is the explosion time. We now proof that the solution is global. Let $m_0 > K$ be sufficiently large, such that $\frac{1}{m_0} < N_0 < m_0$. For any integer $m > m_0$, define the stopping time

$$\tau_m = \inf\left\{t \in [0, \tau_e),\ N(t) \notin \left(\frac{1}{m}, m\right)\right\}.$$

It is clear that τ_m is an increasing sequence as $m \to \infty$. Let $\tau_\infty = \lim_{m\to\infty} \tau_m$, so that $\tau_\infty \leq \tau_e$. To establish the global existence of the solution, we need to prove that $\tau_\infty = \infty$. Suppose, for contradiction, that this statement is false. Then there exist constants T and $\varepsilon \in (0, 1)$, such that

$$\mathbb{P}\{\tau_\infty \leq T\} > \varepsilon.$$

Moreover, there is an integer $m_1 \geq m_0$ such that

$$\mathbb{P}\{\tau_m \leq T\} \geq \varepsilon,\ \forall m \geq m_1.$$

Consider a C^2-function $V : \mathbb{R}^4_+ \to \mathbb{R}_+$, defined by

$$V = S(t) - \ln S(t) + E(t) + K - \ln(E(t) + K) + I(t) - \ln I(t) + R(t) - \ln R(t).$$

The non-negativity of V holds. By applying the *Îto* formula [113], we obtain

$$dV = LVdt - \left(1 - \frac{1}{S}\right)\frac{\sigma IS}{N}dW(t) + \left(1 - \frac{1}{K+E}\right)\frac{\sigma IS}{N}dW(t), \tag{2.9}$$

where

$$\begin{aligned}
LV &= \left(1-\frac{1}{S}\right)\left[\Lambda \mathrm{N}\left(1-\frac{N}{K}\right)-\frac{\beta IS}{N}-cS\right]+\frac{\sigma^2 I^2}{2N^2}+\frac{\sigma^2 I^2 S^2}{2\left(K+E\right)^2 N^2} \\
&\quad +\left(1-\frac{1}{I}\right)\left(\tau E-\gamma I-cI-\mu I\right)+\left(1-\frac{1}{R}\right)\left(\gamma I-cR\right) \\
&\quad +\left(1-\frac{1}{K+E}\right)\left(\frac{\beta IS}{N}-\tau E-cE\right) \\
&= \Lambda N\left(1-\frac{N}{K}\right)-cN-\mu I-\frac{\Lambda N}{S}\left(1-\frac{N}{K}\right)+\frac{\beta I}{N}+3c-\frac{\tau E}{I}+\gamma+\mu-\frac{\gamma I}{R} \\
&\quad -\frac{\beta IS}{N\left(K+E\right)}+\frac{\left(\tau+c\right)E}{K+E}+\frac{\sigma^2 I^2}{2N^2}+\frac{\sigma^2 I^2 S^2}{2\left(K+E\right)^2 N^2} \\
&\quad \leq \Lambda K+\beta+\tau+\gamma+\mu+4c+\sigma^2 \triangleq f_0.
\end{aligned}$$

By integrating both sides of equation (2.9) and taking expectations, we have

$$\mathbb{E}V\left(S\left(t\wedge\tau_m\right),\ E\left(t\wedge\tau_m\right),I\left(t\wedge\tau_m\right),R\left(t\wedge\tau_m\right)\right)\leq \mathbb{E}V\left(S_0,\ E_0,I_0,R_0\right)+f_0 T. \quad (2.10)$$

Define the set $\Omega_m=\{\tau_m\leq T\}$ for $m\geq m_1$, which gives $\mathbb{P}\{\Omega_m\}\geq\varepsilon$. Note that for every $\omega\in\Omega_m$, the value of at least one of the components $S\left(t\wedge\tau_m\right),\ E\left(t\wedge\tau_m\right),I\left(t\wedge\tau_m\right)$, $R\left(t\wedge\tau_m\right)$ is either $\frac{1}{m}$ or m, and hence

$$\begin{aligned}
&V\left(S\left(t\wedge\tau_m\right),\ E\left(t\wedge\tau_m\right),I\left(t\wedge\tau_m\right),R\left(t\wedge\tau_m\right)\right) \\
&\geq \left(\frac{1}{m}-\ln\frac{1}{m}\right)\wedge\left(m-\ln m\right)\wedge\left(\frac{1}{m}+K-\ln\left(\frac{1}{m}+K\right)\right)\wedge\left(m+K-\ln\left(m+K\right)\right).
\end{aligned}$$

This implies that

$$\mathbb{E}\left(1_{\Omega_m}V\left(S\left(t\wedge\tau_m\right),\ E\left(t\wedge\tau_m\right),I\left(t\wedge\tau_m\right),R\left(t\wedge\tau_m\right)\right)\right) \quad (2.11)$$

$$\geq\varepsilon\left[\left(\frac{1}{m}-\ln\frac{1}{m}\right)\wedge\left(m-\ln m\right)\wedge\left(\frac{1}{m}+K-\ln\left(\frac{1}{m}+K\right)\right)\right]. \quad (2.12)$$

Taking the limit as $m \to \infty$ in equations (2.10)-(2.12), we obtain

$$\infty > \mathbb{E}V\left(S_0,\ E_0, I_0, R_0\right) + f_0 T = \infty,$$

which leads to a contraction. Therefore, we conclude that $\tau_e = \infty$. This completes the proof. □

Global Stochastic Stability

Indeed, the stochastic system (2.7) shares the same disease-free equilibrium, i.e. $\left(\frac{(\Lambda-c)K}{\Lambda}, 0, 0, 0\right)$, as its deterministic counterpart. Lahrouz et al. [221] listed definitions of stochastic stability. Following their approach, we establish the global stochastic stability of the disease-free equilibrium.

Theorem 2.3.3. *If $R_0 < 1$, then the stochastic system* (2.7) *converges almost surely exponentially to the diseases-free equilibrium* $\left(\frac{(\Lambda-c)K}{\Lambda}, 0, 0, 0\right)$.

Proof. Let $\omega > 0$ be chosen such that

$$\frac{\tau}{\tau + c} < \omega < \min\left\{\frac{c+\mu}{\beta}, 1\right\}.$$

Applying the $\hat{I}to$ formula, we calculate the derivative along the solutions

$$\begin{aligned} d\ln\left(\omega E + I + R\right) &= \frac{\omega}{\omega E + I + R}\left(\frac{\beta IS}{N} - \tau E - cE\right)dt + \frac{1}{\omega E + I + R}\left(\gamma I - cR\right)dt \\ &\quad + \frac{1}{\omega E + I + R}\left(\tau E - \gamma I - cI - \mu I\right)dt \\ &\quad - \frac{\left(\omega\sigma IS\right)^2}{2\left(\omega E + I + R\right)^2 N^2}dt + \frac{\omega\sigma IS}{\left(\omega E + I + R\right)N}dW\left(t\right) \\ &< \frac{1}{\omega E + I + R}\left\{-\left(-\omega\beta + c + \mu\right)I - \left[\omega\left(\tau + c\right) - \tau\right]E - cR\right\}dt \\ &\quad + \frac{\omega\sigma IS}{\omega E + I + R}dW\left(t\right) \end{aligned}$$

$$< \quad -\varpi dt + \frac{\omega\sigma IS}{(\omega E + I + R)\, N} dW\,(t)\,,$$

where $\varpi = \min\{-\omega\beta + c + \mu, \omega\,(\tau + c) - \tau\}$. By integrating both side, we obtain

$$\ln(\omega E + I + R) < \ln(\omega E\,(0) + I\,(0) + R\,(0)) - \varpi t + \int_0^t \frac{\omega\sigma IS}{(\omega E + I + R)\, N} dW\,(t).$$

According to the strong law of large number for local martingales [235], we obtain

$$\lim_{t\to\infty} \frac{1}{t} \int_0^t \frac{\sigma IS}{(\omega E + I + R)\, N} dW\,(t) = 0, a.s.$$

Thus, we deduce that

$$\lim_{t\to\infty} \sup \frac{1}{t} \ln(\omega E + I + R) < -\varpi < 0, \quad a.s.$$

This implies that all the coordinates E, I, and R in system (2.7) converge almost surely exponentially to zero. □

In contrast to the deterministic system, the stochastic system (2.7) does not possess an endemic equilibrium. However, system (2.7) can be viewed as a perturbed version of the deterministic model (2.1). Therefore, we investigate the behavior of solutions of the SDE system around the endemic equilibrium of the deterministic model [220].

Theorem 2.3.4. *If $R_0 > 1$ and $\mu \leq min\{\frac{\Lambda - c}{2}, c\}$, then the solutions of SDE system* (2.7) *satisfy*

$$\lim_{t\to\infty} \sup \frac{1}{t} \int_0^t \left(\frac{\Lambda}{K} - \frac{\mu I^*}{NN^*}\right)(N - N^*)^2 + \frac{\mu}{N}(I - I^*)(N - N^*)\, dt \leq \sigma^2 N^*,$$

where $N^* = S^* + E^* + I^* + R^*$ represents the endemic equilibrium of the ODE system (2.1).

Proof. Based on Theorem (2.2.2), the ODE system asymptotically stabilizes at the endemic equilibrium. We further analyze the behavior of the corresponding SDE around the equilibrium. To this end, we define the Lyapunov function as

$$V_7 = N - N^* - N^* \ln \frac{N}{N^*}.$$

The derivative of V_7 along the solution of the SDE system (2.7) is given by

$$dV_7 = \left(-\frac{\Lambda}{K} + \frac{\mu I^*}{NN^*}\right)(N - N^*)^2\, dt - \frac{\mu}{N}(I - I^*)(N - N^*)\, dt + \sigma^2 N^* \frac{S^2 I^2}{N^4} dt. \quad (2.13)$$

By integrating equation (2.13) and dividing by t, we obtain

$$\frac{V_7}{t} - \frac{V_7(0)}{t} < \frac{1}{t}\int_0^t \left(-\frac{\Lambda}{K} + \frac{\mu I^*}{NN^*}\right)(N - N^*)^2 dt - \frac{1}{t}\int_0^t \frac{\mu}{N}(I - I^*)(N - N^*) dt + \sigma^2 N^* \frac{S^2 I^2}{N^4}.$$

In Theorem (2.2.2), we demonstrate that the inequality $\frac{\Lambda}{K} - \frac{\mu I^*}{NN^*} > 0$ holds if $\mu < \frac{\Lambda - c}{2}$. Taking the limit as $t \to \infty$ and considering the supremum, the solution of SDE (2.7) satisfies

$$\limsup_{t\to\infty} \frac{1}{t}\int_0^t \left(\frac{\Lambda}{K} - \frac{\mu I^*}{NN^*}\right)(N - N^*)^2 + \frac{\mu}{N}(I - I^*)(N - N^*) dt \leq \sigma^2 N^*.$$

□

Based on the conditions stated, if the ODE system stabilizes at the endemic equilibrium, the SDE model with environmental stochasticity (2.7) is expected to oscillate around the endemic equilibrium under the influence of weak noise [220]. It is important to note that for this stability to hold, the disease-induced death rate must remain within a limited range.

By incorporating both the demographic and environmental stochasticity, our hybrid SDE model is expressed as

$$\begin{cases} dS &= \Lambda \mathrm{N}\left(1-\frac{N}{K}\right)dt - \frac{\hat{\beta} IS}{N}dt - cSdt + \sqrt{\Lambda \mathrm{N}\left(1-\frac{N}{K}\right)}dW_1(t) \\ & \quad -\sqrt{\frac{\hat{\beta} IS}{N}}dW_2(t) - \sqrt{cS}dW_3(t), \\ dE &= \frac{\hat{\beta} IS}{N}dt - \tau Edt - cEdt + \sqrt{\frac{\hat{\beta} IS}{N}}dW_2(t) - \sqrt{\tau E}dW_4(t) - \sqrt{cE}W_5(t), \\ dI &= \tau Edt - \gamma Idt - cIdt - \mu Idt + \sqrt{\tau E}dW_4(t) - \sqrt{\gamma I}dW_6(t) - \sqrt{(c+\mu)I}dW_7(t), \\ dR &= Idt - cRdt + \sqrt{\gamma I}dW_6(t) - \sqrt{cR}dW_8(t), \\ \hat{\beta}dt &= \beta dt + \sigma dW(t). \end{cases} \tag{2.14}$$

The hybrid model (2.14) represents a time-nonhomogeneous SDE that accounts for environmental heterogeneity in the transmission rate [224]. In the following section, we perform simulations of the SDE models, initially investigating the effects of demographic and environmental stochasticity independently, followed by an analysis of the hybrid model (2.14). The simulations are conducted using the Euler-Maruyama method in MATLAB (R2022b) [236], and the figures are generated using DataGraph [237].

For models that incorporate demographic stochasticity, minor adjustments to transition probabilities are applied to preserve non-negativity in simulations, using the methodology described in [109]. For models with environmental stochasticity, a logarithmic transformation of the transmission rate is employed to ensure positivity of transmission rate.

2.4 Results

2.4.1 Demographic Stochasticity and the Probability of Extinction

To examine the influence of demographic stochasticity on the dynamics of disease outbreaks, we analyze the behavior of the SDE model (2.6). In Figures 2.1a-2.1b, the basic reproduction number R_0 is set marginally above one, whereas in Figure 2.1c, R_0 assumes a moderate value. The initial conditions vary across simulations, with Figure 2.1b representing a scenario of high initial infection levels, while Figures 2.1a and 2.1c correspond to cases with low initial infection levels. A total of 800 simulations are conducted over a time span of $t = 150\ 000$. To illustrate the results, we generate both the probability distribution at the final time point and sample paths of infected animal hosts.

When R_0 is slightly above 1, the ODE model stabilizes at an endemic equilibrium with approximately 156 infected individuals. In contrast, the SDE model tends to exhibit low levels of infection (Figures 2.1a-2.1b). As R_0 increases to a moderate level, the ODE model stabilizes at approximately 4 000 infected individuals (Figure 2.1c), whereas the SDE model exhibits a higher likelihood of experiencing significant outbreaks. Furthermore, the estimated probability of disease extinction for the scenarios shown in Figures 2.1a-2.1c is 0.16, 0.0575, and 0.0075, respectively. These values indicate a decreasing probability of disease extinction as either the initial infection level or R_0 increases.

2.4.2 Environmental Stochasticity and Transient Dynamics in Disease Outbreaks

In Figure 2.2, we present effects of environmental stochasticity in system (2.7), where the basic reproduction number R_0 is set to 1.015. We plot sample paths of the number of infected animals over time under varing levels of volatility. In the ODE model, the solution remain near the x-axis before eventually converging to an endemic equilibrium. When environmental noise is introduced, the dispersion of random trajectories around this equilibrium increases, leading to higher peaks and an elevated mean endemic level. Additionally, Figure 2.2 further corroborates our theoretical findings in Theorem 2.3.4. Furthermore, the duration spent near the x-axis is reduced, highlighting the significant role of environmental fluctuations in modulating the transient phase dynamics.

2.4.3 Combined Effects of Demographic and Environmental Stochasticity in the Hybrid Model

To examine the combined impacts of demographic and environmental stochasticity, we conduct simulations of the hybrid model (2.14) across varying levels of volatility. A total of 800 simulations are performed over a time span of $t = 150\,000$ to examine the distribution of infected animals. Both boxplots and sample paths are generated to illustrate the outcomes.

For a small population size, the distribution of infected animals exhibits only minor changes under different levels of noise volatility (Figure 2.3a). Additionally, the probability

of disease extinction at increasing levels of volatility is 0.69, 0.6775, 0.6925, and 0.6825, respectively.

For a moderate population size, both forms of stochasticity play a crucial role. Demographic variation contributes to a higher probability of low infection levels, while environmental stochasticity amplifies the number of infections (Figure 2.3b). Furthermore, the probability of disease extinction under varying levels of volatility is 0.26, 0.2375, 0.255, and 0.225, respectively. In this scenario, the hybrid model may exhibit transient dynamics under conditions of strong volatility (Figure 2.3c).

For a large population size, the probability of low infection levels declines significantly with volatility (Figure 2.3b), indicating that environmental stochasticity plays a dominant role in shaping disease dynamics. The probability of disease extinction under increasing levels of volatility is 0.1625, 0.0525, 0.04375, and 0.01375, respectively.

2.5 Conclusions

Deterministic and stochastic models have been essential in understanding disease dynamics and assessing outbreak risks. In this study, we developed an SEIR model specifically applied for monkeypox transmission within a single host animal population, incorporating logistic growth dynamics and intervention strategies such as mass quarantine and culling. We further developed and analyzed a SDE model that account for both demographic and environmental stochasticity. Our analysis demonstrates that introducing internal stochastic

variation within state variables and external noise in the transmission rate can significantly alter dynamic behaviors of the system.

Our deterministic analysis illustrates that increasing the quarantine and culling rate effectively reduces the basic reproduction number, thereby facilitating disease eradication [189]. However, inappropriate implementation of control measures may lead to unintended consequences, including the potential extinction of the host population [178, 238].

In the stochastic model with demographic stochasticity, the basic reproduction number of the deterministic model serves as a critical threshold. Unlike their deterministic counterparts, stochastic disease outbreaks occur with probabilities influenced by the initial fraction of infected individuals and the R_0 value [109, 239]. As R_0 significantly exceeds one, the likelihood of disease persistence rises.

Analytical and numerical studies indicate that when the deterministic model stabilizes at its endemic equilibrium, the stochastic model subjected to weak environmental noise exhibits oscillatory behavior around this equilibrium. In the presence of significant noise, prior studies have shown that infected and recovered populations eventually decline to extinction, even when $R_0 > 1$ [107, 222]. However, our simulations suggest that outbreaks can still occur under these conditions [169]. Furthermore, we confirmed that environmental noise amplifies outbreaks, increasing both peak infection levels and endemic prevalence, while shortening the duration of transient dynamics [30, 223].

In the above single-stochasticity model, it is evident that the two types of noise exert opposing effects on disease dynamics. Specifically, demographic stochasticity triggers the

likelihood of disease extinction, whereas environmental fluctuations in the transmission rate tend to amplify disease outbreaks. This contrast raises a fundamental question: how does the system behave when both sources of stochasticity act simultaneously? Our results from the hybrid model reveal a population-size-dependent shift in the relative influence of these two sources of stochasticity. In small populations, demographic stochasticity emerges as the dominant driver of disease dynamics. Conversely, in large populations, environmental stochasticity exerts a greater impact, outweighing the effects of demographic fluctuations [240].

Our study underscores the importance of incorporating stochastic effects when designing strategies to control monkeypox transmission. Effective disease management requires not only reducing the basic reproduction number but also accounting for both intrinsic and extrinsic stochastic fluctuations to mitigate outbreak risks effectively.

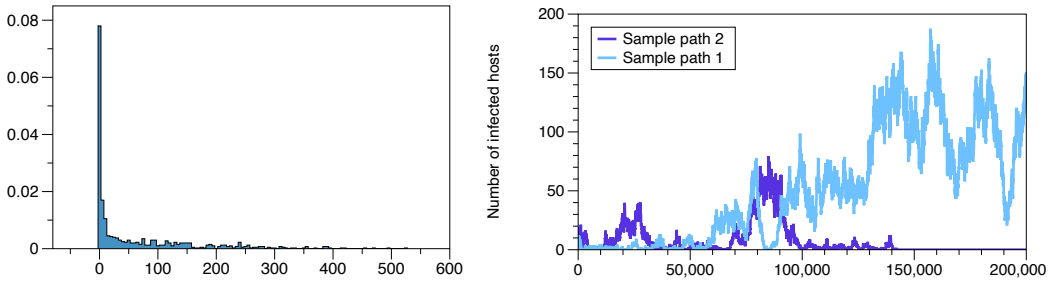

(a) $E_0 = 10,\ I_0 = 0,\ R_0 = 1.001$

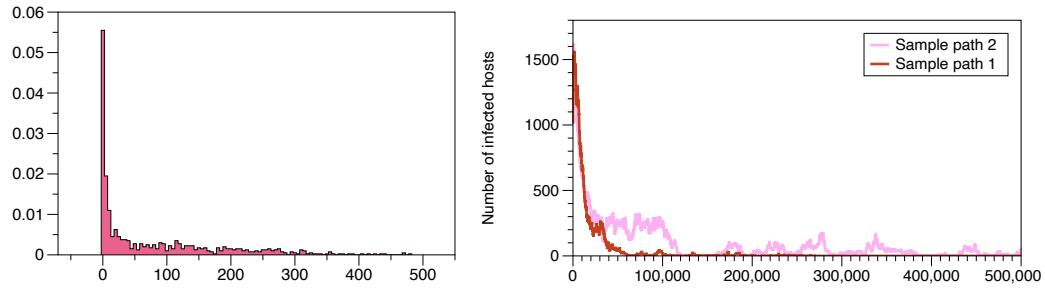

(b) $E_0 = I_0 = 1000,\ R_0 = 1.001$

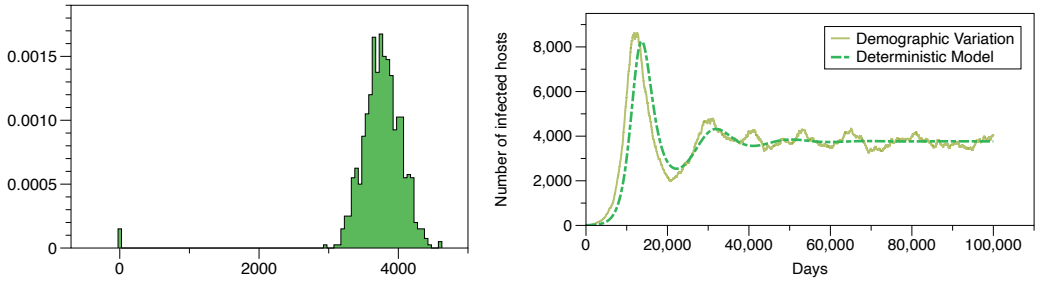

(c) $E_0 = 10,\ I_0 = 0,\ R_0 = 1.015$

Figure 2.1: Impact of demographic variability in model (2.6) under different basic reproduction numbers and initial conditions. The left panel displays probability distributions, while the right panel illustrates sample paths of infected animal hosts. In the figure, $K = 8\ 000\ 000$ and other parameter values see Table 2.1.

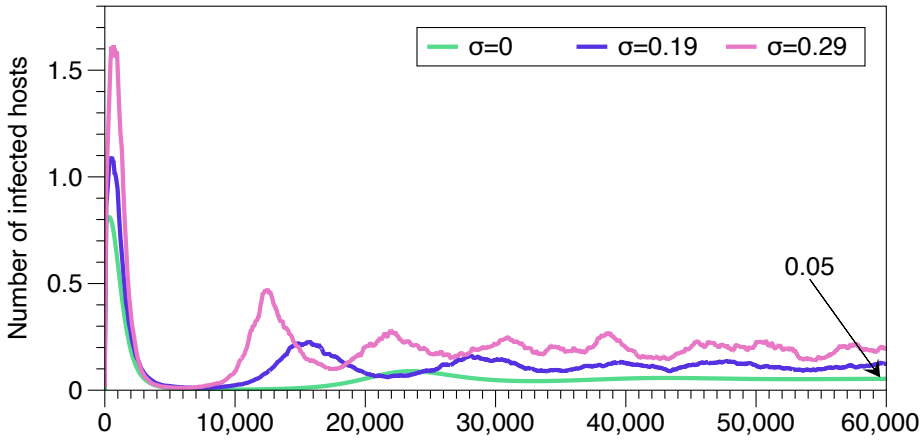

Figure 2.2: Impact of environmental variability on monkeypox disease dynamics in the model considering environmental stochasticity only. The basic reproduction number is set to $R_0 = 1.015$, and the maximal carrying capacity is $K = 800$. Other parameter values are provided in Table 2.1. Initial states are $E_0 = 1$ and $I_0 = 0$.

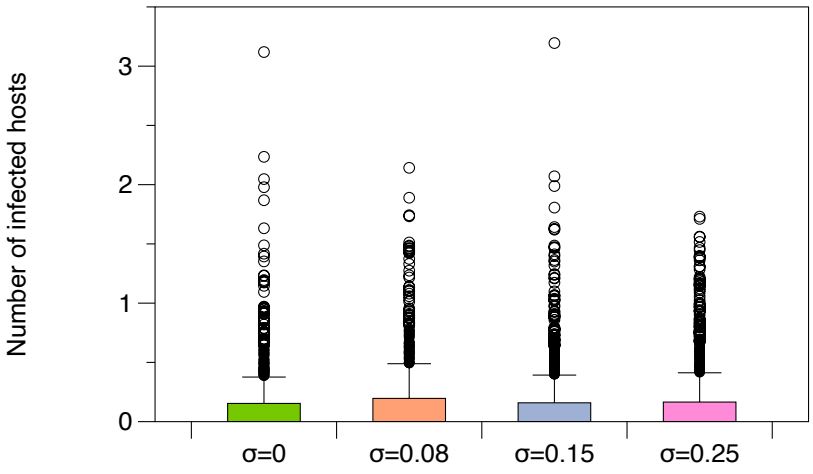

(a) $K = 800$, $R_0 = 1.015$

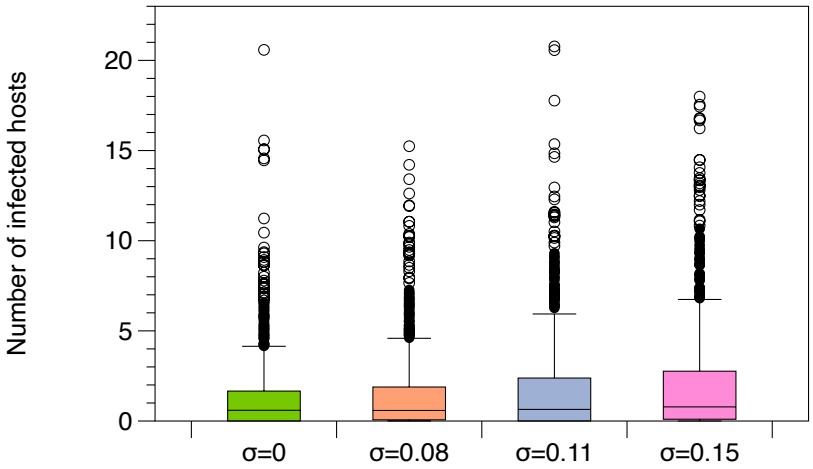

(b) $K = 20\ 000$, $R_0 = 1.015$

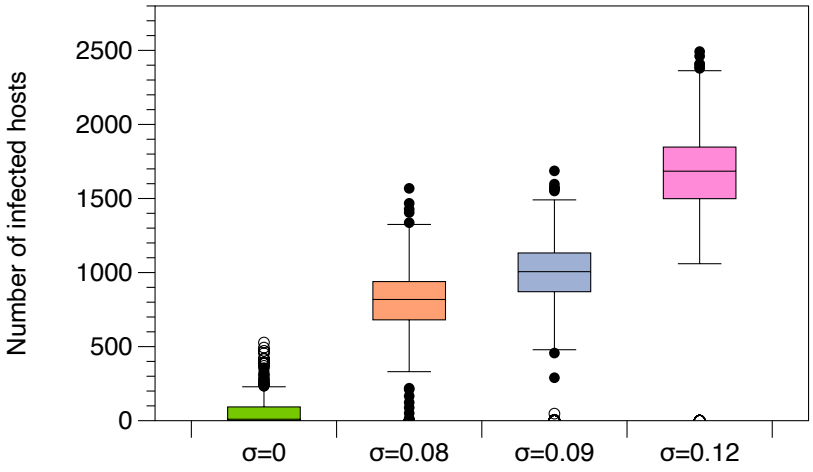

(c) $K = 8\ 000\ 000$, $R_0 = 1.001$

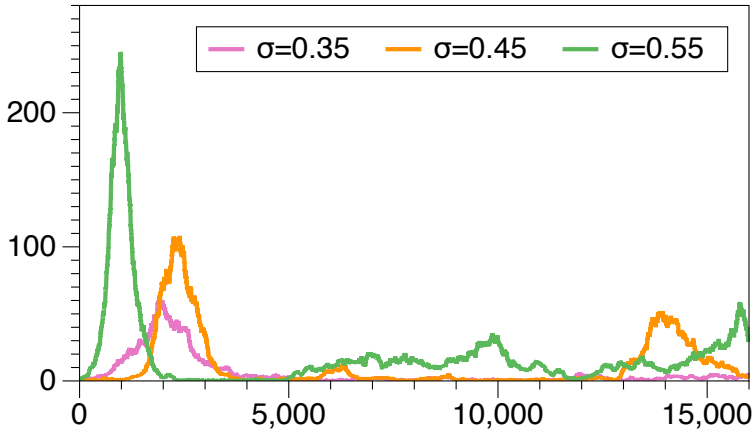

(d) $K = 20\ 000$, $R_0 = 1.015$

Figure 2.3: (a-c) boxplot and (d) sample path of infected animal hosts in the hybrid SDE model under varying levels of volatility. Initial states are $E_0 = 1$ and $I_0 = 0$.

3 Epidemic Spread of Monkeypox in a Reservoir-Target Host System

3.1 Introduction

Based on the classification of pathogens proposed by Wolfe et al. [13] and Lloyd-Smith et al. [2], the consequences of spillover processes during stage II and stage III remains uncertain. Within these stages, spillover events can lead to a range of consequences in target hosts, including disease extinction, outbreaks, endemicity, or population extinction. This chapter aims to explore the potential of stage II and stage III pathogens to cause outbreaks in target host populations. To achieve this, a basic transmission model for monkeypox is developed and applied to examine its dynamics in two distinct animal species.

Distinguishing hosts and their roles in pathogen circulation is a critical first step in modeling their effects. Haydon et al. [9] proposed that reservoirs can only be comprehensively understood in relation to specific target populations. Accordingly, they defined a reservoir as one or more epidemiologically connected populations or environments where a

pathogen can be sustainably maintained and from which transmission to a defined target population occurs. The transmission of a pathogen from reservoir hosts to new target hosts is referred to as spillover [10], during which target hosts serve as recipients [11, 12, 15]. Unlike primary reservoir hosts, target hosts are typically infected incidentally and do not play a role in maintaining the pathogen in nature.

Pathogen spillover is the trigger for disease outbreaks in new hosts, particularly in the context of increased interspecies contacts [15]. The initial spillover event paves the way for successful onward intraspecific transmission, intensifying disease spread within target host populations. Moreover, the transmission of broad host-range pathogens from wildlife to domestic animals may ultimately reach humans through secondary spillover events, where the pathogen is transmitted from new hosts rather than the original reservoir. Therefore, understanding the effects of spillover events on disease outbreaks in target hosts is essential for developing effective intervention strategies.

Despite the crucial nature of spillover, limited attention has been dedicated to evaluating the success of disease outbreak in target populations. Existing studies have shown that once the disease establishes itself in reservoir hosts, the outbreak in target hosts is inevitable [147, 150]. Berge et al. [241] showed that spillover events can be very detrimental to Ebola virus disease by contributing to speed up the disease outbreak. Other research has demonstrated that reducing interspecies transmission can prevent the sustained persistence of the pathogen in target hosts [242].

Traditional methods of calculating the basic reproduction number deriving from deter-

ministic model may prove inadequate in capturing the results of spillover events [21, 98, 134, 243]. As shown in previous studies [72, 98], the basic reproduction number can be expressed as the product of the spillover rate and the spillback rate, where spillback refers to the transmission from the target host population back to the reservoir hosts. This criterion is more suitable for scenarios involving both spillover and spillback transmission. When there is no spillback transmission, the basic reproduction number becomes independent of the spillover rate, prompting the need for a reassessment of its applicability.

An alternative formulation suggests that the basic reproduction number is the maximum of two within-species reproduction numbers in animals and humans, irrespective of the spillover rate [150, 244]. This formulation underscores that, for pathogens in stage II and stage III, the successful establishment of the disease in human populations (i.e., the target host group) requires that the basic reproduction number of the reservoir hosts exceeds one. While mathematically sound, it is questionable whether this is biologically meaningful [21]. It's essential to interpret these comparisons cautiously and consider the underlying biological and ecological factors that may influence transmission dynamics.

Alternative thresholds for structured populations have been examined. In a prior study, the authors introduced a quantity that delineates a major outbreak within the target host population using statistical methods [243]. They revealed that a basic reproduction number exceeding one alone does not adequately account for the occurrence of major outbreaks in the target population resulting from spillover events. Instead, the newly defined threshold quantity emerged as a more appropriate indicator for assessing the potential spillover of

pathogens to target populations and the subsequent generation of significant outbreaks. In previous works [161, 162], using an individual-based, stochastic, discrete-time SIR model, authors provided a group-level threshold to determine the possibility for diseases to remain endemic within a local group, or to be pandemic within the whole community. For agent-based random network models, an epidemic threshold equivalent to basic reproduction number can be derived using random matrix theory [167].

For non-structured models, there are novel investigations on outbreak thresholds. Xu [169] defined a persistence basic reproduction number of a stochastic SIS model based on the profile of stationary distribution. If the invariant density peaks at a positive number instead of zero, the disease will successfully persistent. The study conducted by Kubiak et al. [165] aimed to distinguish between outbreaks caused by a novel pathogen, characterized by either emergence or extinction. The differentiation criteria were grounded in whether the cumulative number of infections surpassed a threshold of 100. This method of categorizing outbreaks based on whether a predefined infection threshold is reached has been widely employed in previous studies [134, 163, 164].

In this study, we adopt a basic reservoir-target model to qualitatively investigate spillover results of monkeypox virus in stage II and stage III. *Funisciurus* spp. are selected as suspect reservoir hosts due to their high capacity for large-scale viral transmission. Non-human primates, particularly *Cercopithecus* spp. are considered targe hosts, as they share a similar ecological niche in the rainforest with squirrels and have been observed to interact with various squirrel species [52]. Using our minimalist two-species epidemiological framework,

we assess the limitation of basic reproduction number and establish an outbreak threshold for target hosts. These results have practical applications for designing and implementing intervention strategies.

3.2 Modelling Monkeypox Transmission

3.2.1 Transmission in Reservoir Hosts

Funisciurus spp. are identified as the suspect reservoir host. Total population of the reservoir host (N_r) can be divided into two distinct classes: susceptible (S_r), and infected (I_r), such that $N_r = S_r + I_r$. As an initial approach, the exposed class is omitted from the model. Furthermore, we exclude the removed class, as it is determined once susceptible and infected hosts are known [245]. Additionally, the demographic dynamics of the reservoir population are not considered.

Susceptible reservoir hosts acquire infection through contact with infected reservoir hosts [32, 36, 52, 246]. We denote β_r as the transmission rate among reservoir hosts and assume a bilinear incidence function. Thus, the reservoir-to-reservoir incidence is represented as $\beta_r I_r S_r$. The number of infected hosts decreases due to recovery or disease-induced mortality, occurring at a rate of μ_r [32, 36, 246]. Considering these processes, the infection dynamics within the reservoir host population are described by the following system of

deterministic differential equations

$$\begin{cases} S_r' = -\beta_r I_r S_r, \\ \\ I_r' = \beta_r I_r S_r - \mu_r I_r. \end{cases} \tag{3.1}$$

The descriptions of model variables and parameters are summarised in Table 3.1. Let S_{r0} be the initial susceptible reservoir hosts and I_{r0} be the initial infected reservoir hosts. The initial conditions of the system (3.1) can be described as

$$S_r(0) = S_{r0},\ I_r(0) = I_{r0}.$$

Since every point with $I_r = 0$ is an equilibrium, the system (3.1) has a line of equilibria [245]. The basic reproduction number for the system (3.1) is given by $R_{0r} = \frac{\beta_r S_{r0}}{\mu_r}$, representing the average number of secondary infections of reservoir hosts that occur when one infected reservoir host is introduced into a completely susceptible population of reservoir hosts of size $N_r \approx S_{r0}$. If $R_{0r} < 1$, the infection dies out. In contrast, if $R_{0r} > 1$, an epidemic occurs within the reservoir host population, with the number of infected hosts reaching a peak before subsequently declining to zero [71, 247]. The peak time thresholds are given by

$$\begin{aligned} S_r^{max} &\triangleq \frac{\mu_r}{\beta_r}, \\ I_r^{max} &\triangleq S_{r0} + I_{r0} - \frac{\mu_r}{\beta_r} - \frac{\mu_r}{\beta_r} \ln \frac{\beta_r S_{r0}}{\mu_r}. \end{aligned} \tag{3.2}$$

Additionally, the number of susceptible reservoir hosts is a nonnegative smooth decreasing function and therefore tends to a limit $S_r(\infty)$ as $t \to \infty$ [245], where $S_r(\infty)$ satisfies

$$\ln \frac{S_{r0}}{S_r(\infty)} = R_{0r} \left(1 - \frac{S_r(\infty)}{S_{r0}}\right). \tag{3.3}$$

Therefore, the cumulative number of infections in reservoir population can be calculated as $S_{r0} - S_r(\infty) = \frac{S_{r0}}{R_{0r}} \ln \frac{S_{r0}}{S_r(\infty)}$.

Table 3.1: Model variables and parameters for host i, where $i = r$ or a represents the reservoir and target hosts, respectively.

Variables and their initial values		
Notation	**Description**	**Initial value**
$S_i(t)$	The number of susceptible hosts on day t	$S_{r0} = 1.31 \times 10^5$ $S_{a0} = 1.07 \times 10^4$
$I_i(t)$	The number of infectious hosts on day t	$I_{r0} = 100, I_{a0} = 0$
Parameters for monkeypox transmission		
Notation	**Description**	**Value**
β_i	Intraspecific transmission rate	$\beta_r = 5.69 \times 10^{-7}$ $\beta_a = 1.71 \times 10^{-7}$
β_{ra}	Spillover rate	2.21×10^{-10}
μ_r	Removal rate of infectious reservoir hosts due to recovery or death	0.05
μ_{a1}	Removal rate of infectious target hosts due to recovery or death	0.05

3.2.2 Transmission in Target Hosts

When the monkeypox virus spills into the target community, specifically *Cercopithecu* spp., the pathogen initiates its transmission within the population. The population dynamics of the target host population (N_a) are structured into two mutually exclusive compartments: susceptible (S_a) and infected (I_a). Pathogen transmission occurs through two distinct mechanisms: a) spillover transmission [45, 143, 248, 249]; and b) intraspecific transmission [24, 44, 48, 250, 251]. These mechanisms are defined as follows.

a) **Spillover:** The virus jumps from reservoir hosts to target hosts. This transmission pathway occurs when target hosts come into contact with infected reservoir hosts, which serve as the primary carriers of the virus. We denote β_{ra} as the spillover rate, representing the transmission from reservoir hosts to target hosts [133, 233]. Therefore, reservoir-to-target incidence is $\beta_{ra} I_r S_a$.

b) **Intraspecific transmission in target hosts:** In addition to spillover transmission, the virus may also spread directly among target hosts. We denote β_a as the intraspecific transmission rate among target hosts, leading to the target-to-target incidence term $\beta_a I_a S_a$.

We assume that the removal rate of infected target hosts, due to recovery or disease-induced mortality, is denoted by μ_{a1}. Incorporating these assumptions, the transmission dynamics of monkeypox within the target host population can be expressed by the following

equation

$$\begin{cases} S_a' = -\beta_{ra} I_r S_a - \beta_a I_a S_a, \\ \\ I_a' = \beta_{ra} I_r S_a + \beta_a I_a S_a - \mu_{a1} I_a. \end{cases} \tag{3.4}$$

Infection within the target host population occurs only after the disease has become established in the reservoir hosts and the spillover process has taken place. Consequently, there are no initial infections in the target host population. Let S_{a0} denote the initial population of susceptible target hosts. Accordingly, the initial conditions for the spillover dynamics in system (3.4) can be described as

$$S_a(0) = S_{a0},\ I_a(0) = 0.$$

System (3.4) does not exhibit a disease-free equilibrium, as $I_r \neq 0$. By summing the two derivatives in system (3.4), we derive $N_a' = -\mu_{a1} I_a$. This implies that the total population of target hosts continuously decreases, satisfying $0 \leq N_a \leq S_{a0}$. Furthermore, since the derivative of a nonnegative, smooth, and decreasing function must tend to zero, it follows that $\lim\limits_{t\to\infty} I_a = 0$.

The logarithm of the number of susceptible hosts (S_a) satisfies the equation

$$(\ln S_a)' = -\beta_{ra} I_r - \beta_a I_a = -\beta_{ra} I_r + \frac{\beta_a}{\mu_{a1}} N_a',$$

and its integration gives

$$\ln \frac{S_a(t)}{S_{a0}} = -t\beta_{ra} I_r + \frac{R_{0a}(N_a(t) - S_{a0})}{S_{a0}}, \tag{3.5}$$

where $R_{0a} = \frac{\beta_a S_{a0}}{\mu_{a1}}$ represents the basic reproduction number for the target host population, quantifying the average number of secondary infections generated by a single infected target host in an entirely susceptible target host population. Formula (3.5) indicates that the susceptible population of target hosts will eventually be depleted under sustained I_r, representing a significant outbreak in target hosts. In the following section, we explore the conditions that lead to an outbreak in the target population, focusing on scenarios where the virus circulates in the reservoir host population and I_r approaches zero over time.

3.2.3 Reservoir-Target Model with Spillover

Given the circulation of monkeypox within the reservoir host population, our goal is to determine whether the spillover process results in an outbreak in the target host population. To explore this, we combine the two subsystems (3.1) and (3.4) into the following unified system

$$\begin{cases} S_r' = -\beta_r I_r S_r, \\ I_r' = \beta_r I_r S_r - \mu_r I_r, \\ S_a' = -\beta_{ra} I_r S_a - \beta_a I_a S_a, \\ I_a' = \beta_{ra} I_r S_a + \beta_a I_a S_a - \mu_{a1} I_a. \end{cases} \tag{3.6}$$

The initial conditions of the system (3.6) can be described as

$$S_r(0) = S_{r0},\ I_r(0) = I_{r0},\ S_a(0) = S_{a0},\ I_a(0) = 0.$$

System (3.6) has numerous equilibria $(S_{r0}, 0, S_{a0}, 0)$. It is straightforward that $\lim_{t\to\infty} I_a = \lim_{t\to\infty} I_r = 0$. The basic reproduction number of system (3.6) using the Next Generation Matrix method can be calculated as

$$R_0 = \max\{R_{0r},\ R_{0a}\}. \tag{3.7}$$

The basic reproduction number $R_0 < 1$ indicates that the virus is eliminated in both species, i.e. $R_{0r} < 1$ and $R_{0a} < 1$. In contrast, when $R_0 > 1$, it implies that the disease will either outbreak in the reservoir host or in the target host. While the definition (3.7) offers insights for evaluating outbreaks within two species, taking the maximum is more suitable for two non-interactive hosts [252].

For virus in stage II and stage III, we assume $R_{0r} > 1 > R_{0a} \geq 0$. Specifically,$R_{0a} < 1$ is assumed to prevent a significant outbreak driven by intraspecific transmission among target hosts. Under these conditions, the definition (3.7) becomes $R_0 = R_{0r}$, representing the overall basic reproduction number of entire system (3.6) is determined by the basic reproduction number of the reservoir host. In this case, the interpretation of $R_0 > 1$ becomes somewhat ambiguous. We can assert that there must be an outbreak in the reservoir host for $R_0 > 1$. However, it doesn't offer a direct indication of the outbreak scenario in the target population, reflecting the insufficiency of basic reproduction number given by equation (3.7).

In fact, the infected population within target hosts experiences an initial increase, followed by a subsequent decline. However, this does not mean there will always be an outbreak

in the target host. For example, the peak of infections in target hosts may be relatively low (Figure 3.1). Generally, the presence of a fractional infected host is not sufficient to be classified as an outbreak. Therefore, we introduce the following threshold to evaluate the outbreak in the target host and assess the impact of spillover.

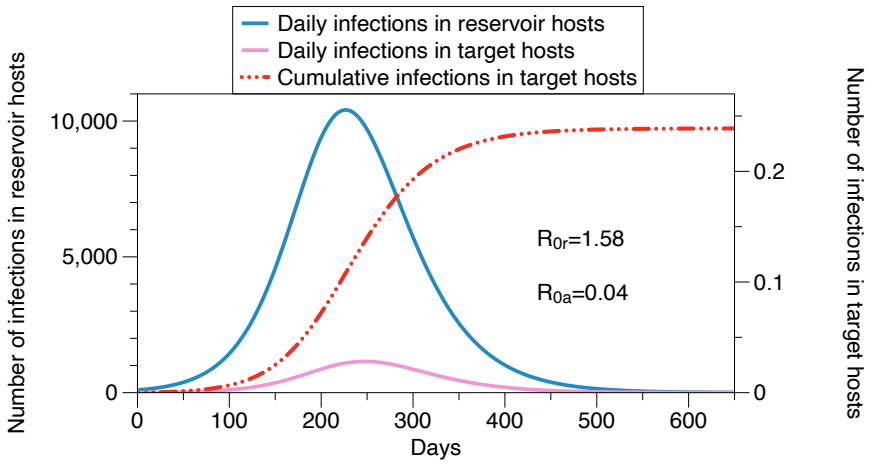

Figure 3.1: Low infections in target hosts in the reservoir-target system (3.6). The spillover rate is set to $\beta_{ra} = 1.21 \times 10^{-11}$, with all other parameter values detailed in Table 3.1.

3.2.4 A Novel Outbreak Threshold

The fundamental criterion for a major outbreak in the target host population is the presence of a sufficient number of infected target hosts. This ensures that trivial emergences, which would otherwise result in extinction, are avoided. To quantify the outbreak dynamics, we begin by analyzing the cumulative infections within the target host population.

The final size relation for the target host population in system (3.6) is given by

$$\ln \frac{S_{a0}}{S_a(\infty)} = \frac{\beta_{ra} S_{r0}}{\mu_r} \left(1 - \frac{S_r(\infty)}{S_{r0}}\right) + R_{0a} \left(1 - \frac{S_a(\infty)}{S_{a0}}\right),$$

where $S_a(\infty) \triangleq \lim_{t\to\infty} S_a$. Furthermore, the cumulative number of infections in the target host population satisfies

$$S_{a0} - S_a(\infty) = S_{a0} \left[1 - \exp\left\{\frac{\beta_{ra}(S_r(\infty) - S_{r0})}{\mu_r} + \frac{\beta_a(S_a(\infty) - S_{a0})}{\mu_{a1}}\right\}\right].$$

Applying the Taylor series expansion, the cumulative number of infections $S_{a0} - S_a(\infty)$ can be approximated as

$$S_{a0} - S_a(\infty) \approx \frac{\beta_{ra} S_{a0}(S_{r0} - S_r(\infty))}{\mu_r} \frac{1}{1 - R_{0a}}. \tag{3.8}$$

The above calculation (3.8) serves as an outbreak threshold for target hosts and can be interpreted as follows. The multiplier $\frac{\beta_{ra} S_{a0}}{\mu_r}$ is an equivalent indicator to the basic reproduction number [155, 156, 253]. It reflects new infections in target host caused by one infected reservoir hosts during period $\frac{1}{\mu_r}$. The multiplication by $S_{r0} - S_0(\infty)$ is employed to emphasize that the prevalence of the monkeypox virus in target hosts depends on the number of infections in reservoir hosts [243]. The first term overall measures the contribution of spillover transmission, and remains independent of the removal rate of infected target hosts.

The second term relates to target-to-target transmission and is greater than one when $R_{0a} < 1$. The multiplication of the first term by the second term illustrates the amplification of spillover results due to onward within-species infection. Notable, when R_{0a} approximates

zero, the total number of infections in target hosts becomes solely dependent on the spillover rate, the basic reproduction number of reservoir hosts, and the initial size of the target population.

Since the final size of the reservoir host population cannot be explicitly solved, we approximate it using equation (3.2) and derive the following lower bound

$$Tot \triangleq \frac{\beta_{ra} S_{a0} \left(S_{r0} - S_r^{max}\right)}{\mu_r} \frac{1}{1 - R_{0a}}. \tag{3.9}$$

It is observed that $S_{a0} - S_a(\infty) > Tot$. We then purpose the outbreak threshold based on the equation (3.9).

Definition 3.2.1. *For any integer k, when the estimation $Tot > k$, we define this as an outbreak in target hosts due to spillover transmission.*

3.2.5 Numerical Methods

We perform simulations of the reservoir-target monkeypox transmission model that incorporates spillover dynamics. In these simulations, we assume the same disease-related parameters, such as recovery rate and disease-induced death rate, for both reservoir and target hosts. This assumption is reasonable, as animal models of clade Ia infection have demonstrated pathology similar to that observed in humans [36, 50]. To reflect ecological differences, the model accounts for variations in population size and transmission rates between the host species. We assume that target hosts have no initial infections and acquire

Table 3.2: Parameter ranges for LHS in sensitivity analysis.

Parameter	**Definition**	**Range**
β_r	Reservoir-to-reservoir transmission rate	$[6.94 \times 10^{-7}, 3.24 \times 10^{-9}]$
β_{ra}	Spillover rate	$[0.4 \times 10^{-18}, 0.4 \times 10^{-7}]$
β_a	Target-to-target transmission rate	$[0.05 \times 10^{-10}, 1.5 \times 10^{-7}]$
S_{a0}	Population size of target hosts	$[1.31 \times 10^{3}, 2.31 \times 10^{5}]$
μ_{a1}	Removal rate of target hosts	$[0.001, 1]$

the disease primarily through spillover transmission, with a spillover rate ranging from 10^{-14} to 10^{-9}. All the parameter values are detailed in Table 3.1.

A rigid deterministic model fails to capture the inherent variability and realistic parametric fluctuations that may play a crucial role in the persistence of disease. To address this limitation, we conduct a sensitivity analysis using Latin Hypercube Sampling (LHS) combined with the Partial Rank Correlation Coefficient (PRCC) method. This approach quantifies the monotonic relationship between model outputs and input parameters. A total of 2 000 parameter sets are generated under the assumption of uniform distributions across specified ranges, as detailed in Table 3.2. The PRCC values are then computed to assess the influence of each parameter on the model output. A positive PRCC indicates a positive correlation between the parameter and the corresponding compartment, while

a negative value implies an inverse relationship. The magnitude of the PRCC reflects the strength of the parameter's effect: the larger the absolute value, the greater the impact.

3.3 Results

3.3.1 Established Threshold as a Reflective Indicator of Outbreak Dynamics in Target Hosts

Figure 3.2 illustrates the number of infections in both reservoir and target hosts. A significant surge is evident in the reservoir host population, where the total number of infected individuals consistently exceeds 800 000. Following spillover events, the monkeypox virus successfully establishes circulation within the target host population. The model-based total number of infections in target hosts is 2.41, while our estimation based on equation (3.9) yields a total of 1.36. Despite some degree of error in the estimation, it remains within an acceptable range and provides a valuable approach for quantifying spillover results in target hosts.

Moreover, the prevalence of the disease in the target host is entirely driven by the epidemiological dynamics within the reservoir hosts (Figure 3.2). The peak of infections in the target hosts lags behind the outbreak in the reservoir hosts. In addition, the observed pattern in the number of infected target hosts reveals a prolonged tail before reaching zero, illustrating a sustained period of transmission dynamics within the target host population.

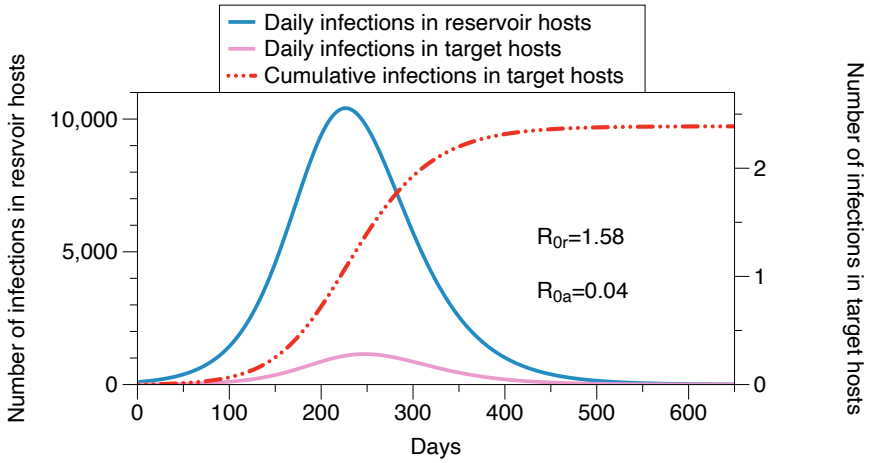

Figure 3.2: Monkeypox outbreaks in reservoir and target hosts for the scenario where $R_{0r} > 1$. Parameter values are provided in Table 3.1.

3.3.2 Spillover Rate Determines Monkeypox Outbreak Dynamics in Target Hosts

We investigate the impacts of intraspecific transmission and spillover dynamics on infection in target hosts, as represented by threshold values of 1 and 10 in Figure 3.3. As the reproduction number of the target population increases, the threshold curve shifts downward and to the left, indicating that even a low spillover rate can result in disease outbreak in the target population. Specifically, for the threshold $k = 1$, in the best scenario characterized by low values of R_{0r} and R_{0a} (1.1 and 0.05, respectively), a spillover rate of 3.5×10^{-10} is sufficient to prevent an outbreak in target hosts. This spillover rate is seven times higher than that required in the worst-case scenario, where R_{0r} andR_{0a} are elevated

(1.5 and 0.7, respectively).

We observe a notable increase in spillover rate tolerance as the threshold value is raised from 1 to 10. This observation is consistent with expectations, as a higher spillover rate would lead to an increased potential for infection spread. On the other hand, for threshold values of 1 and 10, the contour plots exhibit no discernible qualitative differences: a sharp decrease in the beginning followed by a slowed decline. This pattern suggests that the intrinsic combined effects of R_{0r}, R_{0a}, and the spillover rate on the threshold remain largely unaffected by variations in k, indicating robustness of our threshold.

3.3.3 Sensitivity Analysis

Figure 3.4 illustrates the results of the sensitivity analysis for the scenario where $R_{0r} > 1$, which demonstrates a monotonic relationship between the our threshold and input parameters. A strong positive correlation is observed between the threshold and the spillover rate. We highlight the substantial impact of spillover rates on infections in target hosts, emphasizing the intricate interconnectedness between populations. Notably, the findings identify the size of the target population as the second crucial factor, surpassing the contributions of two within-species transmission rates. This correlation underscores the significance of considering population dynamics into outbreak assessments for target hosts.

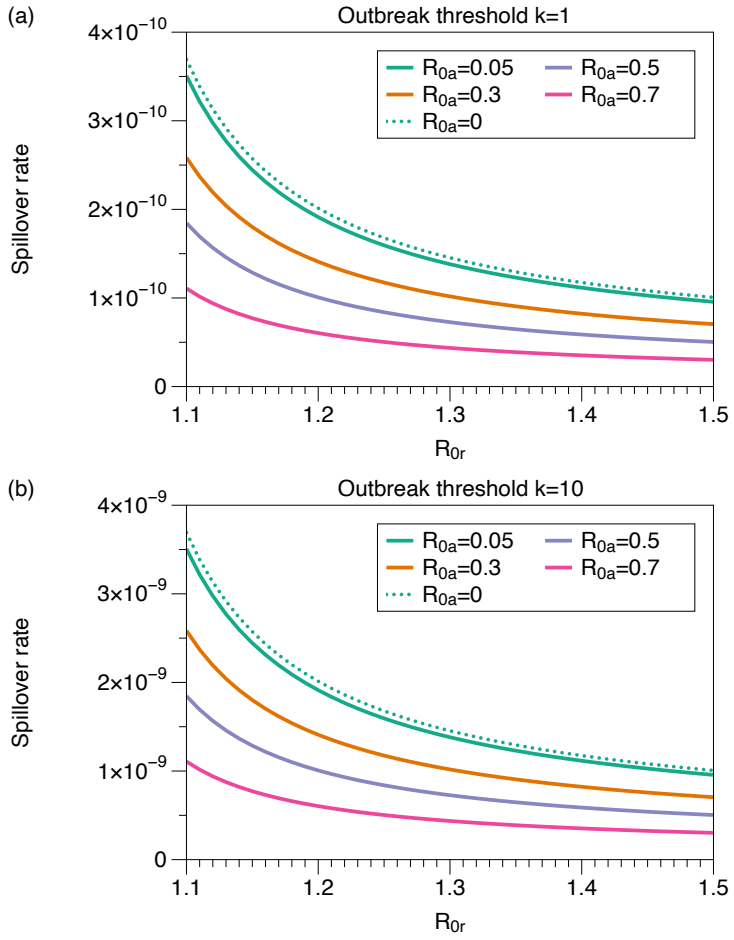

Figure 3.3: Contour plots showing the estimated total infection in target hosts as a function of the spillover rate and the basic reproduction numbers in both reservoir and target hosts. The plots are presented for two threshold values.

3.4 Conclusions

The occurrence of epizootic outbreaks in animals and zoonotic epidemics in humans is driven by the ability of pathogens to propagate across species, as observed in cases such

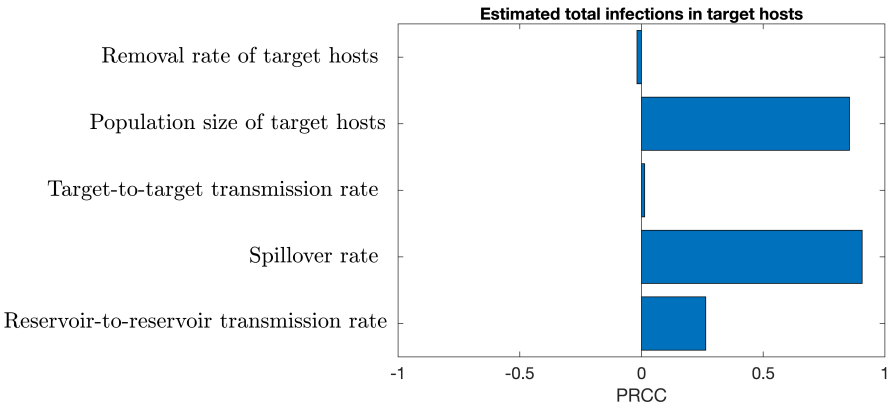

(a) The PRCC value for each parameter.

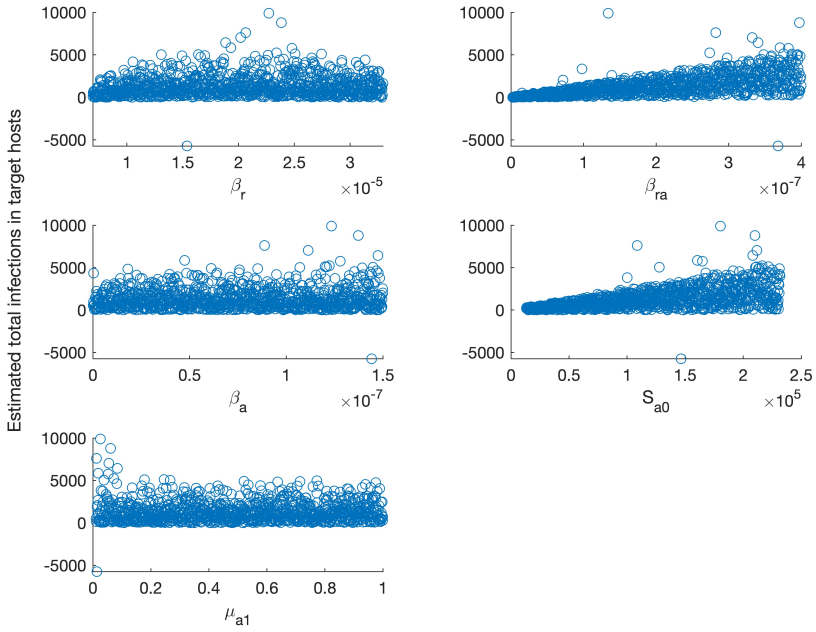

(b) Scatter plot of PRCC value for each parameter.

Figure 3.4: Sensitivity analysis of the estimated total infections in target hosts for the scenario where $R_{0r} > 1$.

as monkeypox, COVID-19, and others. Initial spillover events serve as the foundation for subsequent epidemic and pandemic dynamics, highlighting the critical need for early surveillance and intervention. The basic reproduction number has been pivotal in understanding pathogen spread within populations. However, in the context of spillover, a key limitation emerges: it fails to account for the contribution of reservoir hosts to the infection dynamics of target populations, particularly in two-species models. To address this gap, our study introduces an outbreak threshold specifically designed to assess spillover results, with a focus on monkeypox transmission.

Our findings challenge prior assumptions that a reservoir host reproduction number (R_{0r}) exceeding one is the sole determinant of outbreaks in target populations [150, 244]. While $R_{0r} > 1$ is a necessary condition, we underscore that it is not sufficient on its own [165], especially under low spillover rates. By using total infections in target hosts as a metric, we show that outbreaks are more likely to occur with non-trivial emergencies, offering a biologically meaningful measure of outbreak potential.

The spillover rate emerges as a key driver of outbreak dynamics in target hosts. Frequent reservoir-to-target contacts, coupled with pathogen evolution, can amplify the spillover rate, contributing to substantial outbreaks in the target population. Even in scenarios where intraspecific transmission among target hosts is limited, the potency of the spillover process can trigger and sustain outbreaks in the target population. Consequently, when a pathogen consistently spills over into a target host, it is essential to consider factors beyond within-species transmission alone [134, 147]. Interventions aimed at reducing spillover events are

fundamental to outbreak prevention. Furthermore, our sensitivity analysis identified the crucial role of target host population size in predicting pathogen spread [98, 163], providing valuable insights for the next research.

4 Endemicity of Monkeypox and Target Control Strategies

4.1 Introduction

As observed in monkeypox outbreaks, target host responses to the virus exhibit considerable variability [41, 44, 45, 52, 58, 254, 255]. This variability may be attributed to several factors, including population growth of host species. In this chapter, we incorporate population demographics to provide a more holistic uunderstanding of the effects of pathogen spillover during stage II. We incorporate target control strategies, such as quarantine and culling of target hosts, and assess their potential impact on disease endemicity and the extinction risks faced by target host species. By presenting evidence-based insights, our research aims to offer valuable guidance for managing the consequences of spillover events.

The dynamics of spillover transmission are influenced not only by viral characteristics but also by the intricate interplay between the behavior and ecology of host species [242]. As viruses depend on their hosts for replication and dissemination, the traits and dynamics

of host populations significantly shape spillover outcomes. For zoonosis spillover, it is noteworthy that spillover can occur even in regions with low human population density [256], highlighting the broad reach of these events beyond densely populated areas. Moreover, spillover events can pose significant threats not only to individual hosts but also to entire target populations, potentially driving them toward extinction [21].

One approach to incorporating population demographics is to assume identical patterns for animals and humans, characterized by constant immigration rates and death rates proportional to the population size [147, 150]. Studies have suggested that once the monkeypox virus spills over from reservoir hosts to humans, it inevitably establishes itself within the human population [147, 150]. However, this modeling framework does not account for the conditions under which spillover events drive target hosts to extinction. Moreover, a model incorporating both spillover and spillback processes (i.e., the reverse transmission from target hosts to reservoir hosts) reveals that an increase in monkeypox cases among animal species leads to a corresponding rise in monkeypox cases among humans [145].

Furthermore, studies have demonstrated that the model incorporating population demographics and spillover processes exhibit a unique endemic equilibrium [144, 145, 147, 148, 206]. This equilibrium remains stable when the basic reproduction number, independent of the spillover rate, exceeds one, effectively ruling out the possibility of backward bifurcation in the basic monkeypox transmission model. However, an exception has been identified in the model proposed by Madubueze et al. [205], which introduces backward bifurcation through the incorporation of a contaminated environment. Indeed, previous re-

search has indicated that backward bifurcation can occur in scenarios where both spillover and spillback transmission pathways are present [257].

In a reservoir-target system, management strategies can be specifically tailored to target populations. For instance, in the case of human monkeypox, interventions such as vaccination in human populations have yielded significant effectiveness [143, 144, 148, 258]. Similarly, mathematical modeling of H5N1 transmission has shown that reducing contact among target hosts is the most critical factor in controlling the spread of the disease [19].

Vaccination and drug treatments in animal populations are often impractical or unfeasible due to limited resources and the lack of appropriate diagnostic tools. Consequently, quarantine and culling of target hosts are often employed to manage diseases, particularly in livestock populations [176]. However, there is limited research on the effectiveness of quarantine and culling specifically in target host populations. Using a patch model, Bolzoni et al. [173] found that mass culling within a patch reduces infection in that patch but simultaneously increases the incidence in neighboring areas. In contrast, a stochastic spatial model that distinguished infected premises from their neighbors revealed that neighborhood culling had a significant impact, notably reducing both the number of cases and the total number of culled farms [190].

In this chapter, we develop a mathematical model to describe monkeypox transmission during stage II, integrating demographic factors and target control strategies. The population dynamics of the two host species are modeled distinctly, accounting for interventions such as quarantine and culling of targeted hosts. A fundamental analysis of the

model is conducted, focusing on the derivation of threshold conditions for disease persistence, maximum endemic prevalence, and potential population extinction. Furthermore, the effectiveness of various control measures is evaluated based on the analytical findings.

4.2 SI-SIR Model with Demographics

4.2.1 Model

Given the long-term recurring outbreaks of monkeypox [259], it is essential to account for the population dynamics of host species. In our reservoir-target system, we adopt distinct population growth models for reservoir hosts (*Funisciurus* spp.) and target hosts (*Cercopithecu* spp.). The primary role of reservoir hosts is to contribute infections to target hosts, irrespective of their reproduction type. Moreover, rodents generally exhibit high reproductive rates, short gestation periods, low pathogen virulence, and minimal risk of pathogen-induced extinction [11]. Thus, assuming a constant birth rate and a proportional death rate serves as a reasonable approximation for modeling the population growth of these species.

Conversely, for target hosts such as nonhuman primates, population dynamics are influenced by factors including longer gestation periods, lower reproductive rates and habitat availability. Additionally, to incorporate the effects of interventions such as quarantine and culling, we employ a density-dependent growth model, which can potentially offset population reductions resulting from these measures [198].

Table 4.1: Model variables and parameters.

Variables and their initial values		
Notation	**Description**	**Initial value**
$S_r(t)$	The susceptible population size of reservoir hosts on day t	1.31×10^5
$I_r(t)$	The infectious population size of reservoir hosts on day t	100
$S_a(t)$	The susceptible population size of target hosts on day t	1.07×10^4
$I_a(t)$	The infectious population size of target hosts on day t	0
$R_a(t)$	The recovered population size of target hosts on day t	0
Parameters for monkeypox transmission		
Notation	**Description**	**Value**
β_r	Reservoir-to-reservoir transmission rate	$[5.81 \times 10^{-8}, 4.75 \times 10^{-7}]$
β_{ra}	Spillover rate	$[9.84 * 10^{-10}, 2.60 \times 10^{-6}]$

Λ_r	Intrinsic birth rate of reservoir hosts	500
d_r	Natural death rate of reservoir hosts	0.00061
μ_r	Removal rate of infectious target hosts due to recovery or death	0.05
Λ_a	Intrinsic birth rate of target hosts	0.014
K_a	Maximal carrying capacity of target hosts	50 000
c_a	Quarantine and culling rate of target hosts	0.0137
μ_a	Disease-induced death rate of target hosts	0.005
γ_a	Recovery rate of target hosts	0.0452

We use the subscripts r and a to indicate reservoir and target hosts, respectively. The recruitment and natural death rates of the reservoir host are denoted by Λ_r and d_r, respectively. For the target host, we assume that Λ_a represents the intrinsic birth rate, K_a denotes the maximal carrying capacity, and c_a is a constant quarantine and culling rate [174]. Given the constraints on available resources, we assume that no post-quarantine testing is conducted on animals. In most scenarios, a culling strategy is employed; therefore, the release of populations from quarantine is not considered. The population dynamics of reservoir and target hosts, in the absence of disease, are described by the following system

of ordinary differential equations

$$\begin{aligned} \frac{dN_r\ (t)}{dt} &= \Lambda_r - d_r N_r, \\ \frac{dN_a\,(t)}{dt} &= \Lambda_a N_a \left(1 - \frac{N_a}{K_a}\right) - c_a N_a. \end{aligned}$$

It is evident that the population N_r approaches a positive equilibrium at $\frac{\Lambda_r}{d_r}$, while N_a stabilizes at $\frac{(\Lambda_a - c_a)K_a}{\Lambda_a}$ provided that $\Lambda_a > c_a$. For the remainder of this work, we assume that the condition $\Lambda_a > c_a$ holds. These models capture the limited growth of species and allow us to examine how demographic processes and control measures interact with epidemic transmission within the host populations.

Monkeypox Transmission in Reservoir Hosts with Population Demographics

We extend our previously established monkeypox transmission model in the reservoir host by incorporating demographic factors. The total population of the reservoir host (N_r) is divided into two distinct compartments: susceptible S_r and infective I_r, such that $N_r = S_r + I_r$. The susceptible reservoir host increases through births at a rate Λ_r and decreases due to natural mortality at a rate d_r. Infection among the susceptible reservoir host occurs via contact with infected individuals at a transmission rate β_r [36, 52, 246]. This transmission process leads to a decline in the susceptible population while simultaneously increasing the infected population. The infected reservoir host experienced population reduction through recovery and disease-induced mortality at a rate μ_r [32, 36, 246], along with additional losses due to natural mortality at a rate d_r. By integrating these processes, we derive the following system of deterministic differential equations to describe the infection

dynamics in the reservoir host population

$$\begin{cases} S_r' = \Lambda_r - \beta_r I_r S_r - d_r S_r, \\ I_r' = \beta_r I_r S_r - d_r I_r - \mu_r I_r. \end{cases} \tag{4.1}$$

The descriptions of model variables and parameters are summarised in Table 4.1. Let S_{r0} represent the initial susceptible reservoir host and I_{r0} denote the initial infected reservoir host. Accordingly, the initial conditions for the system (4.1) can be described as

$$S_r(0) = S_{r0},\ I_r(0) = I_{r0}.$$

The system (4.1) exhibits a trivial equilibrium and a disease-free equilibrium $\left(\frac{\Lambda_r}{d_r}, 0\right)$. The stability of the disease-free equilibrium depends on the basic reproduction number of the system, which is defined as $R_{0r} = \frac{\Lambda_r \beta_r}{d_r(d_r+\mu_r)}$. The disease-free equilibrium is globally stable if $R_{0r} \leq 1$ [245, 260]. Furthermore, when $R_{0r} > 1$, the reservoir-only system (4.1) possesses a unique and globally stable endemic equilibrium $\left(\widetilde{S_r}, \widetilde{I_r}\right)$ [245], which is characterized by coordinates

$$\widetilde{S_r} = \frac{d_r + \mu_r}{\beta_r}, \quad \widetilde{I_r} = \frac{(R_{0r} - 1)\, d_r}{\beta_r}.$$

Notably, we detect transient dynamics in system (4.1) when the basic reproduction number exceeds one (Figure 4.1). Before damping converges converging to the endemic equilibrium, the infected reservoir host population remains near the x-axis for a certain period [118, 261]. As the initial infected population increases or as R_{0r} rises, the length of the transient phase decreases. Additionally, the duration of this low-prevalence period

is more sensitive to variations in R_{0r} than to changes in the initial size of the infected population.

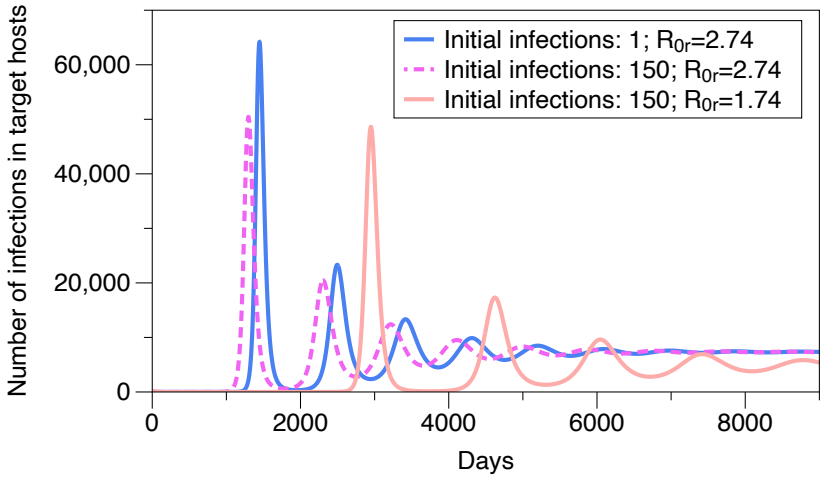

Figure 4.1: Transient dynamics in the reservoir-only system. The parameter values used in the simulations are provided in Table 4.1.

Monkeypox Transmission in Target Hosts with Population Demographics

The total target population is divided into three mutually disjoint compartments, namely susceptible S_a, infective I_a, and recovered R_a, such that $N_a = S_a + I_a + R_a$. The previous model describing the target host population is extended by incorporating logistic growth in the susceptible compartment of the target hosts. Additionally, all compartments experience a decline due to quarantine and culling strategies. Infection in the target host population occurs through spillover from reservoir hosts at a transmission rate β_{ra}. Applying the mass action law, the spillover incidence is given by $\beta_{ra} I_r S_a$. Additionally,

intraspecific transmission within the target host population is not considered in stage II. Therefore, the equation describing the transmission dynamics of monkeypox in the target host population is

$$\begin{cases} S_a' = \Lambda_a N_a \left(1 - \frac{N_a}{K_a}\right) - \beta_{ra} I_r S_a - c_a S_a, \\ I_a' = \beta_{ra} I_r S_a - \gamma_a I_a - c_a I_a - \mu_a I_a, \\ R_a' = \gamma_a I_a - c_a R_a. \end{cases} \tag{4.2}$$

The descriptions of model variables and parameters are summarised in Table 4.1. The system (4.2) exhibits two equilibria: a trivial equilibrium and a disease-free equilibrium $\left(\frac{(\Lambda_a - c_a)K_a}{\Lambda_a}, 0, 0\right)$. In the absence of spillover ($\beta_{ra} = 0$), no infections occur in the target host population. However, when spillover is present, the existence of an endemic equilibrium depends on the number of infections in reservoir hosts. To further investigate this dependency, we proceed with an analysis of the full system.

Reservoir-target System with Population Demographics

By combining systems (4.1) and (4.2), the dynamics of the monkeypox virus in stage II, which incorporates demographic factors, spillover dynamics, and target control strategies, can be described by the following model

$$\begin{cases} S_r' = \Lambda_r - \beta_r I_r S_r - d_r S_r, \\ I_r' = \beta_r I_r S_r - d_r I_r - \mu_r I_r, \\ S_a' = \Lambda_a N_a \left(1 - \frac{N_a}{K_a}\right) - \beta_{ra} I_r S_a - c_a S_a, \\ I_a' = \beta_{ra} I_r S_a - \gamma_a I_a - c_a I_a - \mu_a I_a, \\ R_a' = \gamma_a I_a - c_a R_a. \end{cases} \tag{4.3}$$

The descriptions of model variables and parameters are summarised in Table (4.2). The spillover initial conditions can be described as

$$S_r(0) = S_{r0},\ I_r(0) = I_{r0},\ S_a(0) = S_{a0}, I_a(0) = R_a(0) = 0.$$

We then analyze the existence and stability of the boundary and the endemic equilibrium of system (4.3), providing insights into the conditions under which the infection is eliminated, reaches its peak prevalence, or results in the extinction of the target host population.

4.2.2 Existence of Boundary Equilibria and the Basic Reproduction Number

The system (4.3) exhibits several boundary equilibria. First, it possesses a trivial equilibrium, representing the complete absence of all populations and the disease. Second, it has a reservoir-population-only equilibrium $\left(\frac{\Lambda_r}{d_r}, 0, 0, 0, 0\right)$, where the reservoir population exists without disease, while the target population is entirely absent. Third, a disease-free equilibrium $\left(\frac{\Lambda_r}{d_r}, 0, \frac{(\Lambda_a - c_a)K_a}{\Lambda_a}, 0, 0\right)$ exists, wherein both populations are present but remain free of disease.

If $R_{0r} > 1$, the system (4.3) attains a reservoir-disease-only equilibrium $\left(\widetilde{S_r}, \widetilde{I_r}, 0, 0, 0\right)$. This equilibrium indicates that the disease becomes established within the reservoir population, while the target population is driven to extinction. The extinction of the target population results from the combined effects of spillover infection and the implementation

of quarantine and culling strategies.

The local stability of $\left(\frac{\Lambda_r}{d_r}, 0, \frac{(\Lambda_a - c_a)K_a}{\Lambda_a}, 0, 0\right)$ is determined by the basic reproduction number of system (4.3), which is computed as R_{0r}. Notably, in stage II, the basic reproduction number for the entire system is governed solely by the transmission dynamics within the reservoir population, and remains independent of target control strategies. A detailed stability analysis of all boundary equilibria is presented in the subsequent section.

4.2.3 Stability of Boundary Equilibria

To analyze the local stability of the equilibria, we examine the eigenvalues of the Jacobian matrix derived from system (4.3). The Jacobian matrix yields

$$J_2\left(S_r, I_r, S_a, I_a, R_a\right) = \begin{pmatrix} -I_r\beta_r - d_r & -S_r\beta_r & 0 & 0 & 0 \\ I_r\beta_r & S_r\beta_r - d_r - \mu_r & 0 & 0 & 0 \\ 0 & -\beta_{ra}S_a & J_{33} & J_{34} & J_{34} \\ 0 & \beta_{ra}S_a & \beta_{ra}I_r & -c_a - \gamma_a - \mu_a & 0 \\ 0 & 0 & 0 & \gamma_a & -c_a \end{pmatrix},$$

where

$$\begin{aligned} J_{33} &= \Lambda_a\left(1 - \frac{S_a + I_a + R_a}{K_a}\right) - \frac{\Lambda_a}{K_a}\left(S_a + I_a + R_a\right) - \beta_{ra}I_r - c_a, \\ J_{34} &= \Lambda_a\left(1 - \frac{S_a + I_a + R_a}{K_a}\right) - \frac{\Lambda_a}{K_a}\left(1 - \frac{S_a + I_a + R_a}{K_a}\right). \end{aligned}$$

Theorem 4.2.1. *For system* (4.3)*, we have the following results*

1. *The trivial equilibrium, the reservoir-population-only equilibrium* $\left(\frac{\Lambda_r}{d_r}, 0, 0, 0, 0\right)$, *and the target-population-only equilibrium* $\left(0, 0, \frac{(\Lambda_a - c_a)K_a}{\Lambda_a}, 0, 0\right)$ *are unstable.*

2. *The disease-free equilibrium* $\left(\frac{\Lambda_r}{d_r}, 0, \frac{(\Lambda_a - c_a)K_a}{\Lambda_a}, 0, 0\right)$ *is locally asymptotically stable if* $R_{0r} < 1$.

To prove the stability of the reservoir-disease-only equilibrium, we denote

$$\begin{aligned} c_1^+ &\triangleq \frac{\Lambda_a - \mu_a - \gamma_a + \sqrt{(\Lambda_a - \mu_a - \gamma_a)^2 + 4\Lambda_a\gamma_a}}{2} \, (< \Lambda_a), \\ \widetilde{\beta_1} &\triangleq \frac{c_a \left(c_a + \gamma_a + \mu_a\right)(\Lambda_a - c_a)}{\left(c_a^2 - (\Lambda_a - \mu_a - \gamma_a)\, c_a - \Lambda_a\gamma_a\right)\widetilde{I_r}}. \end{aligned}$$

Theorem 4.2.2. *The reservoir-disease-only equilibrium* $\left(\widetilde{S_r}, \widetilde{I_r}, 0, 0, 0\right)$ *is locally asymptotically stable if* $R_{0r} > 1$, $c_a > c_1^+$, *and* $\beta_{ra} > \widetilde{\beta_1}$.

Proof. The eigenvalues of the Jacobian matrix J_2 at the equilibrium $\left(\widetilde{S_r}, \widetilde{I_r}, 0, 0, 0\right)$ are solutions of the following characteristic equation

$$\left(\lambda^2 + \left(\left(R_{0r} - 1\right) d_r + d_r\right)\lambda + \left(R_{0r} - 1\right) d_r \left(d_r + \mu_r\right)\right) \frac{\left(\lambda^3 + A_1\lambda^2 + A_2\lambda + A_3\right)}{c_a} = 0.$$

where $A_1 = 3c_a + \beta_{ra}\widetilde{I_r} + \mu_a + \gamma_a - \Lambda_a$,

$A_2 = -\left(2c_a + \beta_{ra}\widetilde{I_r} + \mu_a + \gamma_a\right)\Lambda_a + \left(\beta_{ra}\widetilde{I_r} + 2c_a\right)\left(c_a + \mu_a + \gamma_a\right) + c_a\left(\beta_{ra}\widetilde{I_r} + c_a\right)$,

$A_3 = \left(c_a^2 - (\Lambda_a - \mu_a - \gamma_a)\, c_a - \Lambda_a\gamma_a\right)\beta_{ra}\widetilde{I_r} - c_a\left(c_a + \gamma_a + \mu_a\right)(\Lambda_a - c_a)$.

This characteristic equation can be sloved in two parts: a quadratic equation and a cubic equation. The quadratic equation is given by

$$\lambda^2 + \left(\left(R_{0r} - 1\right) d_r + d_r\right)\lambda + \left(R_{0r} - 1\right) d_r \left(d_r + \mu_r\right) = 0,$$

whose solutions possess negative real parts if $R_{0r} > 1$. Next, we consider the cubic term

$$f_1(\lambda) \triangleq \lambda^3 + A_1\lambda^2 + A_2\lambda + A_3. \tag{4.4}$$

One can verify that if $c_a > c_1^+$ and $\beta_{ra} > \widetilde{\beta}_1$, the coefficients $A_i > 0$, for $i = 1, \ldots 3$. To analyze the stability, we calculate $A_1A_2 - A_3$ and collect it in terms of Λ_a as follows

$$H_1(\Lambda_a) \triangleq A_1A_2 - A_3 = a_1\Lambda_a^2 + a_2\Lambda_a + a_3. \tag{4.5}$$

where $a_1 = 2c_a + \mu_a + \gamma_a + \beta_{ra}\widetilde{I}_r > 0$,

$a_2 = -8c_a^2 - 6\beta_{ra}\widetilde{I}_r c_a - 6(\mu_a + \gamma_a)c_a - \beta_{ra}^2\widetilde{I}_r{}^2 - \beta_{ra}\widetilde{I}_r(3\mu_a + 2\gamma_a) - (\mu_a + \gamma_a)^2 < 0$,

$a_3 = (2c_a + \mu_a + \gamma_a)\left(\beta_{ra}\widetilde{I}_r + 2c_a\right)\left(\beta_{ra}\widetilde{I}_r + 2c_a + \mu_a + \gamma_a\right) > 0$.

One can verify that the discriminant of equation (4.5) is non-negative. Denote $x_1 \triangleq \frac{\left(\beta_{ra}\widetilde{I}_r + c_a\right)(c_a+\gamma_a+\mu_a)c_a}{\beta_{ra}\widetilde{I}_r(c_a+\gamma_a)+c_a(c_a+\gamma_a+\mu_a)}$. It follows that $H_1(x_1) > 0$ and $H_1'(x_1) < 0$. Thus, if $\Lambda_a < x_1$, then $H_1(\Lambda_a) > 0$, implying the roots of the cubic equation (4.4) have negative real parts [262]. Noticing that the condition $\Lambda_a < x_1$ holds when $c_a > c_1^+$ and $\beta_{ra} > \widetilde{\beta}_1$. We complete the proof. □

The analysis of boundary equilibria suggests critical insights into population dynamics in disease transmission systems. The instability of the reservoir-population-only equilibrium $\left(\frac{\Lambda_r}{d_r}, 0, 0, 0, 0\right)$ and the target-population-only equilibrium $\left(0, 0, \frac{(\Lambda_a - c_a)K_a}{\Lambda_a}, 0, 0\right)$ indicates that it is impossible for one population to remain unaffected by the disease while the other population goes extinct.

The stability of disease-free equilibrium $\left(\frac{\Lambda_r}{d_r}, 0, \frac{(\Lambda_a - c_a)K_a}{\Lambda_a}, 0, 0\right)$ implies that disease

eradication in both populations requires R_{0r} to be less than one, provided that the initial sizes of the subpopulations are within the basin of attraction of this equilibrium.

The stability of the reservoir-disease-only equilibrium $\left(\widetilde{S_r}, \widetilde{I_r}, 0, 0, 0\right)$ is influenced by the values of c_a and β_{ra}, highlighting a population extinction threshold for the target hosts. Given the persistence of the disease in reservoir hosts and the implementation of moderate quarantine and quarantine strategies ($c_a > c_1^+$), a spillover rate exceeding the threshold $\widetilde{\beta_1}$ places the target population at risk of extinction. Furthermore, this extinction threshold is shaped by disease-related factors affecting both host populations, as well as by population dynamics, excluding the maximum carrying capacity of target hosts.

4.2.4 Existence and Stability of a Unique Endemic Equilibrium

To obtain the endemic equilibrium of system (4.3), we set the right-hand sides equal to zero and obtain

$$\widetilde{S_r} = \frac{d_r + \mu_r}{\beta_r},\ \widetilde{I_r} = \frac{(R_{0r} - 1)\, d_r}{\beta_r}, \widetilde{S_a} = \frac{(c_a + \gamma_a + \mu_a)\, \widetilde{I_a}}{\beta_{ra} \widetilde{I_r}},\ \widetilde{R_a} = \frac{\gamma_a \widetilde{I_a}}{c_a},$$

$$\widetilde{I_a} = \frac{\beta_{ra} \widetilde{I_r} c_a K_a \left(\beta_{ra} \widetilde{I_r} \left(-c_a^2 + \ (\Lambda_a - \mu_a - \ \gamma_a)\, c_a + \Lambda_a \gamma_a\right) + c_a \left(c_a + \gamma_a + \mu_a\right) (\Lambda_a - c_a)\right)}{\left(\beta_{ra} \widetilde{I_r} \left(c_a + \gamma_a\right) + c_a \left(c_a + \gamma_a + \mu_a\right)\right)^2 \Lambda_a}.$$

The above expression demonstrates that the condition $R_{0r} > 1$ is a fundamental prerequisite for the existence of an endemic equilibrium in system (4.3). Furthermore, the realization of this equilibrium necessitates one of the following additional conditions: either

(i) $c_a \leq c_1^+$, or

(ii) $c_a > c_1^+$ and $\beta_{ra} < \widetilde{\beta}_1$.

The derivative of $\widetilde{I}_a$ with respective to β_{ra} yields

$$\frac{d\widetilde{I}_a}{d\beta_{ra}} = \frac{c_a^2 \widetilde{I}_r K_a}{\left(c_a^2 + \left(\beta_{ra}\widetilde{I}_r + \gamma_a + \mu_a\right) c_a + \gamma_a \beta_{ra}\widetilde{I}_r\right)^3 \Lambda_a} \Big(\widetilde{I}_r \beta_{ra} \left(-c_a^2 + (\Lambda_a - 2\mu_a - \gamma_a) c_a + \Lambda_a \gamma_a\right) + c_a \left(c_a + \gamma_a + \mu_a\right)\left(\Lambda_a - c_a\right)\Big).$$

We denote $c_2^+ \triangleq \frac{\Lambda_a - 2\mu_a - \gamma_a + \sqrt{(\Lambda_a - 2\mu_a - \gamma_a)^2 + 4\Lambda_a\gamma_a}}{2} < c_1^+$. If $c_a > c_1^+$, the positive threshold $\widetilde{\beta}_2 \triangleq \frac{c_a(c_a+\gamma_a+\mu_a)(\Lambda_a - c_a)}{(c_a^2 - (\Lambda_a - 2\mu_a - \gamma_a)c_a - \Lambda_a\gamma_a)\widetilde{I}_r} < \widetilde{\beta}_1$. Therefore, we have the following results.

Proposition 4.2.3. *1. If $c_a \leq c_2^+$, the derivative $\frac{d\widetilde{I}_a}{d\beta_{ra}}$ is positive.*

2. If $c_2^+ < c_a \leq c_1^+$, the derivative $\frac{d\widetilde{I}_a}{d\beta_{ra}}$ is positive if $\beta_{ra} < \widetilde{\beta}_2$, while negative if $\beta_{ra} > \widetilde{\beta}_2$.

3. If $c_a > c_1^+$, the derivative $\frac{d\widetilde{I}_a}{d\beta_{ra}}$ is positive if $\beta_{ra} < \widetilde{\beta}_2$, while negative if $\widetilde{\beta}_2 < \beta_{ra} < \widetilde{\beta}_1$,

The analysis of $\widetilde{I}_a$ implies that, under a low quarantine and culling rate, such that $c_a \leq c_2^+$, the endemic value of infected individuals in target hosts increases with the spillover rate. Consequently, the number of infected individuals among target hosts can serve as a key indicator for evaluating the risk of spillover events in this scenario.

On the other hand, under a high quarantine and culling rate, where $c_a > c_2^+$, the endemic equilibrium of infected hosts initially increases with the spillover rate, reaching a maximum at a critical threshold $\widetilde{\beta}_2$. Beyond this threshold, the endemic prevalence decreases as the spillover rate continues to rise. This negative relationship between endemic prevalence

and spillover rate is primarily due to the substantial decline in the susceptible pool of target hosts, resulting from the combined effects of quarantine, culling, and spillover-driven infection. In conclusion, $\widetilde{\beta_2}$ represents the spillover rate threshold at which the endemic prevalence reaches its peak, marking the most impactful spillover level in terms of infection burden within the target hosts.

Theorem 4.2.4. *The endemic equilibrium* $\left(\widetilde{S_r}, \widetilde{I_r}, \widetilde{S_a}, \widetilde{I_a}, \widetilde{R_a}\right)$ *is locally asymptotically stable if exists.*

Proof. The eigenvalues of the Jacobian matrix J_2 at the endemic equilibrium $\left(\widetilde{S_r}, \widetilde{I_r}, \widetilde{S_a}, \widetilde{I_a}, \widetilde{R_a}\right)$ satisfy the characteristic equation

$$\frac{\left(\lambda^2 + R_{0r} d_r \lambda + (d_r + \mu_r) d_r (R_{0r} - 1)\right)}{\left(c_a^2 + c_a\left(\beta_{ra}\widetilde{I_r} + \mu_a + \gamma_a\right) + \gamma_a \beta_{ra}\widetilde{I_r}\right) c_a} \left(A_4\lambda^3 + A_5\lambda^2 + A_6\lambda + A_7\right) = 0,$$

where $A_4 = (\gamma_a + c_a)\beta_{ra}\widetilde{I_r} + c_a(\mu_a + \gamma_a + c_a) > 0,$

$$\begin{aligned}
A_5 &= \left(c_a + \beta_{ra}\widetilde{I_r} + \mu_a + \gamma_a\right) c_a\Lambda_a + \beta_{ra}\widetilde{I_r}\gamma_a\Lambda_a + \beta_{ra}\widetilde{I_r}\gamma_a\left(3c_a + \beta_{ra}\widetilde{I_r} + \mu_a + \gamma_a\right) \\
&\quad + (\mu_a + \gamma_a)^2 c_a + c_a\left(\beta_{ra}\widetilde{I_r} + c_a\right)^2 + 2(\mu_a + \gamma_a)c_a^2 > 0, \\
A_6 &= -c_a^3\left(c_a + \beta_{ra}\widetilde{I_r} + \mu_a + \gamma_a\right) - 3\beta_{ra}\widetilde{I_r}\mu_a c_a^2 + (\gamma_a - \mu_a)\beta_{ra}^2\widetilde{I_r^2}c_a + \left(\gamma_a^2 - \mu_a^2\right)\beta_{ra}\widetilde{I_r}c_a \\
&\quad + (\mu_a + \gamma_a)\beta_{ra}^2\widetilde{I_r^2}\gamma_a + \beta_{ra}\widetilde{I_r}c_a^2\Lambda_a + 2\beta_{ra}\widetilde{I_r}c_a(\mu_a + 2\gamma_a + c_a)\Lambda_a + \beta_{ra}^2\widetilde{I_r^2}\Lambda_a(\gamma_a + c_a) \\
&\quad + (c_a + \mu_a + \gamma_a)c_a(2c_a + \mu_a + \gamma_a)\Lambda_a + (\mu_a + \gamma_a)\gamma_a\beta_{ra}\widetilde{I_r}\Lambda_a, \\
A_7 &= \left(\left(c_a + \beta_{ra}\widetilde{I_r} + \mu_a + \gamma_a\right)c_a + \beta_{ra}\widetilde{I_r}\gamma_a\right)\left(\beta_{ra}\widetilde{I_r}\left(-c_a^2 + (\Lambda_a - \mu_a - \gamma_a)c_a + \Lambda_a\gamma_a\right)\right. \\
&\quad \left. + c_a(c_a + \gamma_a + \mu_a)(\Lambda_a - c_a)\right).
\end{aligned}$$

It is evident that the solutions of the quadratic equation

$$\lambda^2 + R_{0r} d_r \lambda + (d_r + \mu_r)\, d_r\, (R_{0r} - 1) = 0$$

possess negative real parts when $R_{0r} > 1$. Denote the cubic equation

$$f_2(\lambda) \triangleq A_4 \lambda^3 + A_5 \lambda^2 + A_6 \lambda + A_7.$$

One can verify that under conditions either (i) or (ii), the inequalities $A_6 > 0$ and $A_7 > 0$ hold. Next, we determine the sign of $A_5 A_6 - A_4 A_7$, which is

$$H_2(\Lambda_a) \triangleq A_5 A_6 - A_4 A_7 = a_4 \Lambda_a^2 + a_5 \Lambda_a + a_6,$$

where

$$\begin{aligned}
a_4 &= \left(c_a^2 + \left(\beta_{ra}\widetilde{I}_r + \gamma_a + \mu_a\right) c_a + \beta_{ra}\widetilde{I}_r \gamma_a\right)^2 (\, \beta_{ra}\widetilde{I}_r + 2c_a + \gamma_a + \mu_a) > 0, \\
a_5 &= \left(c_a^2 + \left(\beta_{ra}\widetilde{I}_r + \gamma_a + \mu_a\right) c_a + \beta_{ra}\widetilde{I}_r \gamma_a\right) a_{51}, \\
a_{51} &= \left(2\beta_{ra}\widetilde{I}_r + 2\gamma_a + 2\mu_a\right) c_a^3 \\
&\quad + \left(3\gamma_a^2 + \left(6\beta_{ra}\widetilde{I}_r + 6\mu_a\right)\gamma_a + 3\beta_{ra}^2 {\widetilde{I}_r}^2 - \beta_{ra}\widetilde{I}_r \mu_a + 3\mu_a^2\right) c_a^2 \\
&\quad + \left(\beta_{ra}\widetilde{I}_r + \gamma_a + \mu_a\right)\left(\gamma_a^2 + \left(4\beta_{ra}\widetilde{I}_r + 2\mu_a\right)\gamma_a + \beta_{ra}^2 {\widetilde{I}_r}^2 - \beta_{ra}\widetilde{I}_r \mu_a + \mu_a^2\right) c_a \\
&\quad + \beta_{ra}\widetilde{I}_r \gamma_a \left(\gamma_a^2 + \left(2\beta_{ra}\widetilde{I}_r + 2\mu_a\right)\gamma_a + \beta_{ra}^2 {\widetilde{I}_r}^2 + 3\beta_{ra}\widetilde{I}_r \mu_a + \mu_a^2\right) > 0, \\
a_6 &= \left(\beta_{ra}\widetilde{I}_r c_a + \beta_{ra}\widetilde{I}_r \gamma_a + c_a^2 + c_a \gamma_a + c_a \mu_a\right) a_{61} + a_{62} a_{63}, \\
a_{61} &= (c_a^2 + \left(\beta_{ra}\widetilde{I}_r + \gamma_a + \mu_a\right) c_a + \beta_{ra}\widetilde{I}_r \gamma_a) c_a (\beta_{ra}\widetilde{I}_r + c_a)(c_a + \gamma_a + \mu_a), \\
a_{62} &= \left(\beta_{ra}\widetilde{I}_r \gamma_a \left(\beta_{ra}\widetilde{I}_r + 3c_a + \gamma_a + \mu_a\right)\right) + (\gamma_a + \mu_a)^2 c_a + c_a \left(\beta_{ra}\widetilde{I}_r + c_a\right)^2 \\
&\quad + 2(\gamma_a + \mu_a) c_a^2,
\end{aligned}$$

$$
\begin{aligned}
a_{63} \;=\; & -c_a^3\left(\beta_{ra}\widetilde{I}_r \;+\; c_a+\gamma_a+\mu_a\right) - \; 3\beta_{ra}\widetilde{I}_r\mu_a c_a^2 \;+\; \left(\gamma_a \;-\mu_a\right)\beta_{ra}^2\widetilde{I}_r^{\,2}c_a \\
& +\; \left(\gamma_a^2 \;-\mu_a^2\right)\beta_{ra}\widetilde{I}_r c_a + \; \left(\gamma_a+\mu_a\right)\beta_{ra}^2\widetilde{I}_r^{\,2}\gamma_a.
\end{aligned}
$$

It can be verified that $H_2(x_1) > 0$ and $H_2'(x_1) > 0$. Thus, the inequality $A_5A_6 > A_4A_7$ holds when $\Lambda_a > x_1$, ensuring the stability of the equilibrium point. Noticing that $\Lambda_a > x_1$ holds under either condition (i) or (ii). □

It is noticed that Theorem 4.2.4 excludes the occurrence of Hopf bifurcation.

4.3 Results

Figure 4.2 presents contour plots illustrating the endemic infection levels in target hosts as a function of the spillover rate and the basic reproduction number of reservoir hosts. The quarantine and culling rate is set such that $c_a > c_2^+$. The parameter ranges utilized in the analysis are provided in Table 4.1.

In the far-left region of Figure 4.2a, where the spillover rate is low, the endemic infection levels among target hosts is minimally influenced by the basic reproduction number of reservoir hosts. This suggests that control measures aimed at reducing the spillover rate may be effective in mitigating infections in target hosts.

Figure 4.2b indicates that the maximum endemic infection level in target hosts reaches 40. Notably, when the basic reproduction number of reservoir hosts exceeds 5, reductions in the spillover rate may paradoxically lead to an increase in the endemic prevalence. Additionally, when the basic reproduction number of reservoir hosts is approximately 4,

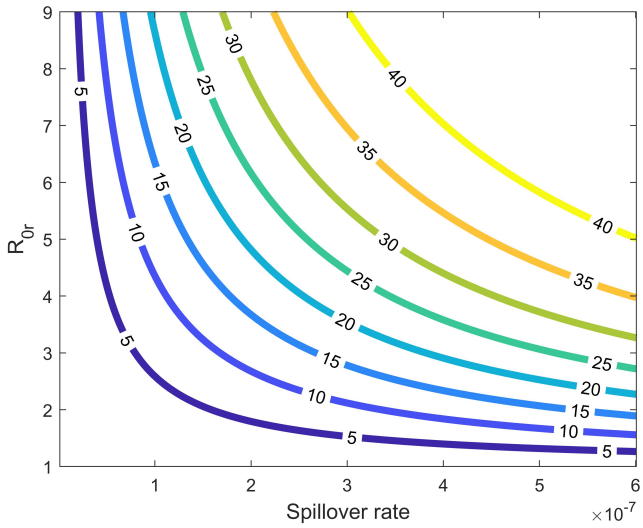

(a)

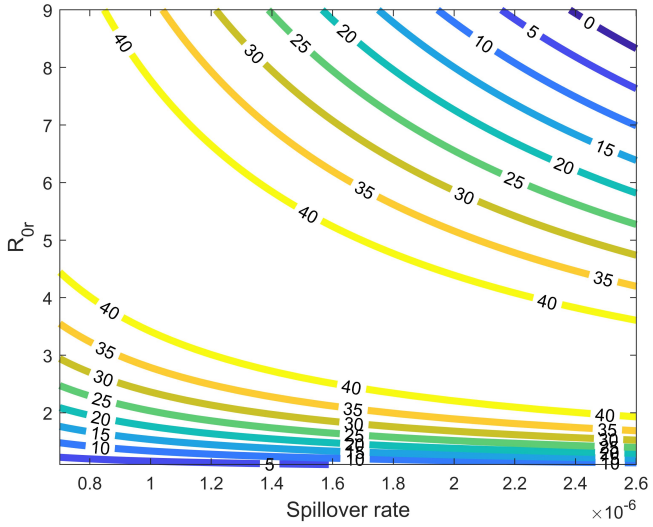

(b)

Figure 4.2: Contour plots of the endemic prevalence of infections in targe hosts in the plane of spillover rate and the basic reproduction number of reservoir hosts.

decreasing the spillover rate from 2.6×10^{-6} to 0.8×10^{-6} results in only minor changes in endemic infection levels in target hosts, highlighting the non-linear relationship between the spillover rate and prevalence dynamics.

4.4 Conclusions

In this Chapter, we introduced a mathematical model to investigate the transmission dynamics of monkeypox during stage II, incorporating population demographics and target control strategies. The primary objective was to identify threshold values associated with disease persistence, peak endemic prevalence, and the potential extinction of target populations. Through a detailed analysis of the transmission dynamics, our work provides valuable insights into the interaction between spillover processes and target control strategies and offers practical recommendations for mitigating spillover impacts.

For monkeypox to persist in target hosts, a basic reproduction number greater than one in reservoir hosts is necessary but not sufficient condition. The spillover of the virus from endemic reservoir hosts to target hosts plays a crucial role in determining infection levels within target populations.

Our findings reveal that under conditions where the disease persists in reservoir hosts and the quarantine and culling rate is weak ($c_a \leq c_1^+$), the system stabilizes around an endemic equilibrium regardless of the spillover rate. In this scenario, the spillover process does not drive the target population to extinction. Conversely, the model predicts that an

additional restriction on the spillover rate, such that $\beta_{ra} < \widetilde{\beta}_1$, is necessary to prevent population extinction. This threshold depends on population- and disease-specific parameters for both host species, excluding the maximum carrying capacity of the target host population. These results align with previous findings, which demonstrated that high spillover rates in less populated environments could heighten the risk of extinction for the entire target host [242].

Under conditions where $c_a \leq c_2^+ \ \left(< c_1^+\right)$, reducing the spillover rate decreases the endemic level [263]. This finding suggests that the number of infections in target hosts at endemic equilibrium can serve as a useful metric to quantify spillover risk. When the quarantine and culling rate of target hosts exceed c_2^+, a critical spillover rate, $\widetilde{\beta}_2$, must be highlighted, as it marks the point at which endemic prevalence reaches its peak. If the spillover rate exceeds $\widetilde{\beta}_2$, an integrated strategy targeting both reservoir transmission and spillover process should be implemented [27]. Such strategies may include the removal of reservoir hosts or reducing interspecific contacts. In contrast, strategies focused exclusively on target control, such as quarantine and culling, are less effective. These target control measures may inadvertently increase infections due to a rise in the number of susceptible individuals driven by density-dependent growth dynamics [176, 190, 198].

5 Environmental Stochasticity in Monkeypox Spillover from Reservoir to Target Hosts

5.1 Introduction

The occurrence of spillover events exhibits an inherently stochastic nature, characterized by the potential for fading out and recurrent episodes [21, 264]. Viral mutations and random host contact patterns play critical roles in shaping this stochasticity. Furthermore, anthropogenic activities, such as globalization and habitat destruction, further exacerbate the random interspecific contacts. Therefore, it is important to model stochastic spillover processes [256]. Existing studies have primarily focused on demographic stochasticity in spillover transmission, analyzing the probability distribution of the first spillover event [133, 134, 233]. In this chapter, we introduce environmental stochasticity and explore its impact on outbreak dynamics within target hosts.

Stochastic bifurcations have been predominantly investigated through simulations due to a lack of general theorem and criteria [107, 119, 120, 121, 122, 123, 124]. A phenomeno-

logical bifurcation (P-bifurcation) is defined as a qualitative shift in the stationary probability density function (PDF) of an observable induced by variations in system parameters [265, 266]. For example, the stationary density function may undergo transitions from one peak to two peaks or a crater-like form [119, 124, 267, 268]. Intrinsic stochasticity has been seen to lead to periodic outbreaks, contrasting with the behavior of the deterministic analogue that would converge to a stable equilibrium [123, 269, 270, 271, 272]. Additionally, quantitative changes in the mean values and variance of the stationary PDF in an eco-epidemiological system has been observed in [107]. However, this P-bifurcation has rarely been studied in zoonotic disease models, and its applications in disease prevention are worth investigating.

In this chapter, we extend the model developed in Chapter 4 to investigate the spillover effects on target hosts in stage III. Our extended deterministic framework incorporates an exposed class and intraspecific transmission among target hosts. We perform a basic analysis of the ODE model, deriving threshold conditions for disease persistence, maximum endemic prevalence, and population extinction. Subsequently, by introducing environmental stochasticity into the spillover rate, we examine the occurrence of P-bifurcation in the SDE model.

5.2 Deterministic Model

5.2.1 Model

We extend the reservoir-target system introduced in Chapter 4. In *Cercopithecus* spp., initial symptoms, such as fever, typically appear between 5 and 9 days post-infection [36, 48], before which the virus remains undetectable. To represent this latent phase of infection, the model is modified to include an exposed class in the infection progression for the target host population. Additionally, intraspecific transmission among target hosts is incorporated into the model, aligning with observations in stage III. By incorporating these two factors, the viral spillover dynamics from reservoir hosts to target hosts in stage III satisfies the following model

$$\begin{cases} S_r' = \Lambda_r - \beta_r I_r S_r - d_r S_r, \\ I_r' = \beta_r I_r S_r - d_r I_r - \mu_r I_r, \\ S_a' = \Lambda_a N_a \left(1 - \frac{N_a}{K_a}\right) - \beta_{ra} I_r S_a - \beta_a I_a S_a - c_a S_a, \\ E_a' = \beta_{ra} I_r S_a + \beta_a I_a S_a - \tau_a E_a - c_a E_a, \\ I_a' = \tau_a E_a - \gamma_a I_a - c_a I_a - \mu_a I_a, \\ R_a' = \gamma_a I_a - c_a R_a. \end{cases} \tag{5.1}$$

The model variables and parameters remain consistent with those presented in Table 4.1, with the inclusion of a new variable, exposed class E_a, and a new parameter, the latent

period τ_a. The spillover initial conditions of system (5.1) yields

$$S_r(0) = S_{r0},\ I_r(0) = I_{r0},\ S_a(0) = S_{a0},\ E_a(0) = I_a(0) = R_a(0) = 0.$$

We then proceed to analyze the basic properties of the entire system (5.1). This includes examining the existence and stability of boundary and endemic equilibria, exploring the conditions necessary for disease persistence, and evaluating the combined effects of spillover transmission, as well as target control measures such as culling and quarantine.

5.2.2 Existence of Boundary Equilibria and the Basic Reproduction Number

The system (5.1) always has the following boundary equilibrium points: a trivial equilibrium $(0, 0, 0, 0, 0, 0)$, a reservoir-population-only equilibrium $\left(\frac{\Lambda_r}{d_r}, 0, 0, 0, 0, 0\right)$, and a disease-free equilibrium $\left(\frac{\Lambda_r}{d_r}, 0, \frac{(\Lambda_a - c_a)K_a}{\Lambda_a}, 0, 0, 0\right)$. Additionally, if $R_{0r} = \frac{\Lambda_r \beta_r}{d_r(d_r+\mu_r)} > 1$, the system admits a reservoir-disease-only equilibrium $\left(\widetilde{S_r}, \widetilde{I_r}, 0, 0, 0, 0\right)$.

The local stability of the disease-free equilibrium is determined by the basic reproduction number R_0. Using the Next Generation Matrix method, R_0 is calculated as the maximum of the two subsystem values, given by

$$R_0 = \max\{R_{0r},\ R_{0a}\}. \tag{5.2}$$

where $R_{0a} = \frac{\beta_a \tau_a (\Lambda_a - c_a) K_a}{(\tau_a + c_a)(\gamma_a + c_a + \mu_a)\Lambda_a}$.

As this chapter focuses on viral spillover to target hosts during stage III, we assume $R_{0a} < 1$. This assumption ensures that, in the absence of reservoir hosts, sustained trans-

mission within the target population is not feasible, thereby highlighting the critical role of spillover events and external inputs in driving disease dynamics. Consequently, for system (5.1), the basic reproduction number simplifies to $R_0 = R_{0r}$.

5.2.3 Stability of Boundary Equilibria

The Jacobian matrix of system (5.1) yields

$$J_3 = \begin{pmatrix} -I_r\beta_r - d_r & -S_r\beta_r & 0 & 0 & 0 & 0 \\ I_r\beta_r & S_r\beta_r - d_r - \mu_r & 0 & 0 & 0 & 0 \\ 0 & -\beta_{ra}S_a & g_{33} & g_{34} & g_{35} & g_{34} \\ 0 & \beta_{ra}S_a & \beta_{ra}I_r + \beta_a I_a & -\tau_a - c_a & \beta_a S_a & 0 \\ 0 & 0 & 0 & \tau_a & -c_a - \gamma_a - \mu_a & 0 \\ 0 & 0 & 0 & 0 & \gamma_a & -c_a \end{pmatrix}.$$

$$g_{33} = \Lambda_a \left(1 - \frac{S_a + E_a I_a + R_a}{K_a}\right) - \frac{\Lambda_a}{K_a}\left(S_a + E_a + I_a + R_a\right) - \beta_{ra}I_r - \beta_a I_a - c_a,$$

$$g_{34} = \Lambda_a \left(1 - \frac{S_a + E_a + I_a + R_a}{K_a}\right) - \frac{\Lambda_a}{K_a}\left(S_a + E_a + I_a + R_a\right),$$

$$g_{35} = \Lambda_a \left(1 - \frac{S_a + E_a + I_a + R_a}{K_a}\right) - \frac{\Lambda_a}{K_a}\left(S_a + E_a + I_a + R_a\right) - \beta_a S_a.$$

Theorem 5.2.1. *For the system* (5.1)*, we have the following results*

(i) The trivial equilibrium and the reservoir-population-only equilibrium $\left(\frac{\Lambda_r}{d_r}, 0, 0, 0, 0, 0\right)$ *are unstable.*

(ii) The disease-free equilibrium $\left(\frac{\Lambda_r}{d_r}, 0, \frac{(\Lambda_a - c_a)K_a}{\Lambda_a}, 0, 0, 0\right)$ *is locally asymptotically stable if* $R_{0r} < 1$.

To determine the stability of the reservoir-disease-only equilibrium, we denote

$$\hat{\Lambda} = \frac{(\tau_a + c_a)(c_a + \gamma_a + \mu_a)c_a}{(c_a + \gamma_a)\tau_a + (c_a + \gamma_a + \mu_a)c_a} (> c_a),$$

$$\hat{\beta} = \frac{(\tau_a + c_a)(c_a + \gamma_a + \mu_a)(\Lambda_a - c_a)c_a}{(\tau_a + c_a)(c_a + \gamma_a + \mu_a)c_a\widetilde{I_r} - ((c_a + \gamma_a)\tau_a + (c_a + \gamma_a + \mu_a)c_a)\Lambda_a\widetilde{I_r}}.$$

Theorem 5.2.2. *The reservoir-disease-only equilibrium* $\left(\widetilde{S_r}, \widetilde{I_r}, 0, 0, 0, 0\right)$ *is locally asymptotically stable if* $R_{0r} > 1$, $\Lambda_a < \hat{\Lambda}$, *and* $\beta_{ra} > \hat{\beta}$.

Proof. The eigenvalues of the Jacobian matrix J_3 at the equilibrium $\left(\widetilde{S_r}, \widetilde{I_r}, 0, 0, 0, 0\right)$ satisfy the characteristic equation

$$\left(\lambda^2 + ((R_{0r} - 1)d_r + d_r)\lambda + (R_{0r} - 1)d_r(d_r + \mu_r)\right)\frac{\left(\lambda^4 + B_1\lambda^3 + B_2\lambda^2 + B_3\lambda + B_4\right)}{c_a} = 0,$$

where $B_1 = 4c_a + \beta_{ra}\widetilde{I_r} + \mu_a + \gamma_a + \tau_a - \Lambda_a$,

$$\begin{aligned}
B_2 &= -\Lambda_a c_a\left(3c_a + \beta_{ra}\widetilde{I_r} + \mu_a + \gamma_a + \tau_a\right) + 3c_a\left(2c_a + \beta_{ra}\widetilde{I_r} + \mu_a + \gamma_a + \tau_a\right) \\
&\quad + \beta_{ra}\widetilde{I_r}(\mu_a + \gamma_a + \tau_a) + (\mu_a + \gamma_a)\tau_a, \\
B_3 &= -\left(2\beta_{ra}\widetilde{I_r} + 2(\gamma_a + \tau_a + \mu_a) + 3c_a\right)\Lambda_a c_a - \beta_{ra}\widetilde{I_r}\Lambda_a(\gamma_a + \tau_a + \mu_a) \\
&\quad - \Lambda_a\tau_a(\gamma_a + \mu_a) + c_a^2\left(4c_a + 3\left(\beta_{ra}\widetilde{I_r} + \mu_a + \gamma_a + \tau_a\right)\right) \\
&\quad + 2\beta_{ra}\widetilde{I_r}(\gamma_a + \tau_a + \mu_a)c_a + (\mu_a + \gamma_a)\tau_a\left(\beta_{ra}\widetilde{I_r} + 2c_a\right),
\end{aligned}$$

$$
\begin{aligned}
B_4 &= -\Lambda_a\left(\beta_{ra}\widetilde{I}_r + c_a\right)\left(c_a+\gamma_a+\mu_a+\tau_a\right)c_a - \beta_{ra}\widetilde{I}_r\gamma_a\tau_a\Lambda_a - \tau_a c_a\left(\gamma_a+\mu_a\right)\Lambda_a \\
&\quad + \left(\beta_{ra}\widetilde{I}_r + c_a\right)c_a\left(c_a+\gamma_a+\mu_a\right).
\end{aligned}
$$

It is obvious that the solutions of the first quadratic equation $\lambda^2+\left(\left(R_{0r}-1\right)d_r+d_r\right)\lambda+\left(R_{0r}-1\right)d_r\left(d_r+\mu_r\right)=0$ possess negative real parts if $R_{0r}>1$.

On the other hand, it can be verified that if $\Lambda_a<\hat{\Lambda}$ and $\beta_{ra}>\hat{\beta}$, then the coefficients $B_i>0$ for $i=1,2,\ldots,4$. Additionally, if $B_1B_2B_3-B_1^2B_4-B_3^2$ is positive, then by Routh-Hurwitz criterion [273, 274, 275], all roots of the fourth-order equation $\lambda^4+B_1\lambda^3+B_2\lambda^2+B_3\lambda+B_4=0$ have negative real parts, implying the stability of the reservoir-disease-only equilibrium.

We solve the solve the determinant expression $B_1B_2B_3-B_1^2B_4-B_3^2$ as

$$
G_1\left(\Lambda_a\right)\triangleq B_1B_2B_3-B_1^2B_4-B_3^2=b_1\Lambda_a^3+b_2\Lambda_a^2+b_3\Lambda_a+b_4,
$$

where

$$
\begin{aligned}
b_1 &= -8c_a^3-\left(8\beta_{ra}\widetilde{I}_r+8\gamma_a+8\mu_a+8\tau_a\right)c_a^2 \\
&\quad +\left(-2\beta_{ra}^2{\widetilde{I}_r}^2-6\beta_{ra}\widetilde{I}_r\left(\gamma_a+\ \mu_a+\tau_a\right)-2\tau_a^2+\left(-6\mu_a-6\gamma_a\right)\tau_a-\ 2\left(\gamma_a+\mu_a\right)^2\right)c_a \\
&\quad -\beta_{ra}^2{\widetilde{I}_r}^2\left(\gamma_a+\mu_a+\tau_a\right)-\left(\tau_a^2\ +\left(3\mu_a+2\gamma_a\right)\tau_a+\left(\gamma_a+\mu_a\right)^2\right)\beta_{ra}\widetilde{I}_r \\
&\quad -\left(\gamma_a+\mu_a\right)\tau_a\left(\gamma_a+\mu_a+\tau_a\right)<0, \\
b_2 &= 48c_a^4\ +\left(56\beta_{ra}\widetilde{I}_r+\ 56\gamma_a+56\mu_a+56\tau_a\right)c_a^3+a_{22}c_a^2+a_{21}c_a+a_{20}>0, \\
a_{22} &= 20\beta_{ra}^2{\widetilde{I}_r}^2+52\beta_{ra}\widetilde{I}_r\left(\gamma_a+\mu_a+\tau_a\right)+\ 20\tau_a^2\ +\left(52\mu_a+\ 52\gamma_a\right)\tau_a+20\left(\gamma_a+\mu_a\right)^2,
\end{aligned}
$$

$$
\begin{aligned}
a_{21} &= 2\beta_{ra}^3 \widetilde{I_r}^3 + 14\beta_{ra}^2 \widetilde{I_r}^2 (\gamma_a + \mu_a + \tau_a) \\
&+ 14\ \beta_{ra}\widetilde{I_r}\left(\tau_a^2 + \left(\frac{19\mu_a}{7} + \frac{15\gamma_a}{7}\right)\tau_a + (\gamma_a + \mu_a)^2\right) \\
&+ 2(\gamma_a + \mu_a + \tau_a)\left(\tau_a^2 + (6\mu_a + 6\gamma_a)\tau_a + (\gamma_a + \mu_a)^2\right) \\
&+ a_{111}\left(\beta_{ra}\widetilde{I_r} + \gamma_a + \mu_a + \tau_a\right), \\
a_{20} &= \beta_{ra}^2 \widetilde{I_r}^2 (\gamma_a + \mu_a + \tau_a) + \beta_{ra}\widetilde{I_r}\left(\tau_a^2 + (4\mu_a + 2\gamma_a)\tau_a + (\gamma_a + \mu_a)^2\right) \\
&+ (\gamma_a + \mu_a)\tau_a(\gamma_a + \mu_a + \tau_a), \\
b_3 &= -96c_a^5 + b_{34}c_a^4 + b_{33}c_a^3 + b_{32}c_a^2 + b_{31}c_a + b_{30} < 0, \\
b_{34} &= -128\beta_{ra}\widetilde{I_r} - 128\gamma_a - 128\mu_a - 128\tau_a, \\
b_{33} &= -56\beta_{ra}^2 \widetilde{I_r}^2 - 144\beta_{ra}\widetilde{I_r}(\gamma_a + \mu_a + \tau_a) - 56\tau_a^2 + (-144\mu_a - 144\gamma_a)\tau_a \\
&- 56(\gamma_a + \mu_a)^2, \\
b_{32} &= -8\beta_{ra}^3 \widetilde{I_r}^3 - 52\beta_{ra}^2 \widetilde{I_r}^2 (\gamma_a + \mu_a + \tau_a) \\
&- 52\beta_{ra}\widetilde{I_r}\left(\tau_a^2 + \left(\frac{34\mu_a}{13} + \frac{30\gamma_a}{13}\right)\tau_a + (\gamma_a + \mu_a)^2\right) \\
&- 8(\gamma_a + \mu_a + \tau_a)\left(\tau_a^2 + \left(\frac{11\mu_a}{2} + \frac{11\gamma_a}{2}\right)\tau_a + (\gamma_a + \mu_a)^2\right), \\
b_{31} &= -6\beta_{ra}^3 \widetilde{I_r}^3 (\gamma_a + \mu_a + \tau_a) - 14\beta_{ra}^2 \widetilde{I_r}^2\left(\tau_a^2 + \left(\frac{19\mu_a}{7} + \frac{15\gamma_a}{7}\right)\tau_a + (\gamma_a + \mu_a)^2\right) \\
&- 6\beta_{ra}\widetilde{I_r}(\gamma_a + \mu_a + \tau_a)\left(\tau_a^2 + \left(\frac{16\mu_a}{3} + 4\gamma_a\right)\tau_a + (\gamma_a + \mu_a)^2\right) \\
&- 6\tau_a(\gamma_a + \mu_a)\left(\tau_a^2 + \left(\frac{7\mu_a}{3} + \frac{7\gamma_a}{3}\right)\tau_a + (\gamma_a + \mu_a)^2\right),
\end{aligned}
$$

$$
\begin{aligned}
b_{30} &= -\beta_{ra}^3 \widetilde{I_r}^3 \left(\tau_a^2 + (3\mu_a + 2\gamma_a)\tau_a + (\gamma_a+\mu_a)^2\right) \\
&\quad - \beta_{ra}^2 \widetilde{I_r}^2 (\gamma_a + \mu_a + \tau_a)\left(\tau_a^2 + (5\mu_a + 3\gamma_a)\tau_a + (\gamma_a+\mu_a)^2\right) \\
&\quad - 3\beta_{ra}\widetilde{I_r}(\gamma_a+\mu_a+\tau_a)^2\tau_a\left(\mu_a + \frac{2\gamma_a}{3}\right)\tau_a^2(\gamma_a+\mu_a)^2(\gamma_a+\mu_a+\tau_a), \\
b4 &= (2c_a+\tau_a)(2c_a + \mu_a+\gamma_a+\tau_a)\left(\beta_{ra}\widetilde{I_r} + 2c_a+\gamma_a+\mu_a\right)\left(\beta_{ra}\widetilde{I_r}\right. \\
&\quad \left. + 2c_a+\tau_a\right)\left(\beta_{ra}\widetilde{I_r} + 2c_a\right)(2c_a+\mu_a+\gamma_a) > 0.
\end{aligned}
$$

We observe that $G_1(0) > 0$, $G_1'(0) < 0$. Let

$$
y_1 \triangleq \frac{\left(\beta_{ra}\widetilde{I_r} + c_a\right)(\tau_a + c_a)(c_a+\gamma_a+\mu_a)c_a}{\left(\beta_{ra}\widetilde{I_r}+c_a\right)(c_a+\gamma_a+\mu_a+\tau_a)c_a + \beta_{ra}\widetilde{I_r}\gamma_a\tau_a + \tau_a c_a(\gamma_a+\mu_a)}.
$$

It follows that $G_1(y_1) > 0$ and $G_1'(y_1) < 0$. Next, we determine the extreme points of the curve $G_1(\Lambda_a)$. The derivative of G_1 with resepect to Λ_a is given by

$$
G_2(\Lambda_a) \triangleq 3b_1\Lambda_a^2 + 2b_2\Lambda_a + b_3.
$$

The roots of $G_2(\Lambda_a) = 0$ are

$$
\Lambda_3^- = \frac{-2b_2 - \sqrt{\Delta_a}}{6b_1}, \Lambda_3^+ = \frac{-2b_2 + \sqrt{\Delta_a}}{6b_1}.
$$

where Δ_a is the discriminant of $G_2(\Lambda_a)$. One can verify that $\Lambda_3^+ > \Lambda_3^- > y_1$. Therefore, the function $G_1(\Lambda_a)$ is always positive if $\Lambda_a < y_1$. Notice that the condition $\Lambda_a < y_1$ holds when $\Lambda_a < \hat{\Lambda}$ and $\beta_{ra} > \hat{\beta}$. This completes the proof. □

From the stability analysis of reservoir-disease-only equilibrium $\left(\widetilde{S_r}, \widetilde{I_r}, 0, 0, 0, 0\right)$, an extinction threshold for the target hosts, $\hat{\beta}$, was derived. Given that the disease persists in

the reservoir hosts and the intrinsic birth rate of the target hosts is low (i.e. $\Lambda_a < \hat{\Lambda}$), an increase in the spillover rate beyond this threshold poses a risk of extinction for the target population. Moreover, this threshold is determined solely by population dynamics and disease-related factors within the target hosts, but remains unaffected by the intraspecies transmission rate among them. This is reasonable since, if spillover events consistently lead to population extinction in the target host, then the further introducing of β_a will exacerbate and accelerate the extinction process.

5.2.4 Existence of a Unique Endemic Equilibrium

The existence of an endemic equilibrium is established in the following proposition.

Proposition 5.2.3. *Let $R_{0r} > 1$. The system (5.1) exhibits a unique endemic equilibrium $\left(\widetilde{S_r}, \widetilde{I_r}, \widehat{S_a}, \widehat{E_a}, \widehat{I_a}, \widehat{R_a}\right)$ if either of the following conditions is satisfied*

(a) $\Lambda_a \geq \hat{\Lambda}$, or

(b) $c_a < \Lambda_a < \hat{\Lambda}$ and $\beta_{ra} < \hat{\beta}$.

Otherwise, no endemic equilibrium exists in the system.

Proof. The system (5.1) is decomposed, with the condition $R_{0r} > 1$ ensures the existence of $\widetilde{S_r}$ and $\widetilde{I_r}$ which represent the equilibrium points of the reservoir subsystem. Then, we solve the equilibrium for the target subsystem by using N_a as a variable in place of S_a,

yeilding

$$\begin{cases} E_a' = \beta_{ra} I_r (N_a - E_a - I_a - R_a) + \beta_a I_a (N_a - E_a - I_a - R_a) - \tau_a E_a - c_a E_a, \\ I_a' = \tau_a E_a - \gamma_a I_a - c_a I_a - \mu_a I_a, \\ R_a' = \gamma_a I_a - c_a R_a, \\ N_a' = \Lambda_a N_a (1 - \frac{N_a}{K_a}) - c_a N_a - \mu_a I_a. \end{cases} \tag{5.3}$$

In system (5.3), the coordinates of endemic equilibrium satisfy

$$\hat{E}_a = \frac{(c_a + \gamma_a + \mu_a)\hat{I}_a}{\tau_a}, \quad \hat{R}_a = \frac{\gamma_a \hat{I}_a}{c_a},$$

and the coordinates $\hat{I}_a$ and $\hat{N}_a$ are determined as the positive intersections of the following two quadratic equations

$$(\beta_a I_a + \beta_{ra}\tilde{I}_r)\left(N_a - \left(1 + \frac{\gamma_a}{c_a} + \frac{c_a + \gamma_a + \mu_a}{\tau_a}\right) I_a\right) - \frac{(\tau_a + c_a)(c_a + \gamma_a + \mu_a)}{\tau_a} I_a = 0, \tag{5.4}$$

$$I_a = \frac{\Lambda_a}{\mu_a}\left(1 - \frac{N_a}{K_a}\right) N_a - \frac{c_a}{\mu_a} N_a. \tag{5.5}$$

By dividing both quadratic equations by N_a and defining $x_a = \frac{I_a}{N_a} < 1$, equations (5.4) and (5.5) can be transferred to

$$I_a = -\frac{(\tau_a + c_a)(c_a + \gamma_a + \mu_a)}{\beta_a \tau_a} \frac{x_a}{(1 + \frac{\gamma_a}{c_a} + \frac{c_a + \gamma_a + \mu_a}{\tau_a})x_a - 1} - \frac{\beta_{ra}\tilde{I}_r}{\beta_a} \tag{5.6}$$

$$I_a = \frac{K_a}{\Lambda_a}(\Lambda_a - c_a - \mu_a x_a) x_a \tag{5.7}$$

The mutually orthogonal asymptotes of hyperbola (5.6) are $x_a = \frac{1}{1 + \gamma_a c_a + \frac{c_a + \gamma_a + \mu_a}{\tau_a}} < 1$ and $I_a = -\frac{(\tau_a + c_a)(c_a + \gamma_a + \mu_a)}{\beta_a \tau_a (1 + \frac{\gamma_a}{c_a} + \frac{c_a + \gamma_a + \mu_a}{\tau_a})} - \frac{\beta_{ra}\tilde{I}_r}{\beta_a}$. Moreover, the hyperbola (5.6) is confined to the

second and fourth quadrants of the coordinate plane, delineated by these asymptotic lines. The quadratic curve (5.6) intersects the x-axis at the point $(\frac{1}{p}, 0)$, where

$$p = \frac{(\tau_a + c_a\ )(c_a + \gamma_a + \mu_a\ )}{\beta_{ra}\tilde{I}_r\tau_a} + 1 + \frac{\gamma_a}{c_a} + \frac{c_a + \gamma_a + \mu_a}{\tau_a}.$$

Simultaneously, the point of intersection between the parabola (5.7) and the x-axis is $\frac{\Lambda_a - c_a}{\mu_a}$. Therefore, there exists a unique positive solution for equations (5.6) and (5.7) if $\frac{\Lambda_a - c_a}{\mu_a} > \frac{1}{p}$, which is equivalent to either (a) $\Lambda_a \geq \hat{\Lambda}$, or (b) $c_a < \Lambda_a < \hat{\Lambda}$ and $\beta_{ra} < \hat{\beta}$. □

The above calculation demonstrates that the condition $R_{0r} > 1$ is a fundamental prerequisite for the existence of an endemic equilibrium in the system (5.1). Furthermore, constraints on the intrinsic birth rate and spillover rate are necessary.

Table 5.1: The number of infections in target hosts at the endemic level varies with the spillover rate, given $R_{0r} > 1$. The parameter values used are the same as those in Figure 4.2.

Spillover rate	**Endemic level of infections in target hosts** ($R_{0a} = 0.64$)	**Endemic level of infections in target hosts** ($R_{0a} = 0$)
$2 * 10^{-6}$	42.848463	44.116446
$1.8 * 10^{-6}$	43.700369	44.559307
$1.6 * 10^{-6}$	44.321647	44.607068
$1.4 * 10^{-6}$	44.628307	44.130994
$1.2 * 10^{-6}$	44.600970	42.959711

We use Maple [276] to compute the endemic infection level in target hosts, as presented in Tables 5.1 and 5.2. Table 5.1 illustrates that the infection count in target hosts initially increases but subsequently declines as the spillover rate rises. This pattern suggests the presence of an extreme spillover rate, as analyzed in Chapter 4. Additionally, we observe that this threshold decreases with R_{0a}, suggesting that in the presence of target intraspecific transmission, more stringent control measures aimed at reducing reservoir outbreaks and limiting interspecies contacts should be implemented earlier.

Table 5.2: The number of infections in target hosts at the endemic level varies with the quarantine and culling rate, given $R_{0r} > 1$. The parameter values used are the same as those in Figure 4.2.

Quarantine and culling rate	**Endemic level of infections in target hosts** ($R_{0a} = 0.64$)	**Endemic level of infections in target hosts** ($R_{0a} = 0$)
0.0137	42.848463	44.116446
0.0135	119.05511	110.00382
0.0131	309.27471	240.98572
$3.9 * 10^{-5}$	42.829717	42.808174
$3.9 * 10^{-6}$	4.3108369	42.959711

On the other hand, the endemic infection level in target hosts is nonlinearly influenced by the quarantine and culling rate, as shown in Table 5.2. This nonlinear relationship

highlights the complexity of disease dynamics and suggests that the effectiveness of control measures may vary depending on the specific epidemiological and ecological conditions. While these strategies may reduce the target host population and, consequently, the prevalence of infection, they may also increase the number of susceptible individuals due to density-dependent effects, potentially leading to a higher prevalence.

5.3 Stochastic Model

5.3.1 Model

We consider the spillover rate, β_{ra}, as a random variable and introduce the Black-Karasinski (BK) process to account for its stochastic nature [114]. The BK process is a well-established mean-reverting stochastic process that ensures nonnegative solutions, a critical property for preserving both the applicability and interpretability of the model. Specifically, the logarithm of the spillover rate, $\ln \beta_{ra}$, follows the dynamics described by the following SDE

$$d \ln \beta_{ra} = r_a \left(\ln \bar{\beta_{ra}} - \ln \beta_{ra} \right) dt + \sigma_{ra} dW_1 (t) ,$$

where $\ln \bar{\beta_{ra}}$ denotes the logarithm of the mean spillover rate, r_a represents the speed of adjustment to the mean $\ln \bar{\beta_{ra}}$, σ_{ra} is the noise volatility , and $W_1 (t)$ is a one-dimensional Wiener process. Specifically, the term $r_a \left(\ln \bar{\beta_{ra}} - \ln \beta_{ra} \right)$ represents the mean-reverting force, pulling the stochastic spillover rate back towards the mean $\ln \bar{\beta_{ra}}$. The last term

$\sigma_{ra} dW_1(t)$ governs the magnitude of random perturbations affecting the spillover rate. The asymptotic distribution of the logarithm of spillover rate follows a normal distribution, which yields

$$\ln \beta_{ra} \ \mathbb{N}\left(\ln \bar{\beta_{ra}}, \frac{\sigma_{ra}^2}{2r_a}\right).$$

By incorporating the stochastic nature of the spillover rate into the deterministic framework (5.1), we have the following SDE system

$$\begin{cases} dS_r = \Lambda_r dt - \beta_r I_r S_r dt - d_r S_r dt, \\ dI_r = \beta_r I_r S_r dt - d_r I_r dt - \mu_r I_r dt, \\ dS_a = \Lambda_a N_a (1 - \frac{N_a}{K_a}) dt - \beta_{ra} I_r S_a dt - \beta_a I_a S_a dt - c_a S_a dt, \\ dE_a = \beta_{ra} I_r S_a dt + \beta_a I_a S_a dt - \tau_a E_a dt - c_a E_a dt, \\ dI_a = \tau_a E_a dt - \gamma_a I_a dt - c_a I_a dt - \mu_a I_a dt, \\ dR_a = \gamma_a I_a dt - c_a R_a dt, \\ d\ln \beta_{ra} = r_a(\ln(\bar{\beta}_{ra}) - \ln \beta_{ra}) dt + \sigma_{ra} dW_1(t). \end{cases} \tag{5.8}$$

In this model, the transmission process among reservoir hosts remains deterministic,whereas stochastic fluctuations in spillover events introduce unpredictable variations in target infections over time. We now proceed to analyze the dynamical behavior of I_a.

5.3.2 Stochastic Bifurcation

Figure 5.1 illustrates the stationary distributions of infected target hosts under varying levels of noise volatility in the spillover rate. Each simulation result represents the expected

value computed from 1 000 independent runs. The corresponding statistical measures for these distributions are summarized in Table 5.3.

In the low-noise scenario, where the volatility is set to 0.08, the resulting distribution exhibits a normal shape, characterized by a central peak, near-zero skewness, and a kurtosis below 3 (Figure 5.1a). With an increase in the noise volatility, a notable shift in the distribution pattern occurs. An additional peak emerges on the right tail, implying a bimodal density with positive skewness (Figure 5.1b). Upon further escalation of volatility to a level of 1, the distribution transitions to a heavy-tailed unimodal form (Figure 5.1c), with both skewness and kurtosis coefficients exceeding those of the normal distribution (> 0.5 and > 3, respectively). Furthermore, in Figures 5.1b and 5.1c, the distribution is observed to be monotonically decreasing as I_a approaches zero.

Table 5.3: Statistics of stationary distributions under volatility.

Volatility	**Mean**	**Variance**	**Skewness**	**Kurtosis**
0.08	0.545124	0.0308167	0.152669	0.263932
0.45	0.564554	0.159145	0.819555	0.954708
1	0.7288	0.594339	2.23127	7.13865
4	20.4514	142.689	23.4486	647.705

Conversely, in high-volatility scenarios (Figure 5.1d), the kurtosis reaches an exceptionally high value of 647.705, highlighting the prevalence of extreme events and the substantial

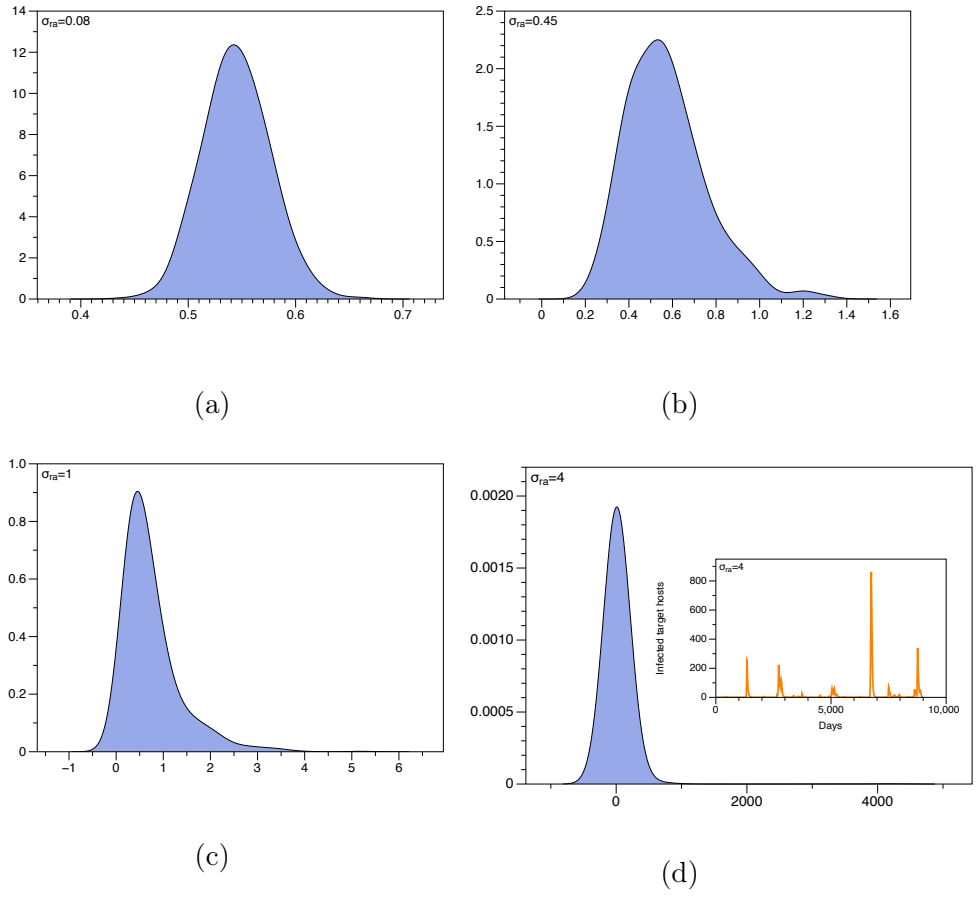

Figure 5.1: Stationary distributions of infected target hosts at the end time of simulations ($t = 9\ 000$) with different levels of volatility of spillover rate. The inner plot in (d) shows a sample path. The corresponding ODE stabilized at the endemic equilibrium with the infections reaching a value 0.54. Used values of parameters are $R_{0r} = 6.15$, $R_{0a} = 0.16$, $\bar{\beta_{ra}} = 3.42 * 10^{-10}$, and $r_a = 0.0081$.

uncertainty associated with large deviations. As depicted in the inner plot of Figure 5.1d, where the sample path of infected target hosts is plotted, multiple outbreaks are evident.

Furthermore, we observe that the distribution is monotonically increasing to a peak value as I_a tends to zero in Figure 5.1d.

In summary, the plots not only illustrate an increase in infections with higher volatility but also reveal the presence of stochastic P-bifurcation.

5.4 Conclusions

To analyze the spillover dynamics of monkeypox from reservoir hosts to target hosts in stage III, we extended the model presented in Chapter 4 by incorporating intraspecific transmission within target hosts. We also introduced an exposed class for target hosts. We started with analyzing the deterministic model and subsequently introduced stochasticity in the spillover rate.

For the ODE model, we developed a population extinction threshold and detected a maximum spillover threshold, as analyzed in Chapter 4. Our deterministic results imply that the existence of endemic equilibrium is independent of intraspecific transmission among target hosts but is primarily governed by the spillover rate and intraspecific transmission within reservoir hosts. This supports previous results that zoonotic spillover, where pathogens jump from animals to humans, plays a more prominent role than intraspecific transmission within the human population [277].

Moreover, our results demonstrate that quarantine and culling, as target host control strategies, are ineffective for disease control and mitigation. This is because, in a reservoir-

target system in stage III transmission, the basic reproduction number of the reservoir hosts is the primary determinant of whether an endemic equilibrium can be sustained and is not influenced by target host control strategies. Additionally, variations in quarantine and culling rates induce nonlinear changes in the endemic infection levels among target hosts, further complicating disease management.

Our stochastic analysis underscores the necessity of incorporating environmental stochasticity into spillover dynamics, particularly given the emergence of P-bifurcation. The stochasticity not only results in an increase in outbreaks among target hosts but also heightens the likelihood of recurrent outbreaks.

6 Reservoir Control Strategies for Mitigating Cross-Species Transmission of Monkeypox

6.1 Introduction

To effectively mitigate the spread of disease in target hosts, management strategies often involve reservoir control measures such as quarantine and culling of reservoir hosts [178, 278]. Das et al. [175] formulated a coupled pig–human transmission model for Nipah virus within a commercial farming context to investigate the dynamics of disease spillover from pigs to humans. Their study incorporated selective culling of infected pigs as a control strategy and demonstrated both backward and Hopf bifurcation phenomena through analytical and numerical approaches. However, in cases where the wildlife reservoir lacks significant conservation value, mass culling—regardless of infection status and potentially to the extent of eradication—may be deemed an acceptable and pragmatic management strategy [177, 178].

The evaluation of mass culling as a reservoir host management strategy is both valu-

able and challenging [279]. Existing studies have demonstrated that such approaches can significantly reduce disease prevalence and mitigate associated risks to other populations [27, 189]. More recent research has compared the relative effctiveness of reservoir control and target control, suggesting that the impact of culling specific targets is comparable to that of reservoir culling [176]. On the other hand, Tchuenche and Bauch [174] developed an age-structured model for human monkeypox transmission, which included an animal infection model with logistic growth and constant mass culling strategies. Their findings revealed a paradoxical effect, whereby culling animal reservoirs could inadvertently increase the prevalence of monkeypox among human juveniles, a demographic more susceptible to infection than adults.

Furthermore, numerous studies have examined the effects of badger culling on limiting the spread of Mycobacterium bovis, the causative agent of bovine tuberculosis (TB), in cattle [178]. McCallum's work [27] highlighted contrasting results from badger culling: while large-scale culling can reduce disease risk in cattle, they may simultaneously increase spillover events around the edge of the culling zone. Another previous study employed a stochastic spatial model, contrasting the outcomes of culling on infected premises alone with neighborhood-wide culls [179]. The authors emphasized that immediate priority should focus on decreasing spillover rates.

The historical implementation of quarantine and culling of reservoir hosts has typically been reactive, initiated after outbreaks were detected in target populations [25, 225]. Preventive measures taken by animal owners included erecting mesh barriers around en-

closures to deter wild rodents from interacting with domestic animals or isolating infected individuals to limit transmission. In addition, culling of reservoir hosts was carried out, accompanied by the proper disposal of carcasses to minimize further risks. The effectiveness and extent of these interventions were largely determined by the level of awareness and the robustness of surveillance systems monitoring target outbreaks. Accordingly, we model quarantine and culling efforts for reservoir hosts as a function of the number of infections in target populations and explore how interactions between spillover events and these control measures influence disease dynamics.

In this study, we present deterministic modeling frameworks to describe the transmission dynamics of monkeypox in stagets II to IV using a two-species epidemiological model. We compare the basic properties of the model without reservoir control to those of models incorporating reservoir control strategies. A detailed analysis is conducted to determine the equilibrium states, and we further investigate the occurrence of saddle-node and Hopf bifurcations in models with reservoir control strategies. From this analysis, we derive threshold values that capture the combined effects of viral circulation within both host species, spillover events, and the impact of quarantine and culling strategies on host populations and disease persistence. These thresholds offer critical insights into the risks associated with emerging infectious diseases within a One Health context. Additionally, the proposed modeling framework is adaptable for studying other cross-species disease systems.

6.2 Model

6.2.1 Spillover of Monkeypox

We select *Funisciurus* spp. as a representative of reservoir hosts for monkeypox (denoted by subscript r). Susceptible species, particularly *Cercopithecus* spp., capable of being infected by *Funisciurus* spp., are identified as target hosts (denoted by subscript a). The total population of hosts (N_r and N_a) is categorized into two distinct classes: susceptible (S_r and S_a) and infected (I_r and I_a), such that $N_r = S_r + I_r$ and $N_a = S_a + I_a$. Infected individuals may exhibit symptoms such as fever, lethargy, and reduced appetite, which can adversely impact reproductive capabilities. Consequently, we assume that the disease suppresses mating behaviors [227] and model the growth of susceptible hosts using a logistic growth framework [280].

Susceptible reservoir hosts can acquire infection through contact with infected reservoir hosts [36, 52, 246]. We denote β_r as the transmission rate among reservoir hosts and assume a bilinear incidence. Target hosts can be infected through two types of transmission: a) spillover (at a rate β_{ra} [45, 143, 248, 249]); and b) intraspecific transmission (at a rate β_a [24, 44, 48, 250, 251]). Based on these considerations, we define our model incorporating

spillover dynamics as follows

$$\begin{cases} S_r' &= \Lambda_r S_r \left(1 - \dfrac{S_r}{K_r}\right) - \beta_r I_r S_r, \\ I_r' &= \beta_r I_r S_r - \mu_r I_r, \\ S_a' &= \Lambda_a S_a \left(1 - \dfrac{S_a}{K_a}\right) - \beta_{ra} I_r S_a - \beta_a I_a S_a, \\ I_a' &= \beta_{ra} I_r S_a + \beta_a I_a S_a - \mu_a I_a. \end{cases} \tag{6.1}$$

The model variables and parameters are summarized in Table 6.1. The spillover initial conditions of system (6.1) yields

$$S_r(0) = S_{r0},\ I_r(0) = I_{r0},\ S_a(0) = S_{a0},\ I_a(0) = 0.$$

We observe that the model (6.1) is decoupled. In the absence of target hosts, the subsystem consisting solely of reservoir hosts exhibits a disease-free equilibrium $(K_r, 0)$. The local stability of this equilibrium is determined by the basic reproduction number, $R_{0r} = \frac{K_r \beta_r}{\mu_r}$ [97]. Similarly, the subsystem for target hosts, in the absence of spillover from reservoir hosts, exhibits a disease-free equilibrium $(K_a, 0)$. The local stability of this equilibrium is governed by the basic reproduction number $R_{0a} = \frac{\beta_a K_a}{\mu_a}$.

6.2.2 Quarantine and Culling of Reservoir Hosts

To mitigate the monkeypox outbreaks, rodents susceptible to monkeypox should be quarantined or culled [225, 226], a strategy effectively implemented during the 2003 outbreaks [25]. We assume that the quarantine period is sufficiently long to ensure that no

uninfected target hosts remain. Consequently, the effects of quarantine and culling are considered equivalent in terms of their impact on epidemic control.

Table 6.1: Model variables and parameters. In the model, $i = r$ or a represents the reservoir and target hosts, respectively.

Notation	**Description**
$S_i(t)$	Number of susceptible hosts on day t
$I_i(t)$	Number of infected hosts on day t
Λ_i	Intrinsic birth rate
K_i	Maximal carrying capacity
β_i	Intraspecific transmission rate
β_{ra}	Spillover rate from reservoir hosts to target hosts
c_r	Scaled quarantine and culling rate based on testing policy
μ_i	Removal rate due to recovery or death

In our model, the quarantine and culling of the reservoir population occurs at a per capita rate $p_r(I_a) \in [0, 1]$, which implies that quarantine and culling occurs at unit time intervals, leading to $\frac{1}{p_r(I_a)}$ quarantined hosts or culls during the average lifetime of a reservoir host in the presence of the target infections [184]. This quarantine and culling rate depends on I_a, as we assume that mass quarantine and culling of reservoir hosts are implemented only after infections in the target host population are detected. Specifically, we set

$p_r(0) = 0$, indicating no quarantined hosts or culls in the absence of confirmed target hosts. We further assume that $p_r' \geq 0$ for $I_a \geq 0$, signifying that quarantine and culling efforts may increase, decrease, or exhibit non-monotonic behavior in response to the number of infected target hosts I_a. Consequently, our model incorporating spillover, quarantine, and culling is given by

$$\begin{cases} S_r' &= \Lambda_r S_r \left(1 - \dfrac{S_r}{K_r}\right) - \beta_r I_r S_r - p_r(I_a) S_r, \\ I_r' &= \beta_r I_r S_r - \mu_r I_r - p_r(I_a) I_r, \\ S_a' &= \Lambda_a S_a \left(1 - \dfrac{S_a}{K_a}\right) - \beta_{ra} I_r S_a - \beta_a I_a S_a, \\ I_a' &= \beta_{ra} I_r S_a + \beta_a I_a S_a - \mu_a I_a. \end{cases} \tag{6.2}$$

There are two possible forms for the function $p_r(I_a)$. The first approach assume a simple linear relationship between p_r and I_a, which is valid when I_a remains relatively small. Specifically, we define $p_r(I_a) = \frac{c_0 q_a I_a}{N_a}$, where q_a represents the diagnose rate of target hosts, and c_0 is a coefficient that reflects changes in the quarantine and culling rate based on the proportion of newly confirmed target hosts. For simplicity, we introduce $c_r = \frac{c_0 q_a}{N_a}$ and refer to this as the scaled quarantine and culling rate based on testing policy [182]. Additionally, we assume $c_0 < \frac{1}{q_a}$ to ensure $c_r I_a < 1$.

Alternatively, a saturating function can be selected. Let C denote the half-saturation constant, which measures the efficiency of quarantine and culling strategy. Then, $p_r(I_a)$ can be modelled as $p_r(I_a) = c_r \dfrac{I_a}{C + I_a}$. This formulation captures the phenomenon where the quarantine and culling rate decreases as the infected host population grows sufficiently

large. In our work, we adopt the linear form and obtain the system

$$\begin{cases} S_r' &= \Lambda_r S_r \left(1 - \dfrac{S_r}{K_r}\right) - \beta_r I_r S_r - c_r I_a S_r, \\ I_r' &= \beta_r I_r S_r - \mu_r I_r - c_r I_a I_r, \\ S_a' &= \Lambda_a S_a \left(1 - \dfrac{S_a}{K_a}\right) - \beta_{ra} I_r S_a \ - \beta_a I_a S_a, \\ I_a' &= \beta_{ra} I_r S_a + \beta_a I_a S_a - \mu_a I_a. \end{cases} \tag{6.3}$$

The model (6.3) with c_r can be interpreted as a perturbation of model (6.1). The model variables and parameters are summarized in Table 6.1. The spillover initial conditions of system (6.3) yields

$$S_r(0) = S_{r0},\ I_r(0) = I_{r0},\ S_a(0) = S_{a0},\ I_a(0) = 0.$$

In the following, we begin by analyzing the fundamental properties of model (6.1), which includes the existence and stability of boundary and endemic equilibria. We then extend this analysis to model (6.3), comparing the results between the two models. Subsequently, we proceed with numerical analyses of the dynamics and bifurcations of model (6.3), offering critical insights into the effects of spillover processes and the implementation of quarantine and culling strategies.

6.3 Model Analysis and Dynamics

6.3.1 Model without Reservoir Control Strategies

Existence of Boundary Equilibria and Basic Reproduction Number

The system (6.1) exhibits several types of equilibria. First, it has a trivial equilibrium $(0, 0, 0, 0)$, which corresponds to the complete extinction of all populations and the absence of disease. Second, there exists a reservoir-population-only equilibrium $(K_r, 0, 0, 0)$, where the reservoir population persists without disease, while the target population is entirely absent. Third, a target-population-only equilibrium $(0, 0, K_a, 0)$ exits, representing the absence of the reservoir population and a disease-free state within the target population. Fourth, a disease-free equilibrium $(K_r, 0, K_a, 0)$ exists, wherein both population are present but remain free of disease.

If $R_{0r} > 1$, the system attains a reservoir-disease-only equilibrium $\left(\frac{\mu_r}{\beta_r}, \frac{\Lambda_r(K_r\beta_r - \mu_r)}{K_r\beta_r^2}, 0, 0\right)$. This equilibrium indicates that the disease becomes endemic within the reservoir population, while the target population remains absent due to infection.

Similarly, if $R_{0a} > 1$, the system has a target-disease-only equilibrium $\left(0, 0, \frac{\mu_a}{\beta_a}, \frac{\Lambda_a(K_a\beta_a - \mu_a)}{K_a\beta_a^2}\right)$, where the disease becomes established in the target population, with no reservoir population due to infection, quarantine, and culling.

Additionally, if $R_{0a} > 1$, the system has another boundary equilibrium $\left(K_r, 0, \frac{\mu_a}{\beta_a}, \frac{\Lambda_a(K_a\beta_a - \mu_a)}{K_a\beta_a^2}\right)$, named as reservoir-disease-free. This equilibrium indicates the disease eradication in the reservoir hosts while it becomes established in the target hosts.

The local stability of $(K_r, 0, K_a, 0)$ is governed by the basic reproduction number R_0, which can be calculated using the Next Generation Matrix method [97]

$$R_0 = \max\{R_{0r},\ R_{0a}\}. \tag{6.4}$$

Stability of Boundary Equilibria

Proposition 6.3.1. *For the system (6.1), we have the following results*

(1) The trivial equilibrium, the reservoir-population-only equilibrium $(K_r, 0, 0, 0)$ *and the target-population-only equilibrium* $(0, 0, K_a, 0)$ *are unstable.*

(2) The disease-free equilibrium $(K_r, 0, K_a, 0)$ *is locally asymptotically stable if* $R_{0r} < 1$ *and* $R_{0a} < 1$.

(3) When $R_{0r} > 1$, *the reservoir-disease-only equilibrium* $\left(\frac{\mu_r}{\beta_r}, \frac{\Lambda_r(K_r\beta_r - \mu_r)}{K_r\beta_r^2}, 0, 0\right)$ *is unstable if* $\beta_{ra} < \frac{\Lambda_a\beta_r R_{0r}}{\Lambda_r(R_{0r}-1)}$ *and locally asymptotically stable if* $\beta_{ra} > \frac{\Lambda_a\beta_r R_{0r}}{\Lambda_r(R_{0r}-1)}$.

(4) When $R_{0a} > 1$, *the target-disease-only equilibrium* $\left(0, 0, \frac{\mu_a}{\beta_a}, \frac{\Lambda_a(K_a\beta_a - \mu_a)}{K_a\beta_a^2}\right)$ *is unstable.*

(5) When $R_{0a} > 1$ *and* $R_{0r} < 1$, *the reservoir-disease-free equilibrium* $\left(K_r, 0, \frac{\mu_a}{\beta_a}, \frac{\Lambda_a(K_a\beta_a - \mu_a)}{K_a\beta_a^2}\right)$ *is locally asymptotically stable.*

This analysis provides critical insights into population dynamics within the disease transmission system. The instability of the reservoir-population-only equilibrium $(K_r, 0, 0,$

0) and the target-population-only equilibrium $(0, 0, K_a, 0)$ indicates that it is impossible for one population to remain unaffected by the disease while the other population goes extinct.

The stability of disease-free equilibrium $(K_r, 0, K_a, 0)$ implies that disease eradication in both populations requires R_{0r} and R_{0a} to be less than one, provided that the initial sizes of the subpopulations are within the basin of attraction of this equilibrium.

For the reservoir-disease-only equilibrium $\left(\frac{\mu_r}{\beta_r}, \frac{\Lambda_r(K_r\beta_r-\mu_r)}{K_r\beta_r^2}, 0, 0\right)$, given the persistence of the disease in the reservoir population and weak spillover (i.e. $\beta_{ra} < \frac{\Lambda_a\beta_r R_{0r}}{\Lambda_r(R_{0r}-1)}$), the target population will be affected but will not go extinct due to the infection. However, when the spillover is strong (i.e. $\beta_{ra} > \frac{\Lambda_a\beta_r R_{0r}}{\Lambda_r(R_{0r}-1)}$), the possibility of target population extinction arises, particularly if the initial subpopulation sizes fall within the basin of attraction of this equilibrium. This highlights the critical role of spillover strength in determining the outcome of disease dynamics, with stronger spillover transmission leading to more deadly consequences for the target population.

The stability of target-disease-only equilibrium $\left(0, 0, \frac{\mu_a}{\beta_a}, \frac{\Lambda_a(K_a\beta_a-\mu_a)}{K_a\beta_a^2}\right)$ and reservoir-disease-free equilibrium $\left(K_r, 0, \frac{\mu_a}{\beta_a}, \frac{\Lambda_a(K_a\beta_a-\mu_a)}{K_a\beta_a^2}\right)$ indicate that once the disease becomes endemic in the target population, the extinction of the reservoir population is impossible. However, disease extinction in the reservoir host population remains feasible when $R_{0r} < 1$. This implies that while the disease may persist in target hosts, effective control strategies can facilitate its eradication in the reservoir population.

Spillover Extinction Threshold

We define $R^* = \frac{\Lambda_r\beta_{ra}}{\Lambda_a\beta_r}\frac{R_{0r}-1}{R_{0r}}$ as the spillover extinction threshold which quantifies the risk

of extinction of the target host population due to spillover transmission. This threshold can be interpreted as follows. The factor $\frac{R_{0r}-1}{R_{0r}}$ accounts for the effect of sustained transmission within the reservoir population, signifying a key condition for disease spillover. This is further adjusted by an adjustment $\frac{\Lambda_r \beta_{ra}}{\Lambda_a \beta_r}$, which represents the relative strength of the spillover transmission rate compared to the internal transmission rate within the reservoir population, weighted by the respective population growth rates.

When this threshold exceeds one, the target population faces a significant risk of extinction due to spillover transmission. It has been observed that a high birth rate in the reservoir population, or a low birth rate in the target population, coupled with an elevated spillover rate, can drive the target population towards extinction. Additionally, this extinction threshold is independent of disease-related factors within the target host population [133]. In summary, this threshold provides a critical measure to assess the conditions under which spillover transmission from the reservoir to the target population becomes dangerous enough to threaten the survival of the target species.

Existence and Stability of a Unique Endemic Equilibrium

To obtain the endemic equilibrium, we set the right hand sides in system (6.1) equal to zero and obtain

$$S_r = \frac{\mu_r}{\beta_r},\ S_a = \frac{\mu_a I_a}{\beta_{ra} I_r + \beta_a I_a},\ I_r = \frac{(R_{0r}-1)\Lambda_r \mu_r}{K_r \beta_r^2}.$$

The coordinate I_a is determined as the solution of the following parabolic equation

$$f(I_a) = \bar{a}_2 I_a^2 + \bar{a}_1 I_a + \bar{a}_0, \tag{6.5}$$

where

$$\begin{aligned}
\bar{a}_2 &= -K_r^2\beta_a^2\beta_r^4 K_a \leq 0,\\
\bar{a}_1 &= \left(K_r\Lambda_a\mu_a(R_{0a}-1)\beta_r^2 - 2K_a\Lambda_r\beta_a\beta_{ra}\mu_r(R_{0r}-1)\right)K_r\beta_r^2,\\
\bar{a}_0 &= (1-R^*)\,(R_{0r}-1)\mu_r K_r\Lambda_a\beta_r^2\beta_{ra}\Lambda_r K_a.
\end{aligned}$$

We denote the discriminant of equation (6.5) as $\bar{\Delta}$, which yeilds

$$\bar{\Delta} = (K_r\Lambda_a(K_a\beta_a-\mu_a)^2\beta_r^2 + 4K_a\Lambda_r\beta_a\beta_{ra}\mu_a(K_r\beta_r-\mu_r))K_r^3\beta_r^6\Lambda_a > 0.$$

Thus, when $R_{0r} > 1$ and $R^* < 1$, the system (6.1) exhibits a unique endemic equilibrium, represented as $\left(\frac{\mu_r}{\beta_r}, \frac{(K_r\beta_r-\mu_r)\Lambda_r}{K_r\beta_r^2}, \frac{(R_{0r}-1)\Lambda_r\mu_r}{K_r\beta_r^2}, I_{a1}\right)$, where

$$I_{a1} = \frac{(K_r\Lambda_a\mu_a(R_{0a}-1)\beta_r^2 - 2K_a\Lambda_r\beta_a\beta_{ra}\mu_r(R_{0r}-1))K_r\beta_r^2 + \sqrt{\bar{\Delta}}}{2K_r^2\beta_a^2\beta_r^4K_a}.$$

Furthermore, it can be verified that for the case $R^* \geq 1$, the coefficient $\bar{a}_1 < 0$, indicating the nonexistence of an endemic equilibrium.

Proposition 6.3.2. *The endemic equilibrium of system (6.1) is locally asymptotically stable when it exists.*

The above analyze indicates that the condition $R_{0r} > 1$ serves as a fundamental prerequisite for the existence of an endemic equilibrium in the system (6.1). This condition ensures the sustained presence of the disease within the reservoir population, thereby creating the potential for spillover into the target population. Furthermore, for population and disease persistence within the target hosts, the spillover extinction threshold $R^* < 1$ must be satisfied.

Notably, while the persistence of disease in the target population is independent of the basic reproduction number of the target population, R_{0a}, it does influence the endemic level of infection. This implies that although spillover-driven persistence is primarily governed by the spillover process and transmission dynamics within the reservoir population, the endemic disease burden in the target population remains shaped by the internal transmission dynamics within that population.

6.3.2 Model with Reservoir Control Strategies

Existence of Boundary Equilibria and Basic Reproduction Number

The system (6.3) with quarantine and culling strategies exhibits the same boundary equilibria as the system (6.1) without these strategies, except for the reservoir-disease-free equilibrium. For system (6.3), the reservoir-disease-free equilibrium is $\left(\frac{K_r(K_a\Lambda_r\beta_a^2-\Lambda_a c_r\mu_a(R_{0a}-1))}{K_a\Lambda_r\beta_a^2}, 0, \frac{\mu_a}{\beta_a}, \frac{\Lambda_a(K_a\beta_a-\mu_a)}{K_a\beta_a^2}\right)$ when $R_{0a} > 1$ and $c_r < \frac{K_a\Lambda_r\beta_a^2}{\Lambda_a\mu_a(R_{0a}-1)}$. This equilibrium indicates that quarantine and culling strategies lead to a reduction in the susceptible population within the reservoir hosts. Furthermore, a moderate level of intervention is necessary to avoid the extinction of the reservoir hosts.

The local stability of $(K_r, 0, K_a, 0)$ in system (6.3) is governed by the basic reproduction number R_0, which can be calculated using the Next Generation Matrix method [97]

$$R_0 = \max\{R_{0r},\ R_{0a}\}. \tag{6.6}$$

It is observed that the basic reproduction number remains unchanged when considering

quarantine and culling strategies. This is reasonable because, in our model, when there is no infection in the target population, no culling occurs; that is, $p_r(0) = 0$.

Stability of Boundary Equilibria

The Jacobian matrix of system (6.3) yields

$$J_5 = \begin{pmatrix} J_{11} & -\beta_r S_r & 0 & -c_r S_r \\ \beta_r I_r & \beta_r S_r - \mu_r - c_r I_a & 0 & -c_r I_r \\ 0 & -\beta_{ra} S_a & \Lambda_a \left(1 - \frac{S_a}{K_a}\right) - \frac{\Lambda_a S_a}{K_a} - \beta_{ra} I_r - \beta_a I_a & -\beta_a S_a \\ 0 & \beta_{ra} S_a & \beta_{ra} I_r + \beta_a I_a & \beta_a S_a - \mu_a \end{pmatrix},$$

where

$$J_{11} = \Lambda_r \left(1 - \frac{S_r}{K_r}\right) - \frac{\Lambda_r S_r}{K_r} - \beta_r I_r - c_r I_a.$$

Proposition 6.3.3. *For system (6.3), we have the following results*

(1) The trivial equilibrium, the reservoir-population-only equilibrium $(K_r, 0, 0, 0)$ *and the target-population-only equilibrium* $(0, 0, K_a, 0)$ *are unstable.*

(2) The disease-free equilibrium $(K_r, 0, K_a, 0)$ *is locally asymptotically stable if* $R_{0r} < 1$ *and* $R_{0a} < 1$.

(3) When $R_{0r} > 1$, *the reservoir-disease-only equilibrium* $\left(\frac{\mu_r}{\beta_r}, \frac{\Lambda_r(K_r\beta_r - \mu_r)}{K_r\beta_r^2}, 0, 0\right)$ *is unstable if* $R^* < 1$ *and locally asymptotically stable if* $R^* > 1$.

(4) When $R_{0a} > 1$ *and* $c_r > \frac{K_a\Lambda_r\beta_a^2}{\Lambda_a\mu_a(R_{0a}-1)}$, *the target-disease-only equilibrium* $\Big(0, 0, \frac{\mu_a}{\beta_a}, \frac{\Lambda_a(K_a\beta_a - \mu_a)}{K_a\beta_a^2}\Big)$ *is locally asymptotically stable.*

(5) Denote $c_1 \triangleq \frac{\beta_a^2 K_a \Lambda_r \mu_r (R_{0r}-1)}{(K_r\beta_r+\Lambda_r)(R_{0a}-1)\mu_a\Lambda_a}$. *When* $R_{0a} > 1$, $c_1 < c_r < \frac{K_a\Lambda_r\beta_a^2}{\Lambda_a\mu_a(R_{0a}-1)}$, *the reservoir-disease-free equilibrium* $\left(\frac{K_r(K_a\Lambda_r\beta_a^2-\Lambda_a c_r\mu_a(R_{0a}-1))}{K_a\Lambda_r\beta_a^2}, 0, \frac{\mu_a}{\beta_a}, \frac{\Lambda_a(K_a\beta_a-\mu_a)}{K_a\beta_a^2}\right)$ *is locally asymptotically stable.*

The stability of the boundary equilibria in system (6.3) — such as the trivial equilibrium, the reservoir-population-only equilibrium $(K_r, 0, 0, 0)$, the target-population-only equilibrium $(0, 0, K_a, 0)$, the disease-free equilibrium $(K_r, 0, K_a, 0)$, and the reservoir-disease-only equilibrium $\left(\frac{\mu_r}{\beta_r}, \frac{\Lambda_r(K_r\beta_r-\mu_r)}{K_r\beta_r^2}, 0, 0\right)$ — is same as their stability in system (6.1). However, the stability of the last two boundary equilibria, the target-disease-only equilibrium $\left(0, 0, \frac{\mu_a}{\beta_a}, \frac{\Lambda_a(K_a\beta_a-\mu_a)}{K_a\beta_a^2}\right)$ and the reservoir-disease-free equilibrium $\left(\frac{K_r(K_a\Lambda_r\beta_a^2-\Lambda_a c_r\mu_a(R_{0a}-1))}{K_a\Lambda_r\beta_a^2}, 0, \frac{\mu_a}{\beta_a}, \frac{\Lambda_a(K_a\beta_a-\mu_a)}{K_a\beta_a^2}\right)$, changes or requires additional constraints.

The target-disease-only equilibrium $\left(0, 0, \frac{\mu_a}{\beta_a}, \frac{\Lambda_a(K_a\beta_a-\mu_a)}{K_a\beta_a^2}\right)$ is locally unstable in system (6.1), but becomes stable in system (6.3) when $R_{0a} > 1$ and $c_r > \frac{K_a\Lambda_r\beta_a^2}{\Lambda_a\mu_a(R_{0a}-1)}$, indicating that the persistence of the disease in the target population, combined with aggressive quarantine and culling, can drive the reservoir population toward extinction if the initial sizes of the subpopulations are within the basin of attraction of this equilibrium.

In contrast, with a moderately aggressive level of quarantine and culling, such that $c_1 < c_r < \frac{K_a\Lambda_r\beta_a^2}{\Lambda_a\mu_a(R_{0a}-1)}$, the outbreak in the reservoir hosts can be controlled. This highlights that the stability of reservoir-disease-free equilibrium $\left(\frac{K_r(K_a\Lambda_r\beta_a^2-\Lambda_a c_r\mu_a(R_{0a}-1))}{K_a\Lambda_r\beta_a^2}, 0, \frac{\mu_a}{\beta_a}, \frac{\Lambda_a(K_a\beta_a-\mu_a)}{K_a\beta_a^2}\right)$ in system (6.3) is governed by the scaled quarantine and culling rate c_r, independent of the basic reproduction number of the reservoir hosts, R_{0r}, which is the

key determinant in system (6.1).

Existence and Number of Endemic Equilibria

For the endemic equilibrium of system (6.3), its coordinates satisfy

$$S_r = \frac{I_a c_r + \mu_r}{\beta_r}, \quad S_a = \frac{\mu_a I_a}{\beta_{ra} I_r + \beta_a I_a}.$$

The coordinates I_r and I_a are the intersections of the following curves

$$c_r \left(\beta_r K_r + \Lambda_r\right) I_a + \beta_r^2 K_r I_r - \Lambda_r \mu_r \left(R_{0r} - 1\right) = 0, \tag{6.7}$$

$$\left(\beta_a I_a + \beta_{ra} I_r\right)^2 K_a - \left(\beta_a I_a + \beta_{ra} I_r\right) \Lambda_a K_a + \mu_a \Lambda_a I_a = 0. \tag{6.8}$$

We express I_r in terms of I_a using equation (6.7), which gives

$$I_r = -\frac{(K_r\beta_r + \Lambda_r)c_r}{K_r\beta_r^2} I_a + \frac{(R_{0r} - 1)\Lambda_r\mu_r}{K_r\beta_r^2}. \tag{6.9}$$

This result indicates that for the endemic equilibrium to exist, the condition $R_{0r} > 1$ must hold, along with $I_a < \frac{(R_{0r}-1)\Lambda_r\mu_r}{(K_r\beta_r+\Lambda_r)c_r}$.

Substituting (6.9) into (6.8) yields the following hyperbolic form

$$f(I_a) = a_2 I_a^2 + a_1 I_a + a_0, \tag{6.10}$$

where

$$\begin{aligned}
a_2 &= -(K_r\beta_a\beta_r^2 - c_r(K_r\beta_r + \Lambda_r)\beta_{ra})^2 K_a \leq 0, \\
a_1 &= (K_r\beta_r + \Lambda_r)\beta_{ra}(2\Lambda_r(K_r\beta_r - \mu_r)\beta_{ra} - K_r\Lambda_a\beta_r^2)K_a c_r + K_r\beta_r^2(K_r\Lambda_a(K_a\beta_a - \mu_a)\beta_r^2 \\
&\quad -2K_a\Lambda_r\beta_a\beta_{ra}(K_r\beta_r - \mu_r)), \\
a_0 &= \left(1 - \tfrac{\Lambda_r\beta_{ra}(R_{0r}-1)}{\Lambda_a\beta_r R_{0r}}\right)(R_{0r} - 1)\mu_r K_r\Lambda_a\beta_r^2\beta_{ra}\Lambda_r K_a.
\end{aligned}$$

It is noticed that if $c_r = 0$, equation (6.10) becomes equation (6.5).

Case 1

When $c_r = \frac{K_r\beta_a\beta_r^2}{(K_r\beta_r+\Lambda_r)\beta_{ra}}$, the coefficient $a_2 = 0$. In this case, if the conditions $R^* < 1$ and $R_{0a} < \frac{1}{1-R^*}$ are satisfied, the system exhibits a unique endemic equilibrium $\check{E}$, where

$$\begin{aligned}\check{I}_a &= \frac{(1-R^*)\beta_{ra}\Lambda_r(R_{0r}-1)K_a\mu_r}{K_r\beta_r^2\mu_a},\\ \check{I}_r &= \frac{\Lambda_r\mu_r(R_{0r}-1)}{\beta_r^2K_r}\left(1-(1-R^*)\,R_{0a}\right).\end{aligned}$$

Case 2

When $c_r \neq \frac{K_r\beta_a\beta_r^2}{(K_r\beta_r+\Lambda_r)\beta_{ra}}$, we denote the discriminant of parabola (6.10) as Δ and collect in terms of c_r, which becomes

$$\Delta = r_2c_r^2 + r_1c_r + r_0, \tag{6.11}$$

where

$$\begin{aligned}r_2 &= \Lambda_a(K_r\beta_r+\Lambda_r)^2\beta_{ra}^2K_a^2 > 0,\\ r_1 &= 2(K_r\beta_r+\Lambda_r)K_a(-2\Lambda_r\beta_{ra}\mu_r(R_{0r}-1) - K_r\Lambda_a(R_{0a}-1)\beta_r^2)\mu_a\beta_{ra},\\ r_0 &= K_r\beta_r^2(K_r\Lambda_a(K_a\beta_a-\mu_a)^2\beta_r^2 + 4K_a\Lambda_r\beta_a\beta_{ra}\mu_a(K_r\beta_r-\mu_r)) > 0.\end{aligned}$$

We further denote the discriminant of Δ as Δ_c, given by

$$\Delta_c = 16(\Lambda_r\beta_{ra}(K_r\beta_r-\mu_r) - \Lambda_a\beta_r^2K_r)(R_{0r}-1)(K_r\beta_r+\Lambda_r)^2\beta_{ra}^3K_a^2\Lambda_r\mu_a^2\mu_r.$$

When $\Delta_c > 0$, then $\Delta = 0$ in (6.11) exhibits two roots, denoted by

$$c^{\pm} = \frac{-r_1+\sqrt{\Delta_c}}{2r_2}.$$

Case 2.1

If $R^* < 1$, then $a_0 > 0$. In this case, parabola (6.10) has a positive root, denoted by I_a^+, which is expressed as

$$I_a^+ = \frac{-a_1 + \sqrt{\Delta}}{2a_2}.$$

To ensure the positivity of I_r, we solve $f\left(\frac{(R_{0r}-1)\Lambda_r\mu_r}{(K_r\beta_r+\Lambda_r)c_r}\right)$, which yields

$$\begin{aligned} f\left(\frac{(R_{0r}-1)\Lambda_r\mu_r}{(K_r\beta_r+\Lambda_r)c_r}\right) = \quad & \frac{\beta_r^4 K_r^2(K_r\beta_r-\mu_r)\Lambda_r}{c_r^2(K_r\beta_r+\Lambda_r)^2}\left(\Lambda_a\mu_a(K_r\beta_r+\Lambda_r)(R_{0a}-1)c_r\right. \\ & \left.-K_a\Lambda_r\mu_r(R_{0r}-1)\beta_a^2\right). \end{aligned}$$

Hence, if $R_{0a} \leq 1$, it follows that $f\left(\frac{(R_{0r}-1)\Lambda_r\mu_r}{(K_r\beta_r+\Lambda_r)c_r}\right) < 0$, which guarantees the existence of a unique endemic equilibrium, E^+. Additionally, if $R_{0a} > 1$ and $c_r < c_1$, the positivity of E^+ is also ensured.

Case 2.2

If $R^* > 1$, then $a_0 < 0$ and $\Delta_c > 0$. Additionally, if $c_r < c^-$ or $c_r > c^+$, the discriminant $\Delta > 0$. We further determine the sign of a_1. We define c_2 as

$$c_2 \triangleq \frac{K_r\beta_r^2(K_r\Lambda_a(K_a\beta_a-\mu_a)\beta_r^2 - 2K_a\Lambda_r\beta_a\beta_{ra}(K_r\beta_r-\mu_r))}{(K_r\beta_r+\Lambda_r)\beta_{ra}(K_r\Lambda_a\beta_r^2 - 2\Lambda_r(K_r\beta_r-\mu_r)\beta_{ra})K_a}$$

Hence, if $c_r > c_2$, the coefficient a_1 is positive. Substituting c_2 into Δ yields

$$\Delta(c_2) = \frac{4(K_r\beta_r-\mu_r)(1-R^*)\mu_a^2\Lambda_r\Lambda_a^2\beta_{ra}\beta_r^6K_r^3}{(K_r\Lambda_a\beta_r^2 - 2\Lambda_r(K_r\beta_r-\mu_r)\beta_{ra})^2} < 0,$$

indicating $c^- < c_2 < c^+$. Therefore, if $c_r > c^+$, we have $a_1 > 0$ and $\Delta > 0$, implying parabola (6.10) has two positive roots $I_a^\pm$, where

$$I_a^- = \frac{-a_1 - \sqrt{\Delta}}{2a_2}.$$

To ensure the positivity of $I_r^{\pm}$, the conditions $f\left(\frac{(R_{0r}-1)\Lambda_r\mu_r}{(K_r\beta_r+\Lambda_r)c_r}\right) < 0$ and $f'\left(\frac{(R_{0r}-1)\Lambda_r\mu_r}{(K_r\beta_r+\Lambda_r)c_r}\right) < 0$ must be satisfied. As discussed above, the first condition $f\left(\frac{(R_{0r}-1)\Lambda_r\mu_r}{(K_r\beta_r+\Lambda_r)c_r}\right) < 0$ is always satisfied if $R_{0a} \leq 1$. If $R_{0a} > 1$, we further verify that $c^+ < c_1$. Therefore, if $R_{0a} > 1$ and $c^+ < c_r < c_1$, we have $\Delta > 0$ and $f\left(\frac{(R_{0r}-1)\Lambda_r\mu_r}{(K_r\beta_r+\Lambda_r)c_r}\right) < 0$.

Additionally, solving for $f'\left(\frac{(R_{0r}-1)\Lambda_r\mu_r}{(K_r\beta_r+\Lambda_r)c_r}\right)$ yields

$$f'\left(\frac{(R_{0r}-1)\Lambda_r\mu_r}{(K_r\beta_r+\Lambda_r)\,c_r}\right) = \frac{d_2c_r^2+d_1c_r+d_0}{c_r\,(K_r\beta_r+\Lambda_r)},$$

where

$$\begin{aligned} d_2 &= -K_a\beta_{ra}\Lambda_a(K_r\beta_r+\Lambda_r)^2, \\ d_1 &= (K_r\beta_r+\Lambda_r)(K_r\Lambda_a(K_a\beta_a-\mu_a)\beta_r^2+2K_a\Lambda_r\beta_a\beta_{ra}(K_r\beta_r-\mu_r)), \\ d_0 &= -2K_aK_r\Lambda_r\beta_a^2\beta_r^2\mu_r(R_{0r}-1). \end{aligned}$$

We denote $g(c_r) \triangleq d_2c_r^2+d_1c_r+d_0$ and its discriminant $\Delta_d = d_1^2-4d_2d_0$. The two roots of $g(c_r)=0$ when $\Delta_d > 0$ are

$$d_c^{\pm} = \frac{-d_1 \pm \Delta_d}{2d_2}.$$

It can be verified that $g(c^+) < 0$ and $g'(c^+) < 0$ when $R_{0a} \leq 1$, indicating $d_c^+ < c^+$. Therefore, if $R_{0a} \leq 1$ and $c_r > c^+$, the positivity of $I_r^{\pm}$ is guaranteed. For the case where $R_{0a} > 1$, the sign of g depends on the relative positions of c^+, c_1, and $d_c^{\pm}$, which is influenced by the spillover rate. Thus, a detailed analysis is omitted.

In summary, either if $R_{0a} \leq 1$ and $c_r > c^+$, or if $R_{0a} > 1$, $c^+ < c_r < c_1$, and $g(c_r) < 0$, the positivity of $I_r^{\pm}$ is ensured, indicating the system exhibits two positive endemic equilibrium $E^{\pm}$.

Conversely, if $R_{0a} > 1$ and $c_r \geq c_1$, then $\Delta > 0$ and $f\left(\frac{(R_{0r}-1)\Lambda_r\mu_r}{(K_r\beta_r+\Lambda_r)c_r}\right) \geq 0$, indicating the system exhibits a unique endemic equilibrium, E^-.

Moreover, if $-2\Lambda_r\beta_{ra}\mu_r(R_{0r}-1) - K_r\Lambda_a(R_{0a}-1)\beta_r^2 < 0$, then $r_1 < 0$, indicating that the equation $\Delta = 0$ has two positive roots $c^{\pm}$. As discussed above, $c^- < c_2$, and the existence of two endemic equilibria requires $c_r > c_2$. Therefore, only when $c_r = c^+$ does the discriminant $\Delta = 0$, causing the two endemic equilibria to coalesce into E^*, where

$$I_a^* = \frac{-a_1}{2a_2}.$$

Case 2.3

If $R^* = 1$, then $a_0 = 0$; additionally, the condition $\Delta = 0$ yield $c_r = -\frac{r_1}{2r_2} = \frac{(K_r\beta_r-\mu_r)(K_a\beta_a+\mu_a)\Lambda_r}{(K_r\beta_r+\Lambda_r)\Lambda_a K_a}$. In this case, solving the quadratic equation (6.10) yields a unique positive root I_a^+, which is

$$I_a^+ = \frac{(K_r\beta_r-\mu_r)\Lambda_r\Lambda_a((K_r\beta_r+\Lambda_r)\Lambda_a K_a c_r - (K_r\beta_r-\mu_r)(K_a\beta_a+\mu_a)\Lambda_r)}{(K_r\beta_a\beta_r^2 - c_r(K_r\beta_r+\Lambda_r)\beta_{ra})^2 K_a}.$$

We observe that I_a^+ is positive when $c_r > -\frac{r_1}{2r_2}$. Moreover, if $R_{0a} \leq 1$, it follows that $f\left(\frac{(R_{0r}-1)\Lambda_r\mu_r}{(K_r\beta_r+\Lambda_r)c_r}\right) < 0$, which guarantees the existence of a unique endemic equilibrium, E^+. On the other hand, if $R_{0a} > 1$ and $\frac{(K_r\beta_r-\mu_r)(K_a\beta_a+\mu_a)\Lambda_r}{(K_r\beta_r+\Lambda_r)\Lambda_a K_a} < c_r < c_1$, the positivity of E^+ is also ensured.

Theorem 6.3.4. *Assume $R_{0r} > 1$, we have the following results for system (6.3)*

1. *If $c_r = \frac{K_r\beta_a\beta_r^2}{(K_r\beta_r+\Lambda_r)\beta_{ra}}$, then the system has a unique endemic equilibrium $\check{E}$, provided that $R^* < 1$ and $R_{0a} < \frac{1}{1-R^*}$.*

2. *If* $c_r \neq \frac{K_r\beta_a\beta_r^2}{(K_r\beta_r+\Lambda_r)\beta_{ra}}$ *and* $R^* < 1$*, then the system has a unique endemic equilibrium* E^+*, provided that one of the following conditions is satisfied*

   a. $R_{0a} \leq 1$.

   b. $R_{0a} > 1$ *and* $c_r < c_1$.

3. *If* $c_r \neq \frac{K_r\beta_a\beta_r^2}{(K_r\beta_r+\Lambda_r)\beta_{ra}}$ *and* $R^* = 1$*, then the system has a unique endemic equilibrium* E^+*, provided that one of the following conditions is satisfied*

   a. $R_{0a} \leq 1$.

   b. $R_{0a} > 1 \quad$ *and* $\quad \frac{(K_r\beta_r-\mu_r)(K_a\beta_a+\mu_a)\Lambda_r}{(K_r\beta_r+\Lambda_r)\Lambda_a K_a} < c_r < c_1$.

4. *If* $c_r \neq \frac{K_r\beta_a\beta_r^2}{(K_r\beta_r+\Lambda_r)\beta_{ra}}$ *and* $R^* > 1$*, then the system has two endemic equilibria* $E^{\pm}$ *when* $c_r > c^+$*, provided that one of the following conditions is satisfied*

   a. $R_{0a} \leq 1$.

   b. $R_{0a} > 1$, $g(c_r) < 0$, *and* $c_r < c_1$.

   These two equilibria coalesce into E^* *if and only if* $c_r = c^+ > 0$.

5. *If* $c_r \neq \frac{K_r\beta_a\beta_r^2}{(K_r\beta_r+\Lambda_r)\beta_{ra}}$ *and* $R^* > 1$*, then the system has a unique endemic equilibrium* E^-*, provided that* $R_{0a} > 1$ *and* $c_r \geq c_1$.

This theorem indicates that when the spillover extinction threshold is less than one, the model with quarantine and culling strategies exhibits at most a unique endemic equilibrium, similar to the model without these strategies. However, it requires additional constraints on

the basic reproduction number of target hosts and the scaled quarantine and culling rate. This is reasonable, as large-scale quarantine measures and extensive culling of reservoir hosts can significantly reduce the reservoir population, disrupting the conditions necessary for the existence of an endemic equilibrium.

Moreover, when the spillover threshold equals or exceeds one, the model (6.1) without quarantine and culling strategies does not exhibit any endemic equilibria due to the widespread infection driving the target population towards extinction. However, with the implementation of these strategies, the system (6.3) can have up to two endemic equilibria. This requires a relative high quarantine and culling rate such that $c_r > c^+$, thereby effectively reducing the spillover source. If the basic reproduction number of target hosts also exceeds one, a moderate quarantine and culling strategies, such that $c_r < c_1$, becomes necessary to ensure the existence of these two equilibria. Beyond this threshold, only a single endemic equilibrium remains.

Stability of Endemic Equilibria

Theorem 6.3.5. *In system (6.3), the endemic equilibrium E^- is unstable if it exists. Conversely, if the endemic equilibrium E^+ exists, it is locally asymptotically stable provided that the following conditions are satisfied*

$$b_3 > 0,\ b_3b_2 - b_1 > 0,\ \textit{and}\ \ b_3b_2b_1 - b_3^2b_{01}b_{02} - b_1^2 > 0,$$

where b_i are the coefficients of the fourth-order equation (6.12).

Proof. Eigenvalues of the Jacobian matrix at the endemic equilibrium

$\left(\frac{I_a c_r+\mu_r}{\beta_r},\ I_r,\ \ \frac{\mu_a I_a}{\beta_{ra} I_r+\beta_a I_a}, I_a\right)$ are solutions of

$$\lambda^4 + b_3\lambda^3 + b_2\lambda^2 + b_1\lambda + b_{01}b_{02} = 0, \tag{6.12}$$

where

$$\begin{aligned} b_3 &= \frac{(b_{31}I_r + b_{30})}{\Lambda_a c_r(K_r\beta_r + \Lambda_r)}, \\ b_2 &= b_{22}I_r^2 + b_{21}I_r + b_{20}, \\ b_1 &= b_{13}I_r^3 + b_{12}I_r^2 + b_{11}I_r + b_{10}, \end{aligned}$$

with

$$\begin{aligned} b_{31} &= ((K_r\beta_{ra}(K_a\beta_a - \Lambda_a) - \Lambda_r\Lambda_a)\beta_r + \Lambda_r\beta_{ra}(K_a\beta_a - \Lambda_a))c_r - K_r\beta_a(K_a\beta_a - \Lambda_a)\beta_r^2, \\ b_{30} &= ((K_r\beta_r + \Lambda_r)\Lambda_a^2 + (\Lambda_r^2 + (-K_a\beta_a + \mu_a + \mu_r)\Lambda_r - K_r\beta_r(K_a\beta_a - \mu_a))\Lambda_a)c_r \\ &\quad +(K_a\beta_a - \Lambda_a)(K_r\beta_r - \mu_r)\Lambda_r\beta_a, \\ b_{22} &= -\frac{1}{(K_r\beta_r + \Lambda_r)^2\Lambda_a c_r^2}\Big(K_r^2(2K_a\beta_a^3 + \Lambda_a c_r^2)\beta_r^4 - K_r((K_aK_r\beta_a\beta_{ra} - \Lambda_a\Lambda_r)c_r \\ &\quad +4K_aK_r\beta_a^2\beta_{ra} + \Lambda_r\beta_a(K_a\beta_a - \Lambda_a))c_r\beta_r^3 + K_a\Lambda_r^2c_r^2\beta_{ra}^2(c_r + 2\beta_a) \\ &\quad +K_r(K_aK_rc_r^2\beta_{ra} + (2K_aK_r\beta_a\beta_{ra} - \Lambda_a\Lambda_r)c_r - 4K_a\Lambda_r\beta_a^2)\beta_{ra}c_r\beta_r^2 \\ &\quad +2\Lambda_r\left(K_aK_rc_r\beta_{ra} + 2\beta_{ra}K_a\beta_aK_r + \frac{\Lambda_r(K_a\beta_a - \Lambda_a)}{2}\right)\beta_{ra}c_r^2\beta_r\Big), \\ b_{21} &= \frac{1}{(K_r\beta_r + \Lambda_r)^2\Lambda_a c_r^2}\left(K_a\beta_{ra}\Lambda_a(K_r\beta_r + \Lambda_r)^2c_r^3 + 4K_aK_r\Lambda_r\beta_r^2(K_r\beta_r - \mu_r)\beta_a^3\right. \\ &\quad +3(K_r\beta_r + \Lambda_r)\left(\frac{\beta_{ra}(K_a\beta_a - \Lambda_a)\Lambda_r^2}{3} + \left(\frac{K_r\Lambda_a\beta_r^2}{3}\right.\right. \\ &\quad +\frac{(-\beta_{ra}K_a\beta_aK_r + \Lambda_a(K_a\beta_a - \Lambda_a - \mu_a))\beta_r}{3} + \left(\left(K_a\beta_a - \frac{\mu_a}{3} - \frac{\mu_r}{3}\right)\Lambda_a\right. \\ &\quad \left.\left.+\frac{2K_a\mu_r\beta_a}{3}\right)\beta_{ra}\right)\Lambda_r + K_r\left(\frac{\mu_r\beta_r}{3} + \left(K_a\beta_a - \frac{\mu_a}{3}\right)\beta_{ra}\right)\beta_r\Lambda_a\Big)c_r^2 \\ &\quad -4\beta_ac_r\left(\frac{3K_r^2\beta_r^3(K_a\beta_a - \frac{\mu_a}{3})\Lambda_a}{4} + \left(\frac{K_r(K_a\beta_a - \Lambda_a)\beta_r^2}{2}\right.\right. \end{aligned}$$

$$
\begin{aligned}
&+\left(\beta_{ra}K_a\beta_aK_r-\frac{\mu_r(K_a\beta_a-\Lambda_a)}{4}\right)\beta_r-\beta_{ra}K_a\mu_r\beta_a\Bigg)\Lambda_r^2\\
&+K_r\beta_r\Bigg(\left(\beta_{ra}K_a\beta_aK_r+\frac{(3K_a\beta_a-\mu_a-\mu_r)\Lambda_a}{4}+\frac{K_a\mu_r\beta_a}{4}\right)\beta_r\\
&-\beta_{ra}K_a\mu_r\beta_a\Bigg)\Lambda_r\Bigg)\Bigg),\\
b_{20}\;&=-\frac{1}{\left(K_r\beta_r+\Lambda_r\right)^2\Lambda_ac_r^2}\Bigg(2K_a\Lambda_r^2\left(K_r\beta_r-\mu_r\right)^2\beta_a^3\\
&-3c_rK_a\left(K_r\beta_r-\mu_r\right)\Lambda_r\Bigg(\left(K_r\beta_r+\Lambda_r\right)\Lambda_a+\frac{\left(\Lambda_r+\mu_r\right)\Lambda_r}{3}\Bigg)\beta_a^2\\
&+c_r\Lambda_a(c_r((K_r\beta_r+\Lambda_r)\Lambda_a+(\Lambda_r+\mu_r)\Lambda_r)(K_r\beta_r+\Lambda_r)K_a\\
&+(\Lambda_r^2+(\mu_a+\mu_r)\Lambda_r+K_r\beta_r\mu_a)(K_r\beta_r-\mu_r)\Lambda_r)\beta_a\\
&-c_r^2((\Lambda_r^2+(\mu_a+\mu_r)\Lambda_r+K_r\beta_r\mu_a)\Lambda_a\\
&+(\Lambda_r+\mu_r)\Lambda_r\mu_a)\Lambda_a(K_r\beta_r+\Lambda_r)\Bigg),\\
b_{13}\;&=\frac{1}{\left(K_r\beta_r+\Lambda_r\right)^3\Lambda_ac_r^2}\Bigg(c_r^3\beta_{ra}K_a\left(K_r\beta_r+\Lambda_r\right)^2\left(\beta_r+2\beta_{ra}\right)\left(K_r\beta_r+\Lambda_r\right)\beta_{ra}\\
&-2\beta_r\Bigg(K_r\Bigg(K_a\beta_a-\frac{\Lambda_a}{2}\Bigg)\beta_r^2+2K_aK_r\beta_a\beta_r\beta_{ra}-K_a\Lambda_r\beta_a\beta_{ra}\Bigg)\left(K_r\beta_r+\Lambda_r\right)^2\beta_{ra}c_r^2\\
&+\left(K_r\beta_r+\Lambda_r\right)\beta_aK_r\left(K_r\left(K_a\beta_a-\Lambda_a\right)\beta_r^2+2K_aK_r\beta_a\beta_r\beta_{ra}-4K_a\Lambda_r\beta_a\beta_{ra}\right)\beta_r^3c_r\\
&+2K_aK_r^2\Lambda_r\beta_a^3\beta_r^5\Bigg),\\
b_{12}\;&=\frac{1}{(K_r\beta_r+\Lambda_r)^3\Lambda_ac_r^2}\Bigg(-\left(\left(3\Lambda_a+\Lambda_r+\mu_r\right)\beta_{ra}+\Lambda_a\beta_r\right)K_a\left(K_r\beta_r+\Lambda_r\right)^3\beta_{ra}c_r^3\\
&+\Bigg(K_r\Lambda_a\left(K_a\beta_a-\Lambda_a-\mu_a\right)\beta_r^3+3\beta_{ra}\left(K_a\left(\Lambda_a+\Lambda_r+\frac{2\mu_r}{3}\right)\beta_a-\frac{\Lambda_a\left(\Lambda_r+\mu_r\right)}{3}\right)K_r\beta_r^2\\
&+4\Lambda_r\left(\beta_{ra}K_a\beta_aK_r-\frac{3\left(\Lambda_a+\frac{\mu_r}{3}\right)K_a\beta_a}{4}+\frac{\Lambda_a\mu_a}{4}\right)\beta_{ra}\beta_r-2\Lambda_rK_a\beta_a\beta_{ra}^2\left(\Lambda_r+3\mu_r\right)\Bigg)\\
&\cdot\left(K_r\beta_r+\Lambda_r\right)^2c_r^2-2\beta_r\left(K_r\beta_r+\Lambda_r\right)\Bigg(\left(\frac{\mu_r}{2}+\Lambda_r\right)K_r^2\left(K_a\beta_a-\Lambda_a\right)\beta_r^3+2\Lambda_rK_r\\
&\cdot\left(\beta_{ra}K_a\beta_aK_r-\frac{3\left(\Lambda_a+\frac{\mu_r}{3}\right)K_a\beta_a}{4}+\frac{\Lambda_a\left(\mu_a+\mu_r\right)}{4}\right)\beta_r^2-4\beta_{ra}K_aK_r\Lambda_r\beta_a\left(\Lambda_r+\mu_r\right)\beta_r\\
&+2K_a\beta_{ra}\Lambda_r^2\mu_r\beta_a\Bigg)\beta_ac_r-6\beta_r^3K_a\Lambda_r\beta_a^3\left(K_r\left(\Lambda_r\;+\frac{\mu_r}{3}\right)\beta_r-\frac{2\Lambda_r\mu_r}{3}\right)K_r\Bigg),
\end{aligned}
$$

$$
\begin{aligned}
b_{11} &= \frac{1}{\left(K_r\beta_r+\Lambda_r\right)^3\Lambda_a c_r^2}\Bigg(\Lambda_a\beta_{ra}\left(\Lambda_a \ + \ \Lambda_r \ +\mu_r\right)\left(K_r\beta_r+ \ \Lambda_r\right)^3 K_a c_r^3 - \ \left(K_r\beta_r \ + \ \Lambda_r\right)^2 \\
&\cdot\Bigg(\beta_{ra}\left(\left(-3K_a\beta_a+\mu_a\right)\Lambda_a+K_a\beta_a\left(K_r\beta_r \ -\mu_r\right)\right)\Lambda_r^2 \ + K_r\Lambda_a\mu_r\beta_r^2\left(K_a\beta_a-\Lambda_a-\mu_a\right) \\
&+\Bigg(-\beta_r\left(K_a\beta_a+ \ K_r\beta_r-\mu_a\right)\Lambda_a^2+\Big(K_r\left(K_a\beta_a-\mu_a\right)\beta_r^2 \\
&+3K_aK_r\beta_a\beta_r\beta_{ra}-6\beta_{ra}\mu_r\left(K_a\beta_a-\frac{\mu_a}{6}\right)\Big)\Lambda_a \ + \ K_a\mu_r\beta_a\beta_{ra} \\
&\left(K_r\beta_r-\mu_r\right)\Bigg)\Lambda_r\Bigg)c_r^2+\Bigg(2K_a\Lambda_r\Bigg(-3\beta_r\Bigg(K_r\left(\frac{\mu_r}{2} \ + \ \Lambda_r\right)\beta_r \\
&-\frac{\Lambda_r\mu_r}{2}\Bigg)\Lambda_a \ + \ \left(\frac{K_r\left(\Lambda_r \ +\mu_r\right)\beta_r^2}{2} \ + \ K_r\Lambda_r\beta_r\beta_{ra} \ - \ 2\beta_{ra}\left(\frac{3\mu_r}{2} \ + \ \Lambda_r\right)\Lambda_r\right) \\
&\cdot\left(K_r\beta_r-\mu_r\right)\Bigg)\left(K_r\beta_r \ + \ \Lambda_r\right)\beta_a^2-\Lambda_a\Bigg(K_r^2\left(\Lambda_r \ +\mu_r\right)\beta_r^2 \ - \ 2K_r\Bigg(\frac{\mu_r^2}{2} \\
&+\frac{\left(\Lambda_r \ +\mu_a\right)\mu_r}{2}+\Lambda_r\mu_a\Bigg)\beta_r+\Lambda_r\mu_a\mu_r\Bigg)\beta_r\Lambda_r\left(K_r\beta_r \ + \ \Lambda_r\right)\beta_a\Bigg)c_r \\
&+6\beta_r\Bigg(K_r\left(\Lambda_r+\frac{2\mu_r}{3}\right)\beta_r\frac{\Lambda_r\mu_r}{3}\Bigg)K_a\left(K_r\beta_r-\mu_r\right)\Lambda_r^2\beta_a^3\Bigg),
\end{aligned}
$$

$$
\begin{aligned}
b_{10} &= \frac{1}{\left(K_r\beta_r+\Lambda_r\right)^3\Lambda_a c_r^2}(-\Lambda_r(\Lambda_r \ +\mu_r)((K_r\Lambda_a\beta_r+\Lambda_a\Lambda_r)c_r \\
&-\beta_a(K_r\beta_r-\mu_r)\Lambda_r)(((K_a\beta_a-\mu_a)\Lambda_a\Lambda_r+K_r\beta_r\Lambda_a(K_a\beta_a-\mu_a))c_r \\
&-2K_a\Lambda_r\beta_a^2(K_r\beta_r-\mu_r))), \\
b_{01} &= \frac{\left(\beta_aI_a+\beta_{ra}I_r-\Lambda_a\right)\left(c_rI_a+\beta_rI_r-\Lambda_r\right)}{\Lambda_a\Lambda_r}>0, \\
b_{02} &= -\frac{a_2I_r\left(I_r+\frac{a_1}{2a_2}\right)}{2K_a\beta_a^2c_r\left(K_r\beta_r+\Lambda_r\right)}.
\end{aligned}
$$

It is noticed that $I_r=-\frac{a_1}{2a_2}$ represents the axis of symmetry of parabola (6.10), so we obtain $b_{02}(I_r^+)>0$ and $b_{02}(I_r^-)<0$. Hence, the equilibrium E^- is locally unstable [275]. Furthermore, if the conditions $b_3>0$, $b_3b_2-b_1>0$, and $b_3b_2b_1-b_3^2b_{01}b_{02}-b_1^2>0$ are satisfied, the endemic equilibrium E^+ is locally stable [281]. □

Hopf Bifurcation

Lemma 6.3.1. *Equation (6.12) exhibits a pair of pure imaginary roots alongside two roots possessing non-zero real parts if and only if one of the following conditions, denoted as A or B, is satisfied:*

A. $b_3 b_1 > 0, b_{01} b_{02} \neq 0,$ *and* $b_3 b_2 b_1 - b_3^2 b_{01} b_{02} - b_1^2 = 0.$

B. $b_3 = 0, b_1 = 0,$ *and* $b_{01} b_{02} < 0.$

Furthermore, Equation (6.12) has a pair of pure imaginary roots and two roots with negative real parts if and only if the following condition, referred to as Condition C, is satisfied:

C. $b_3 > 0, b_1 > 0, b_{01} b_{02} > 0,$ *and* $b_3 b_2 b_1 - b_3^2 b_{01} b_{02} - b_1^2 = 0.$

Theorem 6.3.6. *Let* φ^* *represent a parameter set that satisfies the properties outlined in conditions A, B, or C. If* $\left.\frac{d\mathrm{Re}\lambda(\varphi)}{d\varphi}\right|_{\varphi=\varphi^*} \neq 0,$ *where* $\mathrm{Re}\lambda(\varphi)$ *is the real part of* $\lambda(\varphi)$*, then a Hopf bifurcation occurs at the parameter* φ^* *[273].*

It is noticed a Hopf bifurcation may occur at E^+ when either condition A or condition B in Theorem 6.3.6 is satisfied. Additionally, a Hopf bifurcation may also occur at E^- when either condition A or condition C holds.

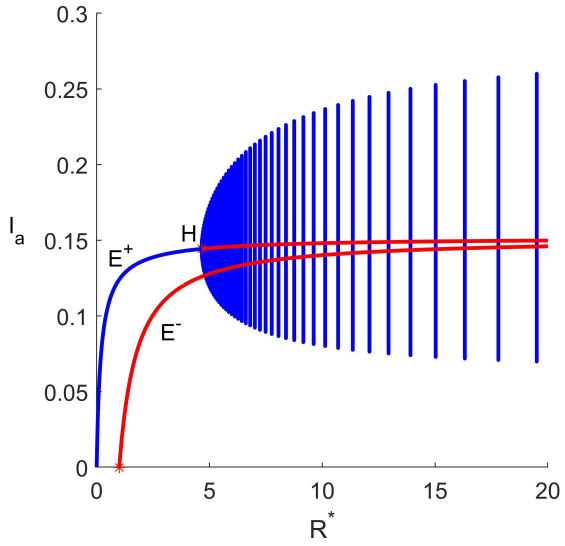
0.3
0.25
0.2
0.15
0.1
0.05
0
I_a
E+
H
E-
0
5
10
15
20
R*

(a) $c_r = 0.4$

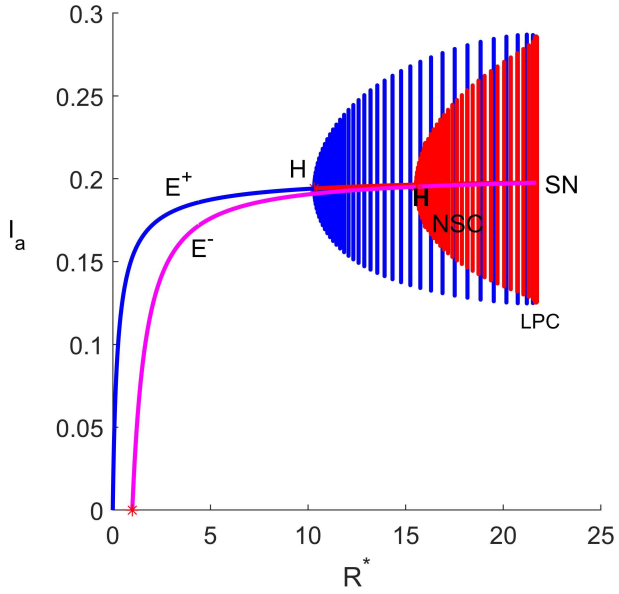
0.3
0.25
0.2
0.15
0.1
0.05
0
I_a
E+
H
H
SN
NSC
E-
LPC
0
5
10
15
20
25
R*

(b) $c_r = 0.3$

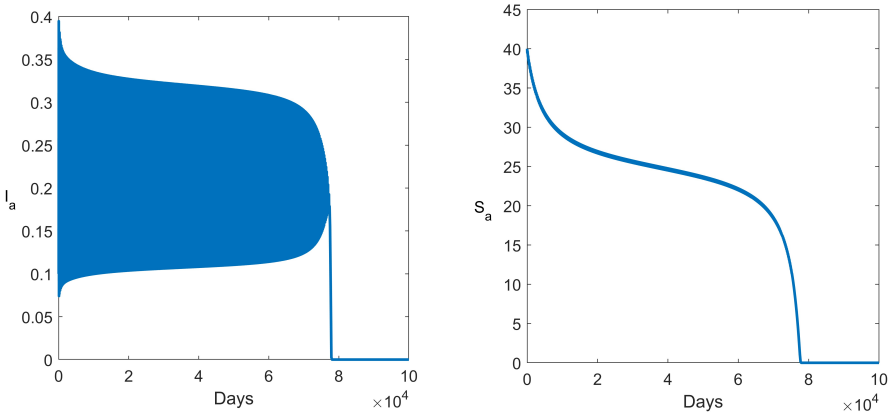

(c) $c_r = 0.3, R^* = 40$ (d) $c_r = 0.3, R^* = 40$

Figure 6.1: (a-b) bifurcation diagrams in (R^*, I_a) plane and (c-d) system solutions. In panel (a), a forward bifurcation occurs at $R^* = 1$. The stability of E^+ transitions from stable (blue line) to unstable (red line) as R^* increases, while E^- is always unstable (red line). Additionally, a stable limit cycle (blue line) bifurcates from supercritical Hopf bifurcation on E^+. In panel (b), a forward occurs at $R^* = 1$ and a saddle-node bifurcation (SN) occurs at $R^* = 21.67$. The stability of E^+ transitions from stable (blue line) to unstable (red line) as R^* increases, while E^- is always unstable (magenta line) when it exits. A stable limit cycle (blue line) bifurcates from supercritical Hopf bifurcation on E^+ while an unstable limit cycle (red line) bifurcates from subcritical Hopf bifurcation on E^-. These two limit cycles collide at the limit point cycle (LPC). The parameters are set as $R_{0r} = 5.82$ and $R_{0a} = 0.086$.

6.4 Simulations

6.4.1 Spillover Processes and Reservoir Control Strategies Shape System Dynamics

Given the basic reproduction number in the reservoir set to the supercritical regime, i.e. $R_{0r} > 1$, we conduct the following simulations. In Figure 6.1, we set $R_{0a} < 1$ and plot the bifurcation diagram in (R^*, I_a) plane by perturbing the spillover rate under different values of c_r. For the selected parameter values, we calculated $c^+ = 0.3$, which represents the minimum quarantine and culling rate required to ensure the existence of two endemic equilibria when the spillover rate is high, such that $R^* > 1$.

When $c_r = 0.4$, under a low spillover rate such that $R^* < 1$, the system stabilizes at a unique endemic equilibrium E^+ (Figures 6.1a and 6.1b). As the spillover rate increases, the system transitions to presenting two coexistence equilibria $E^{\pm}$, where E^- is unstable. With further increase in the spillover rate, the system undergoes a Hopf bifurcation (Figure 6.1a), accompanied by the instability of the equilibrium E^+ and the stabilization of the system into a limit cycle. Moreover, the limit cycle expands to encompass both equilibria as the spillover rate increases. Additionally, since $c_r > c^+$, the discriminant Δ remains positive, indicating that these two equilibria do not collide.

We subsequently examine the case where the scaled quarantine and culling rate, c_r is 0.3, as depicted in Figure 6.1b. Two endemic equilibria exist when $R^* \in (1, 21.67)$. A saddle-node bifurcation occurs when the two equilibria collide. Furthermore, a stable limit

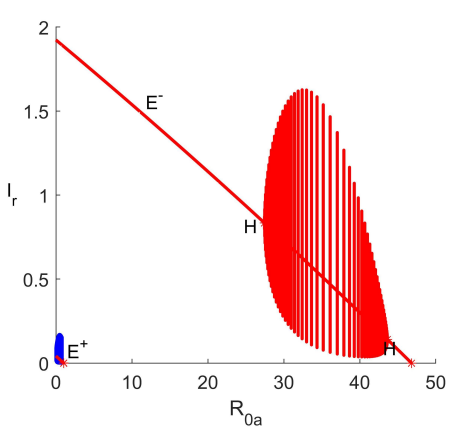

(a) $R^* = 12.35$

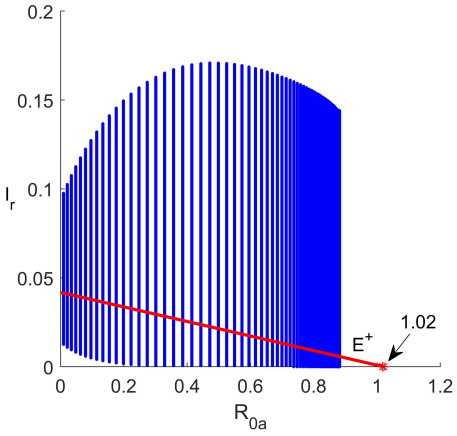

(b) $R^* = 12.35$

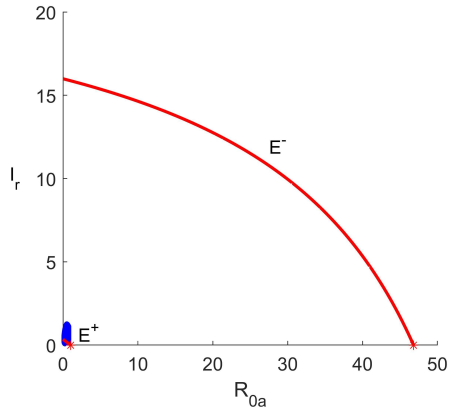

(c) $R^* = 1.49$

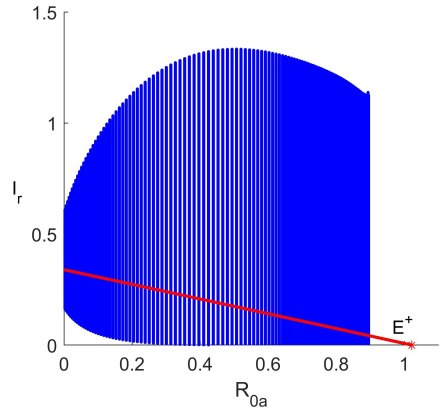

(d) $R^* = 1.49$

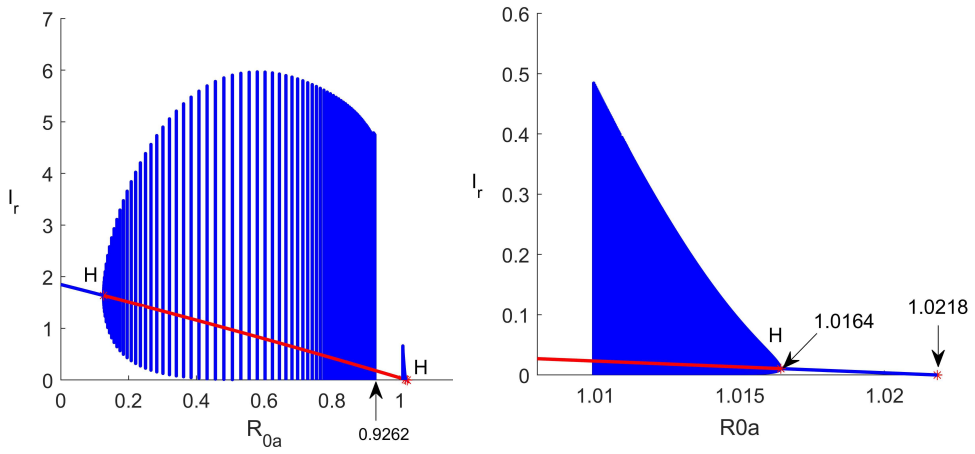

(e) $R^* = 0.26$ (f) $R^* = 0.26$

Figure 6.2: Bifurcation diagram in (R_{0a}, I_r) plane under different R^*. The point LPC represents the limit point of a limit cycle. Panels (a), (c), and (e) illustrate the bifurcation structure over a wide range of R_{0a} values, whereas panels (b), (d), and (f) provide a detailed view of the region where R_{0a} is close to one. The parameters are set to $c_r = 0.3$ and $R_{0r} = 5.82$.

cycle bifurcates from a supercritical Hopf bifurcation at E^+, while an unstable limit cycle emerges from a subcritical Hopf bifurcation at E^-. These two cycles eventually collide at the limit point of cycles (LPC).

Furthermore, in the case of a non-significant spillover rate where two endemic equilibria coexist, a comparison of Figures 6.1a and 6.1b reveals that increasing the scaled quarantine and culling rate either decreases the equilibrium prevalence in the target hosts or reduces

the peak value of the periodic prevalence.

In the case of a significant spillover rate with $c_r = 0.3$, we present the dynamics of the susceptible and infected target hosts in Figures 6.1c and 6.1d. The results reveal that the solution initially oscillates around an endemic level before eventually approaching the boundary point $\left(\frac{\mu_r}{\beta_r}, \frac{\Lambda_r(K_r\beta_r - \mu_r)}{K_r\beta_r^2}, 0, 0\right)$. This outcome indicates the extinction of the target population due to spillover infection.

6.4.2 Effects of Spillover Processes and Target-to-target Transmission

The bifurcation diagram is depicted in the (R_{0a}, I_r) plane by perturbing the target-to-target transmission rate under different spillover rates, as shown in Figure 6.2. Phase portraits corresponding to selected values of R^* and R_{0a} are provided in Figure 6.3. Magnified views of specific regions in Figures 6.2a, 6.2c, and 6.2e are presented in Figures 6.2b, 6.2d, and 6.2f, respectively. In the (R_{0a}, I_r) plane, it is observed that E^- is positioned above E^+ when they coexist, as shown in Figures 6.2a and 6.2c.

When $R^* > 1$, the system admits at most two endemic equilibria, both of which are unstable (Figures 6.2a, 6.2c). Under a low R_{0a}, the system tends toward a stable periodic solution when the equilibria coexist (Figure 6.2b, 6.2d). As R_{0a} increases, the periodic solution expands and progressively approaches the $I_r = 0$ plane (Figures 6.2b, 6.2d). By examining the phase portraits of (S_r, I_r), we observe that the solution remains the $I_r = 0$ plane for a while (Figure 6.3a), indicating transient dynamics. We infer that this behavior,

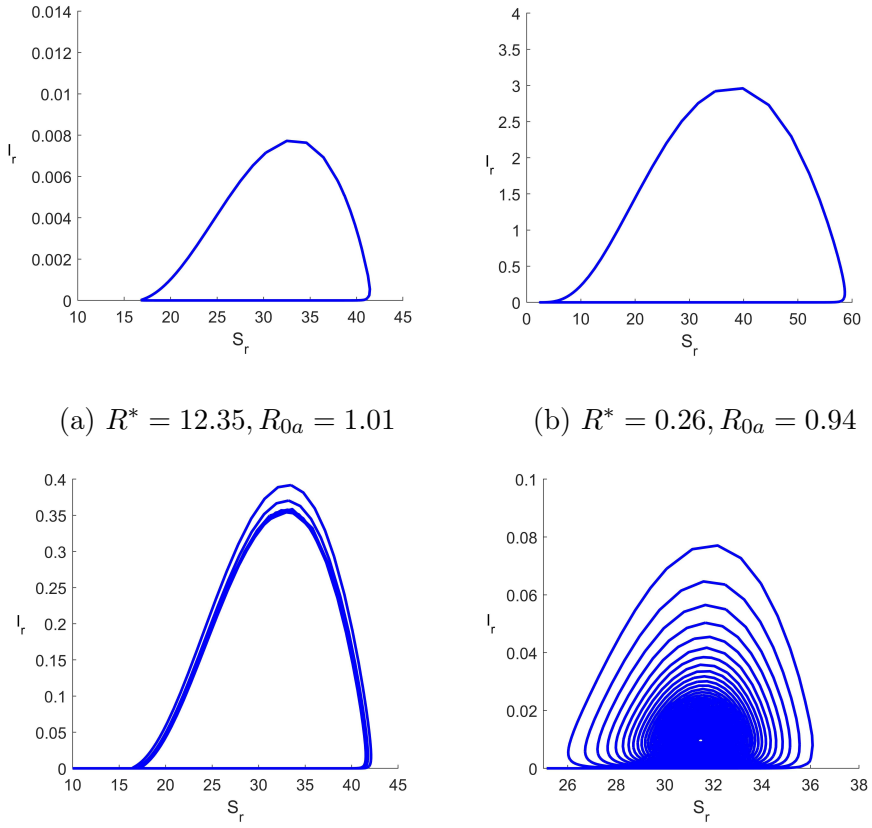

(a) $R^* = 12.35, R_{0a} = 1.01$ (b) $R^* = 0.26, R_{0a} = 0.94$

(c) $R^* = 0.26, R_{0a} = 1.011$ (d) $R^* = 0.26, R_{0a} = 1.0169$

Figure 6.3: Phase portraits of (S_r, I_r) showing (a-c) transient dynamics and (d) a stable equilibrium.

coupled with the further shrinkage of the limit cycle, may contribute to the failure of the bifurcation plotting algorithm, resulting in the incompleteness of the periodic solution around $R_{0a} = 1$ in Figure 6.2b. Conversely, under a high R_{0a}, the system demonstrates at most a single unstable equilibrium (Figures 6.2a, 6.2c). In this case, the system converge toward

the boundary point $\left(0, 0, \frac{\mu_a}{\beta_a}, \frac{\Lambda_a(K_a\beta_a - \mu_a)}{K_a\beta_a^2}\right)$, which reflects the extinction of the reservoir population. This extinction is primarily attributed to elevated infection levels in the target hosts, which lead to intensified quarantine measures and culling efforts. Additionally, the system may exhibit unstable limit cycles for specific parameter combinations (Figure 6.2a).

When R^* decreases to 0.26, the system exhibits a unique equilibrium for $R_{0a} < 1.0218$, and its stability changes with R_{0a} (Figures 6.2e, 6.2f). The system initially stabilizes at the equilibrium before transitioning to a limit cycle. Furthermore, the limit cycle first expands and then contracts, approaching $I_r = 0$. Phase portrait reveals that both coordinates I_r and S_r tend to zero when $R_{0a} = 0.94$, indicating transient dynamics (Figure 6.3b). The appearance of transient dynamics near the origin likely contributes to the incompleteness of the periodic solution in Figure 6.2e when $R_{0a} \in [0.9262, 1.01]$. For a larger value of R_{0a}, the trajectory deviates from the origin in the (S_r, I_r)-plane and stabilizes at a smaller limit cycle (Figure 6.3c). When R_{0a} exceeds 1.0164 but remains less than 1.0218, the system stabilizes at the unique endemic equilibrium again (Figures 6.2f, 6.3d).

Furthermore, a comparison of Figures 6.2a, 6.2c, and 6.2e reveals that a reduction in the spillover rate leads to a decreased equilibrium prevalence in target hosts. This, in turn, reduces the need for quarantine and culling of reservoir hosts, resulting in an increase in the number of infected reservoir hosts.

6.5 Conclusions

In this chapter, we proposed a generalized reservoir-to-target transmission model for monkeypox, applicable to stages II through IV, which integrates reservoir control strategies. Our novel approach, which considers mass quarantine and culling of reservoir hosts based on the number of detected target hosts, is not only biologically meaningful but also provides insight into the interactions between spillover events, target outbreaks, and intervention strategies. To the best of our knowledge, this type of monkeypox model has not been previously explored, despite the considerable epidemic risk posed by reservoir infections and subsequent spillover to target populations. Our findings highlight the necessity of analyzing mass quarantine and culling strategies in two-host models for managing epizootic outbreaks.

In the model without mass quarantine and culling strategies, the target population is vulnerable to extinction under a strong spillover, as indicated by an extinction threshold exceeding one. Importantly, our extinction threshold holds the same significance as the spillover threshold defined by Singh et al. [174], but it offers a more precise functional form that captures the effects of spillover rate, demographic factors of both populations, and disease-related factors in reservoir hosts. Additionally, a high birth rate among target hosts can help mitigate the risk of spillover-induced extinction.

The implementation of mass quarantine and culling does not eradicate the disease in the two populations but significantly reduces its prevalence when it is well-designed [184].

This supports previous research showing that mass quarantine and culling of reservoir hosts lower the risk of spillover [198]. Additionally, these strategies increase the probability of the existence of endemic equilibria, indicating their potential role in biodiversity conservation, particularly in protecting target species vulnerable to extreme spillover events [178]. However, a key finding indicates that the threshold between the level of mass quarantine and culling required to maintain disease endemicity and the point at which reservoir population extinction occurs can be narrow. This is especially true in cases of high spillover rates coupled with intense intraspecific transmission among target hosts [184].

Mathematically, the interactions between spillover events and the implementation of mass quarantine and culling strategies can lead to saddle-node and Hopf bifurcations [187]. Based on these observations, we recommend that mass quarantine and culling be implemented only when supported by appropriate models that indicate their likely effectiveness [282].

7 Conclusions

Pathogens capable of transmission through multiple host species present significant challenges for disease mitigation and control. Such pathogens typically undergo distinct stages of evolutionary adaptation: beginning as infections confined to reservoir hosts (stage I), progressing to spillover infections in target hosts (stage II), followed by an adaptation phase where spillover events coincide with limited onward intraspecific transmission in target hosts (stage III), and ultimately leading to sustained and significant intraspecific transmission within target hosts (stage IV) [2, 13]. Evaluating the effects and outcomes of spillover processes across stages II to IV are fundamental for developing effective intervention strategies.

In this dissertation, monkeypox transmission between reservoir and target hosts is used as an example to elucidate the critical effects of spillover events. Distinguishing between reservoir and target hosts, and understanding their respective roles in disease prevalence, are essential for assessing the consequences of spillover. Important insights are gained through progressive modeling approaches: beginning with a single-host model, advancing to a reservoir-target system without demographic considerations, then incorporating popu-

lation demographics, spillover stochasticity, and target control measures into the reservoir-target system, and finally developing models capable of illustrating reservoir control strategies across stages II to IV. Theoretical and numerical analyses are derived for these models, providing a comprehensive basis for disentangling spillover dynamics.

In Chapter 2, we established a basic framework to model monkeypox transmission within a single host population, incorporating mass quarantine and culling strategies. We first analyzed the local and global dynamics of the deterministic model, demonstrating that effective implementation of quarantine and culling can significantly eradicat the disease [189]. Building upon this framework, we then developed a hybrid stochastic model that accounts for both demographic variations and environmental fluctuations in the transmission rate. A key finding of our study is the population-size-dependent shift in the relative influence of demographic and environmental stochasticity on disease dynamics. Specifically, in small populations, demographic stochasticity plays a dominant role, primarily driving the risk of disease extinction [109]. In contrast, as population size increases, environmental stochasticity exerts a stronger influence, gradually surpassing the effects of demographic fluctuations [240]. Environmental noise not only amplifies both the peak and cumulative number of infections [223] but also modulates the duration of transient dynamics. Depending on the system behavior and intensity of the fluctuations, environmental noise can either shorten or prolong the transient period [30].

Since spillover arises from shedding by reservoir hosts, interspecific contact, and target host exposure, frameworks estimating risk in target hosts should account for these pro-

cesses. In Chapter 3, we analyzed a basic reservoir-target system focusing on spillover transmission from reservoir to target hosts in stages II and III, excluding population demographics. This foundational analysis revealed that the basic reproduction number fails to capture interspecific transmissibility. To address this limitation, we derived a new threshold based on the final size relation, which incorporates both spillover rate and intraspecific transmission rate within target hosts. This threshold provides a more accurate prediction of outbreak risk, emphasizing the spillover rate as a critical determinant [19]. Reducing spillover rates through biosecurity measures, such as constructing fencing in high-risk areas or during animal transportation, is recommended as a primary intervention.

In Chapters 4 and 5, we incorporated demographics to analyze spillover from reservoir to target hosts in stages II and III, respectively. These models also included targeted control strategies such as mass quarantine and culling. Unlike the single-host model in Chapter 2, where quarantine and culling reduce R_0 and effectively control the disease [176], these strategies are ineffective in the reservoir-target system, as the quarantine and culling rate do not impact R_0. Furthermore, our analysis revealed that combining intensified quarantine and culling with strong spillover processes could drive target host population extinction. Interestingly, the extinction threshold is independent of intraspecific transmission in target hosts. This is reasonable since, if spillover events consistently lead to population extinction in the target host, then the further introducing of target-to-target transmission will exacerbate and accelerate the extinction process.

The endemic prevalence in target hosts, influenced significantly by spillover rates [243],

was identified as a key indicator of spillover risk in target hosts. However, under moderate quarantine and culling rates, a nonlinear relationship emerged between spillover rates and endemic prevalence. This relationship led to the identification of a disease severity threshold, which represents the maximum level of endemic infections in target hosts. The expression for this threshold was analytically derived in Chapter 4 and further validated numerically in Chapter 5.

In Chapter 5, we also incorporated stochasticity into the spillover process by introducing a BK process. Our stochastic simulations revealed that the stationary distribution changes with noise volatility, leading to increased variability and asymmetry. This stochastic P-bifurcation highlights the heightened unpredictability of the system, accompanied by an increase in disease incidence.

Lastly, we developed a model capable of analyzing spillover effects on target hosts in stages II to IV, taking into account reservoir control strategies such as mass quarantine and culling of reservoir hosts. Our novel approach, which ties the implementation of quarantine and culling in reservoir hosts to the number of infected target hosts, is both biologically meaningful and mathematically insightful. It captures the interactions between spillover events, target outbreaks, and reservoir control measures. The extinction threshold derived in this model holds similar significance to the spillover threshold defined by Singh et al. [133], but offers a more precise functional form. Notably, this threshold is independent of disease-specific factors in target hosts. Additionally, the interplay between spillover events and the application of quarantine and culling strategies can result in periodic outbreaks,

as indicated by Hopf bifurcation [187]. While these control measures cannot fully eradicate the disease in both populations, they have the potential to reduce its prevalence [184].

In summary, while a basic reproduction number exceeding one in a reservoir-target system is necessary for disease outbreaks and persistence in target hosts, it is not sufficient on its own. When spillover rate is too weak, it is unable to support endemic or epidemic spread [283]. An additional threshold, related to the spillover rate, must also be considered. To manage disease transmission in target hosts during stages II and III, strategies focusing on reservoir management and limiting spillover events are most effective. However, once the pathogen progresses to stage IV in target hosts, control measures specifically targeting the target population become equally essential. We recommend that mass quarantine and culling should be employed only after appropriate models demonstrate its efficacy and feasibility [282].

Future Work

Intense intraspecific transmission within reservoir hosts can significantly influence the likelihood of spillover events. To better capture this relationship, future studies should consider modeling the spillover rate as a function of population dynamics and disease prevalence within reservoir hosts. This approach highlights the need for further pathological and epidemiological investigations to understand how pathogens overcome transmission barriers and the associated dose–response relationships [14]. Similarly, this concept can be extended to reflect how the development of intraspecific transmission among target hosts accumulates as a result of spillover events.

Our reservoir-target host framework serves as an initial step in analyzing spillover effects. Future research could extend this framework by incorporating additional host species. For example, exploring spillover dynamics involving multiple reservoir or target host species may yield valuable insights. Moreover, the role of intermediate hosts in facilitating transmission should not be overlooked, as they may significantly alter outbreak thresholds. In such scenarios, more comprehensive models are necessary to accurately predict spillover impacts.

Lastly, ecological factors within host populations, such as competition or predator-prey relationships, were not included in the current models. Incorporating these factors into future modelling could provide a more nuanced understanding of the ecological drivers of spillover events and disease transmission.

Bibliography

[1] K.E. Jones, N.G. Patel, M.A. Levy, et al. Global trends in emerging infectious diseases. *Nature*, 451(7181):990–993, 2008.

[2] J.O. Lloyd-Smith, D. George, K.M. Pepin, et al. Epidemic dynamics at the human-animal interface. *Science*, 326(5958):1362–1367, 2009.

[3] S. Cleaveland, M.K. Laurenson, and L.H. Taylor. Diseases of humans and their domestic mammals: pathogen characteristics, host range and the risk of emergence. *Philosophical Transactions of the Royal Society of London. Series B: Biological Sciences*, 356(1411):991–999, 2001.

[4] M.B. Joseph, J.R. Mihaljevic, A.L. Arellano, et al. Taming wildlife disease: bridging the gap between science and management. *Journal of Applied Ecology*, 50(3):702–712, 2013.

[5] P. Daszak, A.A. Cunningham, and A.D. Hyatt. Emerging infectious diseases of

wildlife–threats to biodiversity and human health. *Science*, 287(5452):443–449, 2000.

[6] L.H. Taylor, S.M. Latham, and M.E.J. Woolhouse. Risk factors for human disease emergence. *Philosophical Transactions of the Royal Society of London. Series B: Biological Sciences*, 356(1411):983–989, 2001.

[7] P.R. Epstein. Climate change and emerging infectious diseases. *Microbes and Infection*, 3(9):747–754, 2001.

[8] J.M. Hassell, M. Begon, M.J. Ward, and E.M. Fèvre. Urbanization and disease emergence: dynamics at the wildlife–livestock–human interface. *Trends in Ecology and Evolution*, 32(1):55–67, 2017.

[9] D.T. Haydon, S. Cleaveland, L.H. Taylor, and M.K Laurenson. Identifying reservoirs of infection: a conceptual and practical challenge. *Emerging Infectious Diseases*, 8(12):1468–1473, 2002.

[10] E.M. Rees, A. Minter, W.J. Edmunds, et al. Transmission modelling of environmentally persistent zoonotic diseases: a systematic review. *The Lancet Planetary Health*, 5(7):e466–e478, 2021.

[11] L.E. Escobar, A. Velasco-Villa, P.S. Satheshkumar, et al. Revealing the com-

plexity of vampire bat rabies “spillover transmission". *Infectious Diseases of Poverty*, 12(01):102–110, 2023.

[12] A. Borlase, J.W. Rudge, E. Léger, et al. Spillover, hybridization, and persistence in schistosome transmission dynamics at the human–animal interface. *Proceedings of the National Academy of Sciences*, 118(41):e2110711118, 2021.

[13] N.D. Wolfe, C.P. Dunavan, and J. Diamond. Origins of major human infectious diseases. *Nature*, 447(7142):279–283, 2007.

[14] R.K. Plowright, C.R. Parrish, H. McCallum, et al. Pathways to zoonotic spillover. *Nature Reviews Microbiology*, 15(8):502–510, 2017.

[15] J.H. Ellwanger and J.A.B. Chies. Zoonotic spillover: Understanding basic aspects for better prevention. *Genetics and Molecular Biology*, 44(1 Suppl 1):e20200355, 2021.

[16] Food and Agriculture Organization of the United Nations. SARS-CoV-2 in animals situation update. https://www.fao.org/animal-health/situation-updates/sars-cov-2-in-animals/en?utm_source=chatgpt.com, 2024.

[17] M.N. Sparrer, N.F. Hodges, T. Sherman, et al. Role of spillover and spillback in SARS-CoV-2 transmission and the importance of one health in understanding

the dynamics of the COVID-19 pandemic. *Journal of Clinical Microbiology*, 61(7):e01610–22, 2023.

[18] B. Nikolay, H. Salje, M.J. Hossain, et al. Transmission of Nipah virus–14 years of investigations in Bangladesh. *New England Journal of Medicine*, 380(19):1804–1814, 2019.

[19] P.S. Pandit, D.A. Bunn, S.A. Pande, and S.S. Aly. Modeling highly pathogenic avian influenza transmission in wild birds and poultry in west bengal, india. *Scientific reports*, 3(1):2175, 2013.

[20] Centers for Disease Control and Prevention. CDC A(H5N1) bird flu response update, July 19, 2024. https://www.cdc.gov/bird-flu/spotlights/h5n1-response-07192024.html, 2024.

[21] A. Fenton and A.B. Pedersen. Community epidemiology framework for classifying disease threats. *Emerging Infectious Diseases*, 11(12):1815, 2005.

[22] M. Viana, R. Mancy, R. Biek, et al. Assembling evidence for identifying reservoirs of infection. *Trends in Ecology and Evolution*, 29(5):270–279, 2014.

[23] G.A. Poland, R.B. Kennedy, and P.K. Tosh. Prevention of monkeypox with vaccines: a rapid review. *The Lancet Infectious Diseases*, 22(12):e349–e358, 2022.

[24] P. Yuan, Y. Tan, L. Yang, et al. Modeling vaccination and control strategies for outbreaks of monkeypox at gatherings. *Frontiers in Public Health*, 10:1026489, 2022.

[25] K.D. Reed, J.W. Melski, M.B. Graham, et al. The detection of monkeypox in humans in the Western Hemisphere. *New England Journal of Medicine*, 350(4):342–350, 2004.

[26] Centers for Disease Control and Prevention. Update: Multistate Outbreak of Monkeypox – Illinois, Indiana, Kansas, Missouri, Ohio, and Wisconsin, 2003. https://www.cdc.gov/mmwr/preview/mmwrhtml/mm5227a5.htm, 2003.

[27] C.A. Donnelly, R. Woodroffe, D. Cox, et al. Positive and negative effects of widespread badger culling on tuberculosis in cattle. *Nature*, 439(7078):843–846, 2006.

[28] R.K. Plowright, P. Eby, P.J. Hudson, et al. Ecological dynamics of emerging bat virus spillover. *Proceedings of the Royal Society B: Biological Sciences*, 282(1798):20142124, 2015.

[29] L.G. Shoemaker, L.L. Sullivan, I. Donohue, et al. Integrating the underlying structure of stochasticity into community ecology. *Ecology*, 101(2):e02922, 2020.

[30] A. Hastings, K.C. Abbott, K. Cuddington, et al. Effects of stochasticity on the length and behaviour of ecological transients. *Journal of the Royal Society Interface*, 18(180):20210257, 2021.

[31] B.A. Melbourne and A. Hastings. Extinction risk depends strongly on factors contributing to stochasticity. *Nature*, 454(7200):100–103, 2008.

[32] E.A. Falendysz, J.G. Lopera, J.B. Doty, et al. Characterization of Monkeypox virus infection in African rope squirrels (Funisciurus sp.). *PLoS Neglected Tropical Diseases*, 11(8):e0005809, 2017.

[33] M. Kozlov. Monkeypox virus keeps getting better at spreading among humans. *Nature*, 635(8037):13–14, 2024.

[34] E. Petersen, U. Hvid, O. Tomori, et al. Possible scenarios for the spread of mpox outside the endemic focus in Africa. *International Journal of Infectious Diseases*, page 107373, 2024.

[35] T. Wawina-Bokalanga, S. Merritt, E. Kinganda-Lusamaki, et al. Epidemiology and Phylogenomic Characterization of Distinct 2023 and 2024 Mpox outbreaks in Kinshasa, Democratic Republic of the Congo-Evidence for increasingly sustained human-to-human transmission of subclade Ia. *medRxiv*, pages 2024–11, 2024.

[36] R.B. Rosa, E.F. de Castro, M.V. da Silva, et al. In vitro and in vivo models for monkeypox. *Iscience*, 26(1), 2023.

[37] S. Reardon. Mpox is spreading rapidly. here are the questions researchers are racing to answer. *Nature*, 633(8028):16–17, 2024.

[38] J.L. Americo, P.L. Earl, and B. Moss. Virulence differences of mpox (monkeypox) virus clades I, IIa, and IIb. 1 in a small animal model. *Proceedings of the National Academy of Sciences*, 120(8):e2220415120, 2023.

[39] A. Gessain, E. Nakoune, and Y. Yazdanpanah. Monkeypox. *New England Journal of Medicine*, 387(19):1783–1793, 2022.

[40] R. Stephen, F. Alele, J. Olumoh, et al. The epidemiological trend of monkeypox and monkeypox-varicella zoster viruses co-infection in North-Eastern Nigeria. *Frontiers in Public Health*, 10:1066589, 2022.

[41] J.B. Doty, J.M. Malekani, L.N. Kalemba, et al. Assessing monkeypox virus prevalence in small mammals at the human–animal interface in the Democratic Republic of the Congo. *Viruses*, 9(10):283, 2017.

[42] Z. Ježek, B. Grab, M. Szczeniowski, K. Paluku, and M. Mutombo. Clinico-epidemiological features of monkeypox patients with an animal or human source of infection. *Bulletin of the World Health Organization*, 66(4):459, 1988.

[43] A. Yinka-Ogunleye, O. Aruna, M. Dalhat, et al. Outbreak of human monkeypox in Nigeria in 2017–18: a clinical and epidemiological report. *The Lancet Infectious Diseases*, 19(8):872–879, 2019.

[44] J. Guarner, B.J. Johnson, C.D. Paddock, et al. Monkeypox transmission and pathogenesis in prairie dogs. *Emerging Infectious Diseases*, 10(3):426, 2004.

[45] C.L. Hutson, K.N. Lee, J. Abel, et al. Monkeypox zoonotic associations: insights from laboratory evaluation of animals associated with the multi-state US outbreak. *The American Journal of Tropical Medicine and Hygiene*, 76(4):757–768, 2007.

[46] K. Brown and P.A. Leggat. Human monkeypox: current state of knowledge and implications for the future. *Tropical Medicine and Infectious Disease*, 1(1):8, 2016.

[47] E.R. Mega. Why scientists fear monkeypox spreading in wild animals. *Nature*, 2022.

[48] S. Parker, A. Nuara, R.M.L. Buller, and D.A. Schultz. Human monkeypox: an emerging zoonotic disease. *Future Microbiology*, 2(1):17–34, 2007.

[49] M.G. Reynolds, J.B. Doty, A.M. McCollum, V.A. Olson, and Y. Nakazawa.

Monkeypox re-emergence in Africa: a call to expand the concept and practice of One Health. *Expert Review of Anti-infective Therapy*, 17(2):129–139, 2019.

[50] M. Domán, E. Fehér, R. Varga-Kugler, F. Jakab, and K. Bányai. Animal models used in monkeypox research. *Microorganisms*, 10(11):2192, 2022.

[51] K. Li, Y. Yuan, L. Jiang, et al. Animal host range of mpox virus. *Journal of Medical Virology*, 95(2):e28513, 2023.

[52] S. Parker and R.M. Buller. A review of experimental and natural infections of animals with monkeypox virus between 1958 and 2012. *Future Virology*, 8(2):129–157, 2013.

[53] M.S. Tiee, R.J. Harrigan, H.A. Thomassen, and T.B. Smith. Ghosts of infections past: using archival samples to understand a century of monkeypox virus prevalence among host communities across space and time. *Royal Society Open Science*, 5(1):171089, 2018.

[54] E.A. Falendysz, J.G. Lopera, F. Lorenzsonn, et al. Further assessment of monkeypox virus infection in Gambian pouched rats (Cricetomys gambianus) using in vivo bioluminescent imaging. *PLoS Neglected Tropical Diseases*, 9(10):e0004130, 2015.

[55] Africa CDC. Monkeypox. https://africacdc.org/disease/monkeypox/, 2024.

[56] D. Forni, C. Molteni, R. Cagliani, and M. Sironi. Geographic structuring and divergence time frame of monkeypox virus in the endemic region. *The Journal of Infectious Diseases*, 227(6):742–751, 2023.

[57] H.A. Thomassen, T. Fuller, S. Asefi-Najafabady, et al. Pathogen-host associations and predicted range shifts of human monkeypox in response to climate change in central Africa. *PLoS One*, 8(7):e66071, 2013.

[58] M. Curaudeau, C. Besombes, E. Nakouné, et al. Identifying the most probable mammal reservoir hosts for monkeypox virus based on ecological niche comparisons. *Viruses*, 15(3):727, 2023.

[59] A.W. Rimoin, P.M. Mulembakani, S.C. Johnston, et al. Major increase in human monkeypox incidence 30 years after smallpox vaccination campaigns cease in the Democratic Republic of Congo. *Proceedings of the National Academy of Sciences*, 107(37):16262–16267, 2010.

[60] J. Cohen. Monkeypox is a new global threat. African scientists know what the world is up against. *Science News*, 2022.

[61] P.L. Earl, J.L. Americo, and B. Moss. Lethal monkeypox virus infection of CAST/EiJ mice is associated with a deficient gamma interferon response. *Journal of Virology*, 86(17):9105–9112, 2012.

[62] Y. Xiang and A. White. Monkeypox virus emerges from the shadow of its more infamous cousin: family biology matters. *Emerging Microbes and Infections*, 11(1):1768–1777, 2022.

[63] The New York Times. N.Y.C. rat sightings double to unsettling 60,000 in last year, health data shows. https://www.nbcnewyork.com/investigations/i-team-rat-sightings-doubled-in-nyc-over-past-12-months-according-to-health-data/4070243/, 2023.

[64] The New York Times. N.Y.C. rats: They're in the park, on your block and even at your table. https://www.nytimes.com/2021/11/05/nyregion/nyc-rats-sightings.html, 2023.

[65] Centers for Disease Control and Prevention. Technical report 2: Multi-national mpox outbreak, United States, 2022. https://www.cdc.gov/poxvirus/mpox/cases-data/technical-report/report-2.html, 2022.

[66] J.G. Breman, J. Bernadou, and J.H. Nakano. Poxvirus in West African non-

human primates: serological survey results. *Bulletin of the World Health Organization*, 55(5):605, 1977.

[67] E. Chaix, M. Boni, L. Guillier, et al. Risk of monkeypox virus (mpxv) transmission through the handling and consumption of food. *Microbial Risk Analysis*, 22:100237, 2022.

[68] M.S. Hakim and S.A. Widyaningsih. The recent re-emergence of human monkeypox: Would it become endemic beyond Africa? *Journal of Infection and Public Health*, 16(3):332–340, 2023.

[69] Centers for Disease Control and Prevention. Examining animals with suspected mpox. https://archive.cdc.gov/#/details?url=https://www.cdc.gov/poxvirus/mpox/veterinarian/examination.html, 2022.

[70] C.L. Hutson, V.A. Olson, D.S. Carroll, et al. A prairie dog animal model of systemic orthopoxvirus disease using West African and Congo Basin strains of monkeypox virus. *Journal of General Virology*, 90(2):323–333, 2009.

[71] H.W. Hethcote. The mathematics of infectious diseases. *SIAM Review*, 42(4):599–653, 2000.

[72] A. Fenton, D.G. Streicker, O.L. Petchey, and A.B. Pedersen. Are all hosts

created equal? Partitioning host species contributions to parasite persistence in multihost communities. *The American Naturalist*, 186(5):610–622, 2015.

[73] A. Dobson. Population dynamics of pathogens with multiple host species. *The American Naturalist*, 164(S5):S64–S78, 2004.

[74] R.M. Anderson and R.M. May. Population biology of infectious diseases: Part i. *Nature*, 280(5721):361–367, 1979.

[75] S. Busenberg and P. Van den Driessche. Analysis of a disease transmission model in a population with varying size. *Journal of Mathematical Biology*, 28(3):257–270, 1990.

[76] W. Derrick and P. Van den Driessche. A disease transmission model in a non-constant population. *Journal of Mathematical Biology*, 31(5):495–512, 1993.

[77] J.A. Jacquez, C.P. Simon, J. Koopman, L. Sattenspiel, and T. Perry. Modeling and analyzing HIV transmission: the effect of contact patterns. *Mathematical Biosciences*, 92(2):119–199, 1988.

[78] J. Mena-Lorcat and H.W. Hethcote. Dynamic models of infectious diseases as regulators of population sizes. *Journal of Mathematical Biology*, 30(7):693–716, 1992.

[79] J.S. Zhou and H.W. Hethcote. Population size dependent incidence in models for diseases without immunity. *Journal of Mathematical Biology*, 32:809–834, 1994.

[80] R.M. Anderson, H.C. Jackson, R.M. May, and A.M. Smith. Population dynamics of fox rabies in Europe. *Nature*, 289(5800):765–771, 1981.

[81] F. Brauer. Models for the spread of universally fatal diseases. *Journal of Mathematical Biology*, 28:451–462, 1990.

[82] H.J. Bremermann and H. Thieme. A competitive exclusion principle for pathogen virulence. *Journal of Mathematical Biology*, 27(2):179–190, 1989.

[83] A.R.S. Castañeda, E.E. Ramirez-Torres, L.E. Valdés-García, et al. Modified SEIR epidemic model including asymptomatic and hospitalized cases with correct demographic evolution. *Applied Mathematics and Computation*, 456:128122, 2023.

[84] J. Zhang, J.Q. Li, and Z.E. Ma. Global analysis of SIR epidemic models with population size dependent contact rate. *Journal of Engineering Mathematics*, 21:259–267, 2004.

[85] L.Q. Gao and H.W. Hethcote. Disease transmission models with density-

dependent demographics. *Journal of Mathematical Biology*, 30(7):717–731, 1992.

[86] K. Dietz and J.A.P. Heesterbeek. Daniel bernoulli's epidemiological model revisited. *Mathematical Biosciences*, 180(1-2):1–21, 2002.

[87] R. Ross. *The prevention of malaria.* John Murray, 1911.

[88] W.O. Kermack and A.G. McKendrick. A contribution to the mathematical theory of epidemics. In *Papers of a mathematical and physical character*, volume 115, pages 700–721. The Royal Society London. Series A, 1927.

[89] R. Ross. Some a priori pathometric equations. *British Medical Journal*, 1(2830):546, 1915.

[90] W.H. Hamer. *The milroy lectures on epidemic diseases in england: The evidence of variability and of persistency of type.* Bedford Press, 1906.

[91] M. Begon, M. Bennett, R.G. Bowers, et al. A clarification of transmission terms in host-microparasite models: numbers, densities and areas. *Epidemiology and Infection*, 129(1):147–153, 2002.

[92] J. Antonovics. Transmission dynamics: critical questions and challenges.

Philosophical Transactions of the Royal Society B: Biological Sciences, 372(1719):20160087, 2017.

[93] O. Diekmann, J.A.P. Heesterbeek, and M.G. Roberts. The construction of next-generation matrices for compartmental epidemic models. *Journal of the Royal Society Interface*, 7(47):873–885, 2010.

[94] J.A.P. Heesterbeek. A brief history of R_0 and a recipe for its calculation. *Acta Biotheoretica*, 50(3):189–204, 2002.

[95] J.J. Dennehy. Bacteriophages as model organisms for virus emergence research. *Trends in Microbiology*, 17(10):450–457, 2009.

[96] O. Diekmann, J.A.P. Heesterbeek, and J.A.J. Metz. On the definition and the computation of the basic reproduction ratio R_0 in models for infectious diseases in heterogeneous populations. *Journal of Mathematical Biology*, 28:365–382, 1990.

[97] P. Van den Driessche and J. Watmough. Reproduction numbers and sub-threshold endemic equilibria for compartmental models of disease transmission. *Mathematical Biosciences*, 180(1-2):29–48, 2002.

[98] J. Li, D. Blakeley, and R.J. Smith. The failure of R_0. *Computational and Mathematical Methods in Medicine*, 527610, 2011.

[99] A.G. McKendrick. Applications of mathematics to medical problems. *Proceedings of the Edinburgh Mathematical Society*, 44:98–130, 1926.

[100] D.J. Daley and J.M. Gani. *Epidemic modelling: an introduction*. Number 15. Cambridge University Press, 1999.

[101] A.D. Barbour. The principle of the diffusion of arbitrary constants. *Journal of Applied Probability*, 9(3):519–541, 1972.

[102] N.G. Becker and K. Dietz. The effect of household distribution on transmission and control of highly infectious diseases. *Mathematical Biosciences*, 127(2):207–219, 1995.

[103] I. Nasell. Endemicity, persistence, and quasi-stationarity. *IMA Volumes in Mathematics and Its Applications*, 125:199–228, 2002.

[104] S. Lambert, P. Ezanno, M. Garel, and E. Gilot-Fromont. Demographic stochasticity drives epidemiological patterns in wildlife with implications for diseases and population management. *Scientific Reports*, 8(1):16846, 2018.

[105] T. Britton and D. Lindenstrand. Epidemic modelling: aspects where stochasticity matters. *Mathematical biosciences*, 222(2):109–116, 2009.

[106] A. Bodini, S. Pasquali, A. Pievatolo, and F. Ruggeri. Underdetection in

a stochastic SIR model for the analysis of the COVID-19 Italian epidemic. *Stochastic Environmental Research and Risk Assessment*, 36(1):137–155, 2022.

[107] I. Bashkirtseva, L. Ryashko, and T. Ryazanova. Analysis of regular and chaotic dynamics in a stochastic eco-epidemiological model. *Chaos, Solitons and Fractals*, 131:109549, 2020.

[108] D.A. Rand and H.B. Wilson. Chaotic stochasticity: a ubiquitous source of unpredictability in epidemics. *Proceedings of the Royal Society of London. Series B: Biological Sciences*, 246(1316):179–184, 1991.

[109] K.F. Nipa, S.R.J. Jang, and L.J.S. Allen. The effect of demographic and environmental variability on disease outbreak for a dengue model with a seasonally varying vector population. *Mathematical Biosciences*, 331:108516, 2021.

[110] K.F. Nipa and L.J.S. Allen. Disease emergence in multi-patch stochastic epidemic models with demographic and seasonal variability. *Bulletin of Mathematical Biology*, 82(12):152, 2020.

[111] D.H. Nguyen, G. Yin, and C. Zhu. Long-term analysis of a stochastic SIRS model with general incidence rates. *SIAM Journal on Applied Mathematics*, 80(2):814–838, 2020.

[112] N. Dalal, D. Greenhalgh, and X.R. Mao. A stochastic model of AIDS and condom use. *Journal of Mathematical Analysis and Applications*, 325(1):36–53, 2007.

[113] T. Gard. *Introduction to stochastic differential equations*. Marcel Dekker Inc, 1988.

[114] E.J. Allen. Environmental variability and mean-reverting processes. *Discrete and Continuous Dynamical Systems–B*, 21(7):2073–2089, 2016.

[115] L.J.S. Allen. A primer on stochastic epidemic models: Formulation, numerical simulation, and analysis. *Infectious Disease Modelling*, 2(2):128–142, 2017.

[116] A. Morozov, K. Abbott, K. Cuddington, et al. Long transients in ecology: Theory and applications. *Physics of Life Reviews*, 32:1–40, 2020.

[117] S. Haldar, K. Chakraborty, K. Das, and T. Kar. Bifurcation and control of an eco-epidemiological system with environmental fluctuations: a stochastic approach. *Nonlinear Dynamics*, 80:1187–1207, 2015.

[118] A. Hastings, K.C. Abbott, K. Cuddington, et al. Transient phenomena in ecology. *Science*, 361(6406):eaat6412, 2018.

[119] X.L. Zou, D.J. Fan, and K. Wang. Stationary distribution and stochastic Hopf

bifurcation for a predator-prey system with noises. *Discrete and Continuous Dynamical Systems–B*, 18(5), 2013.

[120] A. Tesfay, D. Tesfay, S.L. Yuan, et al. Stochastic bifurcation in single-species model induced by α-stable lévy noise. *Journal of Statistical Mechanics: Theory and Experiment*, 2021(10):103403, 2021.

[121] S.R. Dtchetgnia Djeundam, R. Yamapi, T.C. Kofane, and M.A. Aziz-Alaoui. Deterministic and stochastic bifurcations in the hindmarsh-rose neuronal model. *Chaos: An Interdisciplinary Journal of Nonlinear Science*, 23(3), 2013.

[122] S. Mariappan. Stochastic dynamics of vortex-acoustic lock-in: stochastic bifurcation and resonance. *Journal of Fluid Mechanics*, 941:A38, 2022.

[123] A. Din. The stochastic bifurcation analysis and stochastic delayed optimal control for epidemic model with general incidence function. *Chaos: An Interdisciplinary Journal of Nonlinear Science*, 31(12):123101, 2021.

[124] R. Yamapi, G. Filatrella, M. Aziz-Alaoui, and H.A. Cerdeira. Effective Fokker-Planck equation for birhythmic modified van der pol oscillator. *Chaos: An Interdisciplinary Journal of Nonlinear Science*, 22(4), 2012.

[125] M.S. Bartlett. Deterministic and stochastic models for recurrent epidemics. In

Proceedings of the Third Berkeley Symposium on Mathematical Statistics and Probability, volume 4, page 109. Berkeley, 1956.

[126] L.J.S. Allen. An introduction to stochastic epidemic models. In *Mathematical Epidemiology, Lecture Notes in Mathematics*, pages 81–130. Brauer, 2008.

[127] L.J.S. Allen and X.Y. Wang. Stochastic models of infectious diseases in a periodic environment with application to cholera epidemics. *Journal of Mathematical Biology*, 82(6):48, 2021.

[128] J.E. Simpson, P.J. Hurtado, J. Medlock, et al. Vector host-feeding preferences drive transmission of multi-host pathogens: West Nile virus as a model system. *Proceedings of the Royal Society B: Biological Sciences*, 279(1730):925–933, 2012.

[129] M.L. Childs, N. Nova, J. Colvin, and E.A. Mordecai. Mosquito and primate ecology predict human risk of yellow fever virus spillover in Brazil. *Philosophical Transactions of the Royal Society B*, 374(1782):20180335, 2019.

[130] A. Iggidr, G. Sallet, and M.O. Souza. On the dynamics of a class of multi-group models for vector-borne diseases. *Journal of Mathematical Analysis and Applications*, 441(2):723–743, 2016.

[131] N.R. Faria, M.U.G. Kraemer, S.C. Hill, et al. Genomic and epidemiological monitoring of yellow fever virus transmission potential. *Science*, 361(6405):894–899, 2018.

[132] A.D. Washburne, D.E. Crowley, D.J. Becker, et al. Percolation models of pathogen spillover. *Philosophical Transactions of the Royal Society B*, 374(1782):20180331, 2019.

[133] S. Singh, D.J. Schneider, and C.R. Myers. Using multitype branching processes to quantify statistics of disease outbreaks in zoonotic epidemics. *Physical Review E*, 89(3):032702, 2014.

[134] M. Voinson, A. Alvergne, S. Billiard, and C. Smadi. Stochastic dynamics of an epidemic with recurrent spillovers from an endemic reservoir. *Journal of Theoretical Biology*, 457:37–50, 2018.

[135] K. LoGiudice, S.T.K. Duerr, M.J. Newhouse, et al. Impact of host community composition on Lyme disease risk. *Ecology*, 89(10):2841–2849, 2008.

[136] B.F. Allan, R.B. Langerhans, W.A. Ryberg, et al. Ecological correlates of risk and incidence of West Nile virus in the United States. *Oecologia*, 158:699–708, 2009.

[137] V.O. Ezenwa, M.S. Godsey, R.J. King, and S.C. Guptill. Avian diversity and West Nile virus: testing associations between biodiversity and infectious disease risk. *Proceedings of the Royal Society B: Biological Sciences*, 273(1582):109–117, 2006.

[138] R.S. Ostfeld and F. Keesing. Biodiversity and disease risk: the case of Lyme disease. *Conservation Biology*, 14(3):722–728, 2000.

[139] J.E. Vinson and A.W. Park. Vector-borne parasite invasion in communities across space and time. *Proceedings of the Royal Society B*, 286(1917):20192614, 2019.

[140] M.E. Craft, P.L. Hawthorne, C. Packer, and A. Dobson. Dynamics of a multihost pathogen in a carnivore community. *Journal of Animal Ecology*, 77(6):1257–1264, 2008.

[141] J. Liu, H. Xiao, F. Lei, et al. Highly pathogenic H5N1 influenza virus infection in migratory birds. *Science*, 309(5738):1206–1206, 2005.

[142] P.C. Cross, D.J. Prosser, A.M. Ramey, E.M. Hanks, and K.M. Pepin. Confronting models with data: the challenges of estimating disease spillover. *Philosophical Transactions of the Royal Society B*, 374(1782):20180435, 2019.

[143] P. Yuan, Y. Tan, L. Yang, et al. Assessing transmission risks and control strategy for monkeypox as an emerging zoonosis in a metropolitan area. *Journal of Medical Virology*, 95(1):e28137, 2023.

[144] S. Usman and I.I. Adamu. Modeling the transmission dynamics of the monkeypox virus infection with treatment and vaccination interventions. *Journal of Applied Mathematics and Physics*, 5(12):2335, 2017.

[145] C.P. Bhunu, S. Mushayabasa, and J. Hyman. Modelling HIV/AIDS and monkeypox co-infection. *Applied Mathematics and Computation*, 218(18):9504–9518, 2012.

[146] P. Emeka, M. Ounorah, F. Eguda, and B. Babangida. Mathematical model for monkeypox virus transmission dynamics. *Epidemiol Open Access*, 8(3):348, 2018.

[147] I. Lauko, G. Pinter, and R.E. TeWinkel. Equilibrium analysis for an epidemic model with a reservoir for infection. *Letters in Biomathematics*, 5(1):255–274, 2018.

[148] S. Majee, S. Jana, and T.K. Kar. Dynamical analysis of monkeypox transmission incorporating optimal vaccination and treatment with cost-effectiveness. *Chaos: An Interdisciplinary Journal of Nonlinear Science*, 33(4), 2023.

[149] O.J. Peter, S. Kumar, N. Kumari, et al. Transmission dynamics of monkeypox virus: a mathematical modelling approach. *Modeling Earth Systems and Environment*, pages 1–12, 2022.

[150] K. Royce and F. Fu. Mathematically modeling spillovers of an emerging infectious zoonosis with an intermediate host. *PloS One*, 15(8):e0237780, 2020.

[151] F. Saldaña, N. Stollenwerk, J.B. Van Dierdonck, and M. Aguiar. Modeling spillover dynamics: understanding emerging pathogens of public health concern. *Scientific Reports*, 14(1):9823, 2024.

[152] D. Bichara, A. Iggidr, and L. Smith. Multi-stage vector-borne zoonoses models: A global analysis. *Bulletin of Mathematical Biology*, 80:1810–1848, 2018.

[153] C.X. Ding, Z.P. Qiu, and H.P. Zhu. Multi-host transmission dynamics of schistosomiasis and its optimal control. *Mathematical Biosciences and Engineering*, 12(5):983–1006, 2015.

[154] D.M. Bichara. Global analysis of multi-host and multi-vector epidemic models. *Journal of Mathematical Analysis and Applications*, 475(2):1532–1553, 2019.

[155] J.W. Rudge, J.P. Webster, D.B. Lu, et al. Identifying host species driving transmission of schistosomiasis japonica, a multihost parasite system, in China. *Proceedings of the National Academy of Sciences*, 110(28):11457–11462, 2013.

[156] J. Turner, R.G. Bowers, and M. Baylis. Two-host, two-vector basic reproduction ratio (R_0) for bluetongue. *PloS One*, 8(1):e53128, 2013.

[157] L. Binkley, J. O'Quin, B. Jourdan, et al. Quantifying intra-and inter-species contact rates at supplemental feeding sites in ethiopia to inform rabies maintenance potential of multiple host species. *Transboundary and Emerging Diseases*, 69(6):3837–3849, 2022.

[158] L. Bolzoni, G.A. De Leo, M. Gatto, and A.P. Dobson. Body-size scaling in an SEI model of wildlife diseases. *Theoretical Population Biology*, 73(3):374–382, 2008.

[159] J. Bielby, S.J. Price, C. Monsalve-CarcaÑo, and J. Bosch. Host contribution to parasite persistence is consistent between parasites and over time, but varies spatially. *Ecological Applications*, 31(3):e02256, 2021.

[160] M. Jesse, R. Mazzucco, U. Dieckmann, H. Heesterbeek, and J.A. Metz. Invasion and persistence of infectious agents in fragmented host populations. *PLoS One*, 6(9):e24006, 2011.

[161] P.C. Cross, J.O. Lloyd-Smith, P.L.F. Johnson, and W.M. Getz. Duelling timescales of host movement and disease recovery determine invasion of disease in structured populations. *Ecology letters*, 8(6):587–595, 2005.

[162] P.C. Cross, P.L.F. Johnson, J.O. Lloyd-Smith, and W.M. Getz. Utility of R0 as a predictor of disease invasion in structured populations. *Journal of the Royal Society Interface*, 4(13):315–324, 2007.

[163] M.E. Craft, E. Volz, C. Packer, and L.A. Meyers. Distinguishing epidemic waves from disease spillover in a wildlife population. *Proceedings of the Royal Society B: Biological Sciences*, 276(1663):1777–1785, 2009.

[164] E.L. Davis, T.C.D. Lucas, A. Borlase, et al. Contact tracing is an imperfect tool for controlling COVID-19 transmission and relies on population adherence. *Nature Communications*, 12(1):5412, 2021.

[165] R.J. Kubiak, N. Arinaminpathy, and A.R. McLean. Insights into the evolution and emergence of a novel infectious disease. *PLoS Computational Biology*, 6(9):e1000947, 2010.

[166] M. Hartfield and S. Alizon. Introducing the outbreak threshold in epidemiology. *PLoS Pathogens*, 9(6):e1003277, 2013.

[167] M. Pardo-Araujo, D. García-García, D. Alonso, and F. Bartumeus. Epidemic thresholds and human mobility. *Scientific Reports*, 13(1):11409, 2023.

[168] J. Humplik, A.L. Hill, and M.A. Nowak. Evolutionary dynamics of infectious

diseases in finite populations. *Journal of Theoretical Biology*, 360:149–162, 2014.

[169] C. Xu. Global threshold dynamics of a stochastic differential equation SIS model. *Journal of Mathematical Analysis and Applications*, 447(2):736–757, 2017.

[170] M.G. Roberts and J.A.P. Heesterbeek. A new method for estimating the effort required to control an infectious disease. *Proceedings of the Royal Society of London B: Biological Sciences*, 270(1522):1359–1364, 2003.

[171] J.V. Greenman and A.S. Hoyle. Exclusion of generalist pathogens in multihost communities. *The American Naturalist*, 172(4):576–584, 2008.

[172] D.R. Cox, C.A. Donnelly, F.J. Bourne, et al. Simple model for tuberculosis in cattle and badgers. *Proceedings of the National Academy of Sciences*, 102(49):17588–17593, 2005.

[173] L. Bolzoni, R.D. Marca, M. Groppi, et al. Dynamics of a metapopulation epidemic model with localized culling. *Discrete and Continuous Dynamical Systems–B.*, 25(6):2307–2330, 2020.

[174] J.M. Tchuenche and C.T. Bauch. Can culling to prevent monkeypox infec-

tion be counter-productive? Scenarios from a theoretical model. *Journal of Biological Systems*, 20(03):259–283, 2012.

[175] Samhita Das, Pritha Das, and Parthasakha Das. Control of Nipah virus outbreak in commercial pig-farm with biosecurity and culling. *Mathematical Modelling of Natural Phenomena*, 15:64, 2020.

[176] X. O'Neill, A. White, and M. Boots. The evolution of parasite virulence under targeted culling and harvesting in wildlife and livestock. *Evolutionary Applications*, 16(10):1697–1707, 2023.

[177] M.F. Abakar, H.Y. Azami, P.J. Bless, et al. Transmission dynamics and elimination potential of zoonotic tuberculosis in morocco. *PLoS Neglected Tropical Diseases*, 11(2):e0005214, 2017.

[178] H. McCallum. Models for managing wildlife disease. *Parasitology*, 143(7):805–820, 2016.

[179] M.J. Keeling, M.E.J. Woolhouse, D.J. Shaw, et al. Dynamics of the 2001 UK foot and mouth epidemic: stochastic dispersal in a heterogeneous landscape. *Science*, 294(5543):813–817, 2001.

[180] A. Abdelrazec, S. Lenhart, and H.P. Zhu. Transmission dynamics of West Nile

virus in mosquitoes and corvids and non-corvids. *Journal of Mathematical Biology*, 68(6):1553–1582, 2014.

[181] A.J. Terry and S.A. Gourley. Perverse consequences of infrequently culling a pest. *Bulletin of Mathematical Biology*, 72:1666–1695, 2010.

[182] H. Gulbudak and M. Martcheva. Forward hysteresis and backward bifurcation caused by culling in an avian influenza model. *Mathematical Biosciences*, 246(1):202–212, 2013.

[183] E. Shim and A.P. Galvani. Evolutionary repercussions of avian culling on host resistance and influenza virulence. *PloS one*, 4(5):e5503, 2009.

[184] E. Tanner, A. White, P.W.W. Lurz, et al. The critical role of infectious disease in compensatory population growth in response to culling. *The American Naturalist*, 194(1):E1–E12, 2019.

[185] L. Bolzoni, L. Real, and G. De Leo. Transmission heterogeneity and control strategies for infectious disease emergence. *PLoS One*, 2(8):e747, 2007.

[186] E. Miguel, V. Grosbois, A. Caron, et al. A systemic approach to assess the potential and risks of wildlife culling for infectious disease control. *Communications Biology*, 3(1):353, 2020.

[187] Y. Nie, X. Sun, H. Hu, and Q. Hou. Bifurcation analysis of a sheep brucellosis model with testing and saturated culling rate. *Mathematical Biosciences and Engineering*, 20(1):1519–1537, 2023.

[188] W.K. Zhou, Y.N. Xiao, and J.M. Heffernan. A two-thresholds policy to interrupt transmission of West Nile Virus to birds. *Journal of Theoretical Biology*, 463:22–46, 2019.

[189] J.C. Prentice, G. Marion, P.C.L. White, R.S. Davidson, and M.R. Hutchings. Demographic processes drive increases in wildlife disease following population reduction. *PloS One*, 9(5):e86563, 2014.

[190] T.G. Hallam and G.F. McCracken. Management of the panzootic white-nose syndrome through culling of bats. *Conservation Biology*, 25(1):189–194, 2011.

[191] R. Woodroffe, S. Cleaveland, O. Courtenay, M.K. Laurenson, and A. Artois. Infectious diseases in the management and conservation of wild canids. *The Biology and Conservation of Wild Canids*, pages 123–142, 2004.

[192] M. Viana, J.A. Benavides, A. Broos, et al. Effects of culling vampire bats on the spatial spread and spillover of rabies virus. *Science Advances*, 9(10):eadd7437, 2023.

[193] D.E. te Beest, T.J. Hagenaars, J.A. Stegeman, M.P.G. Koopmans, and M. van Boven. Risk based culling for highly infectious diseases of livestock. *Veterinary Research*, 42:1–9, 2011.

[194] M.J. Keeling, M.E.J. Woolhouse, R.M. May, G. Davies, and B.T. Grenfell. Modelling vaccination strategies against foot-and-mouth disease. *Nature*, 421(6919):136–142, 2003.

[195] G. Wasserberg, E.E. Osnas, R.E. Rolley, and M.D. Samuel. Host culling as an adaptive management tool for chronic wasting disease in white-tailed deer: a modelling study. *Journal of Applied Ecology*, 46(2):457–466, 2009.

[196] J.E. Gross and M.W. Miller. Chronic wasting disease in mule deer: disease dynamics and control. *The Journal of Wildlife Management*, pages 205–215, 2001.

[197] A. Potapov, E. Merrill, and M.A. Lewis. Wildlife disease elimination and density dependence. *Proceedings of the Royal Society B: Biological Sciences*, 279(1741):3139–3145, 2012.

[198] M. Choisy and P. Rohani. Harvesting can increase severity of wildlife disease epidemics. *Proceedings of the Royal Society B: Biological Sciences*, 273(1597):2025–2034, 2006.

[199] American Veterinary Medical Foundation. Mpox (monkeypox). https://www.avma.org/resources-tools/one-health/veterinarians-and-public-health/monkeypox#:~:text=The%20name%20mpox%20stems%20from,also%20can%20harbor%20the%20virus, 2024.

[200] L. Khodakevich, Z. Jezek, and K. Kinzanzka. Isolation of monkeypox virus from wild squirrel infected in nature. *Lancet*, 327(8472):98, 1986.

[201] J.K. Omifolaji, E.T. Ikyaagba, A.A. Alarape, et al. Diversity and distribution of anomalures and squirrels in Oban Hills of Nigeria. *Hystrix: The Italian Journal of Mammalogy*, 33(1), 2022.

[202] M.G. Reynolds, D.S. Carroll, and K.L. Karem. Factors affecting the likelihood of monkeypox's emergence and spread in the post-smallpox era. *Current Opinion in Virology*, 2(3):335–343, 2012.

[203] C.L. Hutson, D.S. Carroll, J. Self, et al. Dosage comparison of Congo Basin and West African strains of monkeypox virus using a prairie dog animal model of systemic orthopoxvirus disease. *Virology*, 402(1):72–82, 2010.

[204] C.L. Hutson, Y.J. Nakazawa, J. Self, et al. Laboratory investigations of African pouched rats (Cricetomys gambianus) as a potential reservoir host species for monkeypox virus. *PLoS Neglected Ttropical Diseases*, 9(10):e0004013, 2015.

[205] C.E. Madubueze, I.O. Onwubuya, G.N. Nkem, and Z. Chazuka. The transmission dynamics of the monkeypox virus in the presence of environmental transmission. *Frontiers in Applied Mathematics and Statistics*, 8:1061546, 2022.

[206] O.J. Peter, F.A. Oguntolu, M.M. Ojo, et al. Fractional order mathematical model of monkeypox transmission dynamics. *Physica Scripta*, 97(8):084005, 2022.

[207] M. Ngungu, E. Addai, A. Adeniji, U.M Adam, and K. Oshinubi. Mathematical epidemiological modeling and analysis of monkeypox dynamism with non-pharmaceutical intervention using real data from United Kingdom. *Frontiers in Public Health*, 11:1101436, 2023.

[208] A.I. Ward and G.C. Smith. Predicting the status of wild deer as hosts of Mycobacterium bovis infection in Britain. *European Journal of Wildlife Research*, 58:127–135, 2012.

[209] L. Bolzoni, E. Bonacini, C. Soresina, and M. Groppi. Time-optimal control strategies in SIR epidemic models. *Mathematical Biosciences*, 292:86–96, 2017.

[210] L. Bolzoni and G.A. De Leo. Unexpected consequences of culling on the eradication of wildlife diseases: the role of virulence evolution. *The American Naturalist*, 181(3):301–313, 2013.

[211] L.J.S. Allen. *An introduction to stochastic processes with applications to biology*. CRC press, 2010.

[212] H. Andersson and T. Britton. *Stochastic epidemic models and their statistical analysis*, volume 151. Springer Science & Business Media, 2012.

[213] I. Sazonov, M. Kelbert, and M.B. Gravenor. A two-stage model for the SIR outbreak: Accounting for the discrete and stochastic nature of the epidemic at the initial contamination stage. *Mathematical Biosciences*, 234(2):108–117, 2011.

[214] L.J.S. Allen, S.R. Jang, and L. Roeger. Predicting population extinction or disease outbreaks with stochastic models. *Letters in Biomathematics*, 2017.

[215] L.J.S. Allen and G.E. Lahodny Jr. Extinction thresholds in deterministic and stochastic epidemic models. *Journal of Biological Dynamics*, 6(2):590–611, 2012.

[216] A. Gray, D. Greenhalgh, L.J. Hu, X.R. Mao, and J.F. Pan. A stochastic differential equation SIS epidemic model. *SIAM Journal on Applied Mathematics*, 71(3):876–902, 2011.

[217] N.T. Dieu. Asymptotic properties of a stochastic SIR epidemic model with

Beddington–DeAngelis incidence rate. *Journal of Dynamics and Differential Equations*, 30(1):93–106, 2018.

[218] Q. Liu and D.Q. Jiang. Threshold behavior in a stochastic SIR epidemic model with Logistic birth. *Physica A: Statistical Mechanics and its Applications*, 540:123488, 2020.

[219] E. Bernardi and A. Lanconelli. A note about the invariance of the basic reproduction number for stochastically perturbed SIS models. *Studies in Applied Mathematics*, 148(4):1543–1562, 2022.

[220] L. Zhu and H.X. Hu. A stochastic SIR epidemic model with density dependent birth rate. *Advances in Difference Equations*, 2015:1–12, 2015.

[221] A. Lahrouz, L. Omari, and D. Kiouach. Global analysis of a deterministic and stochastic nonlinear SIRS epidemic model. *Nonlinear Analysis: Modelling and Control*, 16(1):59–76, 2011.

[222] Q.S. Yang, D.Q. Jiang, N.Z. Shi, and C.Y. Ji. The ergodicity and extinction of stochastically perturbed SIR and SEIR epidemic models with saturated incidence. *Journal of Mathematical Analysis and Applications*, 388(1):248–271, 2012.

[223] N. Shakiba, C.J. Edholm, B.O. Emerenini, et al. Effects of environmental variability on superspreading transmission events in stochastic epidemic models. *Infectious Disease Modelling*, 6:560–583, 2021.

[224] K. Hwang, C. Edholm, O. Saucedo, L.J.S. Allen, and N. Shakiba. A hybrid epidemic model to explore stochasticity in COVID-19 dynamics. *Bulletin of Mathematical Biology*, 84(9):91, 2022.

[225] S. Newey. Pet hamsters belonging to monkeypox patients should be isolated or killed, say health chiefs. https://www.telegraph.co.uk/global-health/science-and-disease/pet-hamsters-belonging-monkeypox-patients-should-isolated-killed/, 2022.

[226] R.R. Musafir, A. Suryanto, and I. Darti. Optimal control of a fractional-order monkeypox epidemic model with vaccination and rodents culling. *Results in Control and Optimization*, 14:100381, 2024.

[227] H.W. Hethcote. Epidemiology models with variable population size. In *Mathematical Understanding of Infectious Disease Dynamics*, pages 63–89. World Scientific, 2009.

[228] J.H. Swart. Hopf bifurcation and stable limit cycle behavior in the spread of

infectious disease, with special application to fox rabies. *Mathematical Biosciences*, 1989.

[229] L.Q. Gao, J. Mena-Lorca, and H.W. Hethcote. Variations on a theme of SEI endemic models. In *Differential Equations and Applications to Biology and Industry*, pages 191–207. World Scientific, 1994.

[230] P.F. Hsieh and A.W.J. Stoddart. *Analytic theory of differential equations: the proceedings of the conference at Western Michigan University, Kalamazoo, from 30 April to 2 May 1970*, volume 183. Springer, 2006.

[231] E.J. Allen. *Modeling with Itô stochastic differential equations*, volume 22. Springer Science and Business Media, 2007.

[232] E.J. Allen, L.J.S. Allen, A. Arciniega, and P.E. Greenwood. Construction of equivalent stochastic differential equation models. *Stochastic Analysis and Applications*, 26(2):274–297, 2008.

[233] A. Nandi and L.J.S. Allen. Probability of a zoonotic spillover with seasonal variation. *Infectious Disease Modelling*, 6:514–531, 2021.

[234] K. Mamis and M. Farazmand. Stochastic compartmental models of the COVID-19 pandemic must have temporally correlated uncertainties. *Proceedings of the Royal Society A*, 479(2269):20220568, 2023.

[235] X.R. Mao. *Stochastic differential equations and applications*. Elsevier, 2007.

[236] Matlab for artificial intelligence. https://www.mathworks.com, 2022.

[237] Datagraph. https://www.visualdatatools.com/DataGraph/, 2022.

[238] J. Lee, Y. Ko, and E. Jung. Effective control measures considering spatial heterogeneity to mitigate the 2016–2017 avian influenza epidemic in the Republic of Korea. *PLoS One*, 14(6):e0218202, 2019.

[239] C.J. Edholm, B.O. Emerenini, A.L. Murillo, et al. Searching for superspreaders: Identifying epidemic patterns associated with superspreading events in stochastic models. *Understanding Complex Biological Systems with Mathematics*, pages 1–29, 2018.

[240] R. Lande. Risks of population extinction from demographic and environmental stochasticity and random catastrophes. *The American Naturalist*, 142(6):911–927, 1993.

[241] B. Tsanou, J.M.S. Lubuma, A.J.O. Tassé, and H.M. Tenkam. Dynamics of host-reservoir transmission of Ebola with spillover potential to humans. *Electronic Journal of Qualitative Theory of Differential Equations*, 2018(14):1–32, 2018.

[242] M. Toorians, A. MacPherson, and T.J. Davies. Unravelling transmission in epidemiological models and its role in the disease-diversity relationship. 2021.

[243] N.I. Samia, K.L. Kausrud, H. Heesterbeek, et al. Dynamics of the plague–wildlife–human system in Central Asia are controlled by two epidemiological thresholds. *Proceedings of the National Academy of Sciences*, 108(35):14527–14532, 2011.

[244] A. Feukouo Fossi, J. Lubuma, C. Tadmon, and B. Tsanou. Mathematical modeling and nonstandard finite difference scheme analysis for the environmental and spillover transmissions of Avian Influenza A model. *Dynamical Systems*, 36(2):212–255, 2021.

[245] F. Brauer, C. Castillo-Chavez, and C. Castillo-Chavez. *Mathematical models in population biology and epidemiology*, volume 2. Springer, 2012.

[246] E.A. Falendysz, J.G. Lopera, T.E. Rocke, and J.E. Osorio. Monkeypox virus in animals: current knowledge of viral transmission and pathogenesis in wild animal reservoirs and captive animal models. *Viruses*, 15(4):905, 2023.

[247] M. Turkyilmazoglu. Explicit formulae for the peak time of an epidemic from the SIR model. *Physica D: Nonlinear Phenomena*, 422:132902, 2021.

[248] Centers for Disease Control and Prevention. Mpox in animals and pets. https://www.cdc.gov/mpox/about/mpox-in-animals-and-pets.html?CDC_AAref_Val=https://www.cdc.gov/poxvirus/mpox/veterinarian/mpox-in-animals.html, 2024.

[249] R.A. Weinstein, A. Nalca, A.W. Rimoin, et al. Reemergence of monkeypox: prevalence, diagnostics, and countermeasures. *Clinical Infectious Diseases*, 41(12):1765–1771, 2005.

[250] L.D. Nolen, L. Osadebe, J. Katomba, et al. Introduction of monkeypox into a community and household: risk factors and zoonotic reservoirs in the Democratic Republic of the Congo. *The American Journal of Tropical Medicine and Hygiene*, 93(2):410, 2015.

[251] E. Gomez-Lucia. Monkeypox: some keys to understand this emerging disease. *Animals*, 12(17):2190, 2022.

[252] R.D. Holt, A.P. Dobson, M. Begon, R.G. Bowers, and E.M. Schauber. Parasite establishment in host communities. *Ecology Letters*, 2003.

[253] W.S. Hart, H. Park, Y.D. Jeong, et al. Analysis of the risk and preemptive control of viral outbreaks accounting for within-host dynamics: SARS-

CoV-2 as a case study. *Proceedings of the National Academy of Sciences*, 120(41):e2305451120, 2023.

[254] C. Besombes, F. Mbrenga, L. Schaeffer, et al. National Monkeypox Surveillance, Central African Republic, 2001–2021. *Emerging Infectious Diseases*, 28(12):2435, 2022.

[255] N. Haddad. The presumed receptivity and susceptibility to monkeypox of European animal species. *Infectious Diseases Now*, 52(5):294–298, 2022.

[256] D.J. Becker, A.D. Washburne, C.L. Faust, et al. Dynamic and integrative approaches to understanding pathogen spillover. *Philosophical Transactions of the Royal Society B*, 374(1782):20190014, 2019.

[257] V.A. Bokil and C.A. Manore. Coexistence of competing species with a directly transmitted pathogen. *Oregon State University*, 2010.

[258] M. Banuet-Martinez, Y. Yang, B. Jafari, et al. Monkeypox: a review of epidemiological modelling studies and how modelling has led to mechanistic insight. *Epidemiology and Infection*, 151:e121, 2023.

[259] B.K. Titanji, B. Tegomoh, S. Nematollahi, M. Konomos, and P.A. Kulkarni. Monkeypox: a contemporary review for healthcare professionals. In *Open*

Forum Infectious Diseases, volume 9, page ofac310. Oxford University Press, 2022.

[260] M. Hoti, X. Huo, and K.Q. Lan. Stability and phase portraits of susceptible-infective-removed epidemic models with vertical transmissions and linear treatment rates. 2017.

[261] A. Hastings. Transients: the key to long-term ecological understanding? *Trends in Ecology and Evolution*, 19(1):39–45, 2004.

[262] F. Nani and H.I. Freedman. A mathematical model of cancer treatment by immunotherapy. *Mathematical Biosciences*, 163(2):159–199, 2000.

[263] K.R. Manlove, L.M. Sampson, B. Borremans, et al. Epidemic growth rates and host movement patterns shape management performance for pathogen spillover at the wildlife–livestock interface. *Philosophical Transactions of the Royal Society B*, 374(1782):20180343, 2019.

[264] K.A. Alexander, C.J. Carlson, B.L. Lewis, et al. The ecology of pathogen spillover and disease emergence at the human-wildlife-environment interface. In *The connections between ecology and infectious disease*, pages 267–298. Springer, 2018.

[265] L. Arnold, C. Jones, K. Mischaikow, G. Raugel, and L. Arnold. *Random dynamical systems*. Springer, 1995.

[266] X.F. Zhang and R. Yuan. Stochastic bifurcation and density function analysis of a stochastic logistic equation with distributed delay and weak kernel. *Mathematics and Computers in Simulation*, 195:56–70, 2022.

[267] M. Ishikawa. Stochastic bifurcations in the plankton-fish system. *Transactions of the Institute of Systems, Control and Information Engineers*, 28(12):453–459, 2015.

[268] A. Zakharova, T. Vadivasova, V. Anishchenko, A. Koseska, and J. Kurths. Stochastic bifurcations and coherencelike resonance in a self-sustained bistable noisy oscillator. *Physical Review E–Statistical, Nonlinear, and Soft Matter Physics*, 81(1):011106, 2010.

[269] G. Rozhnova and A. Nunes. Fluctuations and oscillations in a simple epidemic model. *Physical Review E–Statistical, Nonlinear, and Soft Matter Physics*, 79(4):041922, 2009.

[270] A.J. Black, A.J. McKane, A. Nunes, and A. Parisi. Stochastic fluctuations in the susceptible-infective-recovered model with distributed infectious pe-

riods. *Physical Review E–Statistical, Nonlinear, and Soft Matter Physics*, 80(2):021922, 2009.

[271] L.F. Olsen and W.M. Schaffer. Chaos versus noisy periodicity: alternative hypotheses for childhood epidemics. *Science*, 249(4968):499–504, 1990.

[272] D. Alonso, A.J. McKane, and M. Pascual. Stochastic amplification in epidemics. *Journal of the Royal Society Interface*, 4(14):575–582, 2007.

[273] T. Asada and H. Yoshida. Coefficient criterion for four-dimensional Hopf bifurcations: a complete mathematical characterization and applications to economic dynamics. *Chaos, Solitons and Fractals*, 18(3):525–536, 2003.

[274] S. Bosi and D. Desmarchelier. Local bifurcations of three and four-dimensional systems: A tractable characterization with economic applications. *Mathematical Social Sciences*, 97:38–50, 2019.

[275] Z.J. Jing, Z.R. Liu, and J.Q. Shen. Hopf bifurcation and other dynamical behaviors for a fourth order differential equation in models of infectious disease. *Acta Mathematicae Applicatae Sinica*, 10:401–410, 1994.

[276] Maplesoft. https://www.maplesoft.com/, 2022.

[277] G. Lo Iacono, A. Cunningham, E. Fichet-Calvet, et al. Using modelling to dis-

entangle the relative contributions of zoonotic and anthroponotic transmission: the case of Lassa fever. *PLoS Neglected Tropical Diseases*, 9(1):e3398, 2015.

[278] C. Gortázar, E. Ferroglio, U. Höfle, K. Frölich, and J. Vicente. Diseases shared between wildlife and livestock: a European perspective. *European Journal of Wildlife Research*, 53:241–256, 2007.

[279] M. Boadella, J. Vicente, F. Ruiz-Fons, J. De la Fuente, and C. Gortázar. Effects of culling eurasian wild boar on the prevalence of Mycobacterium bovis and Aujeszky's disease virus. *Preventive Veterinary Medicine*, 107(3-4):214–221, 2012.

[280] Á.G.C. Pérez, E. Avila-Vales, and G.E. García-Almeida. Bifurcation analysis of an SIR model with logistic growth, nonlinear incidence, and saturated treatment. *Complexity*, 2019(1):9876013, 2019.

[281] H. Hethcote, Z.E. Ma, and S.B. Liao. Effects of quarantine in six endemic models for infectious diseases. *Mathematical Biosciences*, 180(1-2):141–160, 2002.

[282] N. Beeton and H. McCallum. Models predict that culling is not a feasible strategy to prevent extinction of tasmanian devils from facial tumour disease. *Journal of Applied Ecology*, 48(6):1315–1323, 2011.

[283] S. Blumberg and J.O. Lloyd-Smith. Inference of R_0 and transmission heterogeneity from the size distribution of stuttering chains. *PLoS Computational Biology*, 9(5):e1002993, 2013.